TECHNICAL TRANSACTIONS
CZASOPISMO TECHNICZNE

MECHANICS
MECHANIKA

ISSUE 4-M (14)
ZESZYT 4-M (14)

YEAR 2016 (113)
ROK 2016 (113)

WYDAWNICTWO POLITECHNIKI KRAKOWSKIEJ

TECHNICAL TRANSACTIONS | CZASOPISMO TECHNICZNE

MECHANICS | MECHANIKA

ISSUE 4-M (14) | ZESZYT 4-M (14)
YEAR 2016 (113) | ROK 2016 (113)

Basic version of each Technical Transactions magazine is its online version
Pierwotną wersją każdego zeszytu Czasopisma Technicznego jest jego wersja online
www.ejournals.eu/Czasopismo-Techniczne www.technicaltransactions.com www.czasopismotechniczne.pl

TECHNICAL TRANSACTIONS | CZASOPISMO TECHNICZNE
MECHANICS | MECHANIKA
4-M/2016

NORBERT RADEK*, ŁUKASZ J. ORMAN**, ANDREJ KAPJOR***,
AUGUSTÍN SLADEK****

EFFICIENT SURFACES FOR BOILING HEAT TRANSFER ENHANCEMENT

WYDAJNE POWIERZCHNIE WYMIENNIKOWE DLA WYMIANY CIEPŁA PRZY WRZENIU

A b s t r a c t

The paper discusses the use of efficient surfaces for heat transfer enhancement during a nucleate boiling heat transfer. Distilled water under ambient pressure was the working fluid in the presented experiment. The application of a brass mesh of 0.63 mm aperture and 0.20 mm wire diameter on the surface of a copper heater led to considerable improvement in the value of heat flux at low temperature differences of a few Kelvin, where the enhancement ratio exceeded 2. Such modified surfaces could be used in the design of more efficient heat exchangers e.g. in refrigeration systems.

Keywords: boiling heat transfer, *microstructures*

S t r e s z c z e n i e

Artykuł dotyczy wykorzystania wydajnych powierzchni do intensyfikacji wrzenia. Czynnikiem roboczym w badaniach była woda destylowana. Zastosowanie siatki mosiężnej o prześwicie 0,63 mm i o grubości drutu 0,20 mm na powierzchni wymiennikowej skutkowało znacznym wzrostem gęstości strumienia ciepła w obszarze małych przegrzań, gdzie stopień intensyfikacji wymiany ciepła przekroczył 2. Takie modyfikowane powierzchnie mogą być wykorzystywane do projektowania bardziej wydajnych wymienników ciepła, np. w systemach chłodniczych.

Słowa kluczowe: wymiana ciepła przy wrzeniu, *mikropowierzchnie*

DOI: 10.4467/2353737XCT.16.224.5973

* D.Sc. Ph.D. Eng. Norbert Radek, Assoc. Prof., Centre for Laser Technologies of Metals, Faculty of Mechatronics and Machine Design, Kielce University of Technology.

** D.Sc. Ph.D. Eng. Łukasz J. Orman, Chair of Sanitary Networks and Systems, Faculty of Environmental, Geomatic and Energy Engineering, Kielce University of Technology.

*** D.Sc. Ph.D. Eng. Andrej Kapjor, Department of Power Engineering, Faculty of Mechanical Engineering, University of Žilina, Slovakia.

**** Prof. D.Sc. Ph.D. Eng. Augustín Sladek, Department of Technology Engineering, Faculty of Mechanical Engineering, University of Žilina, Slovakia.

1. Introduction

Boiling mode is a phase-change process which is characterised by significant heat flux values being exchanged at relatively low temperature differences. Such heat exchangers are commonly used for example in refrigeration or electronics. Smooth heat exchangers can be covered with additional structures and the morphology of the heater surface itself can also be changed by means of various techniques e.g. through roughening or machining. Different kinds of microstructures can also be applied on heaters in order to enhance boiling. Such enhancement means elevating the exchanged heat fluxes in a device at the same temperature difference or enabling the same heat flux to be dissipated at a lower temperature difference.

One common kind of structures used for boiling augmentation are metal meshes. They are cheap to produce and easy to attach to heaters with different methods. Asakavičjus et al. [1] considered boiling of R-113, ethanol and water inside a heat pipe with an internal coating of up to 12 mesh layers. It was given that mesh layers enhance boiling heat transfer in comparison to the smooth surface and boiling on microstructures proved to occur at much lower heat fluxes. Vasil'yev [2] experimentally analysed water boiling on a horizontal heater with a single stainless steel mesh layer. The wire diameters of the meshes were 0.055 mm, 0.09 mm, 0.15 mm and 0.26 mm, while aperture (distance between the wires): 0.08 mm, 0.14 mm, 0.40 mm and 0.73 mm, respectively. It was reported that the heat transfer coefficient increased as the aperture value became smaller. The most significant augmentation was observed for the mesh of 0.055 wire diameter and aperture 0.08 mm. The investigations performed by Li et al. [3] concentrated on water boiling under ambient pressure on a copper heater covered with meshes. The wire diameter was 0.056 mm, while the number of layers was up to 9, producing a structure of the height up to 0.82 mm and porosity 0.693–0.737. All of the meshed surfaces improved boiling in comparison with the smooth surface. Li and Peterson [4] were experimentally analysing water boiling under ambient pressure on a horizontal copper surface with a copper mesh coating. The authors found out that the application of such meshes enhanced boiling heat transfer in comparison with the smooth surface. The meshes had a wire diameter of $d = 56$ μm and aperture (distance between the wires) $a = 119.3$ μm, $d = 114$ μm and $a = 139.7$ μm as well as $d = 191$ μm and $a = 232.8$ μm. The observations revealed that for smaller apertures higher heat flux values could be dissipated from the surface. In order to determine the impact of volumetric porosity, samples of 6 mesh layers were produced and compacted to various porosity values. Only a low influence of porosity was detected. Other kinds of structures can be applied on heaters in order to enhance boiling heat transfer. Danilova et al. [5] analysed boiling of R-22 and R-717 on steel tubes with aluminum porous coating made with the flame spraying technique. Heat transfer coefficient of the porous covering was observed to be 2 to 5 times higher in comparison to the smooth surface. The paper by Cieśliński [6] experimentally considers water boiling heat transfer on horizontal heaters produced with copper with electrochemically deposited microstructures. The height of such aluminum, copper and silver coverings was 0.3–1.1 mm. It was reported by the author that the heat transfer coefficient value of the copper layer was the highest – about four times larger than the one noted for the smooth surface. Yang et al. [7] experimentally analysed boiling of water on foams of the height

1 mm, 2 mm, 3 mm, 4 mm and 5 mm. Heat transfer coefficients of foam layers were reported to be two to three times higher than those of the smooth surface.

2. Material and method

There are many types of microstructures, however mesh layers seem to be very efficient as given in the literature and they have been chosen for the analysis. The tests have been performed on the non-isothermal surface of a 3 mm thick fin with a brass mesh of 0.63 mm aperture and 0.20 mm wire diameter. Such a mesh is a commercially available product applied, for example, for filtering purposes. Sintering at the temperature of ca. 900°C was used to produce durable bonds between the copper fin (base) and the attached brass mesh. This process occurred in the oxygen-free atmosphere (with nitrogen and hydrogen) so that oxidation of the elements could be avoided.

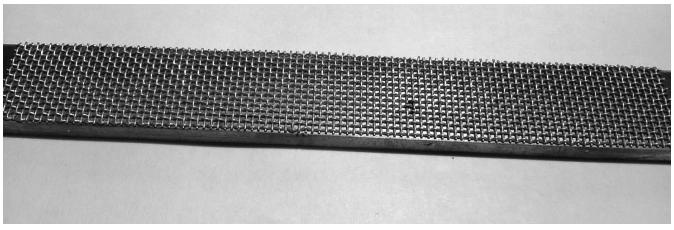

Fig. 1. Photo of the sample – copper base with the brass mesh

Figure 1 presents a photograph of the sample. The fin is placed and sealed in the vessel with boiling water. Its surface open to the atmosphere is observed with a thermovision camera system to determine the temperature gradient along it with heating power being regulated by means of an autotransformer. The inner surface is in contact with distilled water that is boiled in the vessel. Here, the methodology presented by Orzechowski [8] has been used. This technique is based on the assumption of exponential dependence of the heat transfer coefficient on the difference between the surface and saturation temperatures – called superheat (θ). As a result of the application of numerical differentiation procedure of the obtained temperature distribution along the length of the investigated element, it is possible to determine the local values of the heat transfer coefficient (and, consequently, heat flux) through the application of the linear fitting of the experimental results.

3. Results and discussion

The experiments have been performed under ambient pressure with distilled water as the boiling fluid. The surface that was observed with the infrared camera was covered with a special black paint in order to reduce possible errors caused by the incorrect value of emissivity and the influence of the surroundings on the measurements. The results of the superheat gradient were used to produce numerically the first derivative values. Then

the heat flux was determined. The results of both surfaces are particularly different in the range of small superheat values. However, as the temperature differences become larger (the surface becomes hotter and more bubbles are created), the impact of the additional porous metal layer gets smaller and the obtained results seem to approach those that were recorded for the smooth surface. It is very visible in Fig. 2, where the heat flux (determined using procedure described in [8]) has been presented vs. wall superheat.

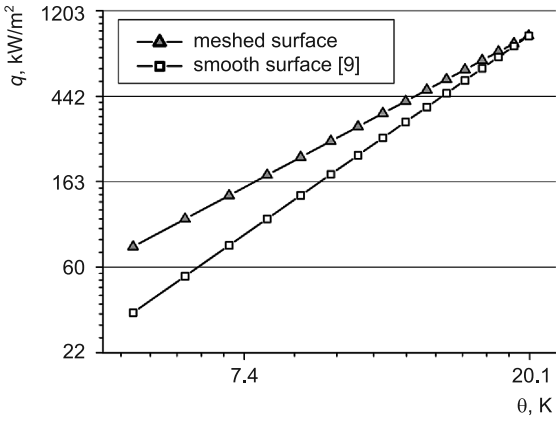

Fig. 2. Heat flux vs. wall superheat

Based on the above figure of changes of the hear flux values as a function of superheat in logarithmic coordinates, it can be stated that the boiling process is enhanced mainly for low temperature differences. This may be attributed to the fact that the mesh microstructure offers additional locations where vapour bubbles can be grown. The overheating of the mesh provides favourable conditions for efficient heat transfer. Here, the contact surface between the extended surface with the mesh and the fluid is much larger than in the case of a technically smooth surface. Nevertheless, a constant growth in temperature leads to the increased vapour production of superheats over 15 K. As a consequence, vapour seems to accumulate within the surface. This phenomenon is more pronounced in the case of the mesh layer, because vapour removal and liquid inflow is hampered due to increased resistance. This might be the prime reason behind worsening of heat transfer conditions for considerable superheat values. If temperature is increased even further, the burn-out of the heater can take place. Very large accumulation of vapour may lead to the occurrence of a permanent vapour blanket on the heater surface that acts as a thermal insulation. Here, a transition to film boiling occurs, which is an unfavourable phenomenon due to lower heat fluxes and large temperatures. Figure 3 summarises the results of heat transfer enhancement due to the application of an additional mesh layer. A steady deterioration of heat dissipation conditions can be easily observed for the analysed type of coating.

It is worth noting that the application of the analysed brass mesh can result in elevated heat fluxes. For the superheat of 5 K ,the enhancement ratio was almost 2.2 as given in Fig. 3. The heat flux dissipated from the meshed surface can, thus, be over twice higher than that from the smooth reference surface without any layers for the same superheat value.

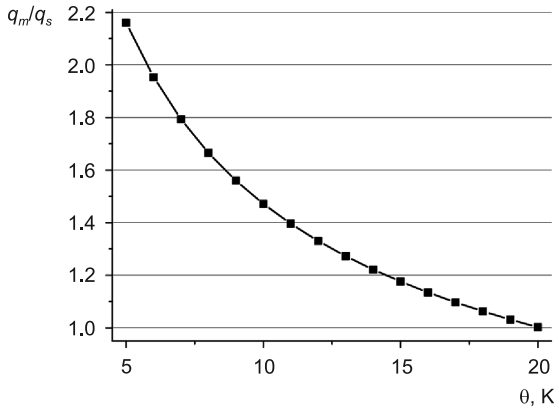

Fig. 3. Ratio of the heat flux for the surface with the meshed layer (q_m) and the smooth surface (q_s) – data from Fig. 2

This indicates better heat transfer conditions and can also be used to produce smaller heat exchangers that are still able to remove the same heat flux.

4. Summary and conclusions

There are many different techniques to enhance boiling. The majority are passive (e.g. application of additional microstructures). Here, metallic coatings seem to be the most favourable – including steel of different types [10, 11]. However, some involve the use of electrostatic field for boiling of dialectic fluids, which could be inferred from [12, 13]. The presented results indicate significant possibilities in heat transfer enhancement with the use of mesh layers. However, microstructures can also be used in flow boiling (as considered in [14, 15]). Generally, they tend to augment boiling in the range of low temperature differences. At higher heat fluxes more vapour is produced and gets accumulated within the additional coating, which hampers heat and mass transfer conditions.

Further work of the authors can be directed to search for new types of coatings – including those that are produced as a combination of a microstructure (e.g. meshes) and a modification of the surface with laser or electrospark deposition. This could further enhance boiling heat transfer. What is more, different boiling fluids, such as commercial refrigerants, nanofluids or new cooling agents can be used instead of water.

Acknowledgements: *This article was created within the frame of the project KEGA 026ŽU-4/2014 "The heat transfer from the heat exchange surfaces based on natural convection"*

References

[1] Asakavičjus I.P., Žukauskas A.A., Gajgalis V.A., Eva V.K., *Teplootdača freona-113, etilovogo spirta i vody v setčatych fitiljach*, Lietuvos TSR Moksly akademijos darbai, B serija, vol. I **104**, 1978, 87-93.

[2] Vasil'yev A.A., *Heat transfer and critical heat flux densities in boiling of water under a vacuum on walls covered with a single layer of mesh*, Heat Transfer Research, vol. **24** (7), 1992, 913-921.

[3] Li C., Peterson G.P., Wang Y., *Evaporation/boiling in thin capillary wicks (I) – wick thickness effects*, J. of Heat Transfer, vol. **128**, 2006, 1312-1319.

[4] Li C., Peterson G.P., *Evaporation/boiling in thin capillary wicks (II) – effects of volumetric porosity and mesh size*, J. of Heat Transfer, vol. **128**, 2006, 1320-1328.

[5] Danilova G.N., Dyundin V.A., Bosishanskaya A.V., Soloviyov A.G., Vol'nykh Yu.A., Kozyrev A.A., *Effect of surface conditions on boiling heat transfer of refrigerants in shell-and--tube evaporators*, Heat Transfer – Soviet Research, vol. **22** (1), 1990, 56-65.

[6] Cieśliński J.T., *An experimental study of nucleate pool boiling heat transfer from a flat horizontal plate covered with porous coatings*, Archive of Thermodynamics, vol. **12** (1–4), 1991, 69-76.

[7] Yang Y., Ji X., Xu J., *Pool boiling heat transfer on copper foam covers with water as working fluid*, Int. J. of Thermal Sciences, vol. **49**, 2010, 1227-1237.

[8] Orzechowski T., *Wymiana ciepła przy wrzeniu na żebrach z mikropowierzchnią strukturalną*, Wyd. Politechniki Świętokrzyskiej, Kielce 2003 [in Polish].

[9] Orman Ł.J., *Nucleate boiling heat transfer on a smooth surface of a fin*, XII Int. Symp. „Heat Transfer and Renewable Sources of Energy", Międzyzdroje 2008, 363-369.

[10] Ulewicz R., Mazur M., Bokuvka O., *Structure and mechanical properties of fine-grained steels*, Periodica Polytechnica Transportation Engineering, vol. **41**, 2013, 111-115.

[11] Mazur M., Ulewicz R., Novy F., Szataniak P., *The structure and mechanical properties of domex 700 MC steel*, Komunikacie, vol. **15** (4), 2013, 54-57.

[12] Radziszewski L., *The influence of the surface load exerted by a piezoelectric contact sensor on testing results: Part I, The displacement field in the solid*, Archives of Acoustics, vol. **28**, 2003, 71-91.

[13] Radziszewski L., *The influence of the surface load exerted by a piezoelectric contact sensor on testing results: Part II, The electrical transients generated by piezoelectric sensor*, Archives of Acoustics, vol. **28**, 2003, 93-100.

[14] Piasecka M., *An application of enhanced heating surface with mini-reentrant cavities for flow boiling research in minichannels*, Heat and Mass Transfer, vol. **49** (2), 2013, 261-275.

[15] Hożejowska S., Piasecka M., Poniewski M., *Boiling heat transfer in vertical minichannels. Liquid crystal experiments and numerical investigations*, Int. J. of Thermal Sciences, vol. **48** (6), 2009, 1049-1059.

TECHNICAL TRANSACTIONS | CZASOPISMO TECHNICZNE
MECHANICS | MECHANIKA
4-M/2016

MAGDALENA MAZUR*

FATIGUE PROPERTIES OF FINE-GRAINED STEELS APPLIED IN COMPONENTS OF SEMITRAILERS

WŁASNOŚCI ZMĘCZENIOWE STALI DROBNOZIARNISTYCH W KONSTRUKCJI NACZEP SAMOCHODOWYCH

A b s t r a c t

The article presents preliminary fatigue test results of selected grades of constructional steel used for producing elements of semitrailers and trailers, which are made by WIELTON S.A. company. Demand for fatigue tests of fine-grained steel has been reported by designers looking for new applications of high strength steel in new constructions. Fractorapnic analysis of the selected elements proved strong relation between fatigue structure and microstructure of the materials.

Keywords: fatigue properties, *trailers construction*, *higher-strength steel*, *fractographic analysis*

S t r e s z c z e n i e

W niniejszym artykule dokonano analizy badań zmęczeniowych dla stali drobnoziarnistych w zakresie zmęczenia wysokocyklowego, materiałów konstrukcyjnych naczep samochodowych produkowanych przez firmę WIELTON S.A. Prowadzone badania są wynikiem zainteresowania konstruktorów poszukiwaniem nowych możliwości wykorzystania stali wysokowytrzymałych w nowych modelach naczep. Analiza fraktograficzna wybranych elementów potwierdza silną zależność struktury przełomu zmęczeniowego z mikrostrukturą materiału.

Słowa kluczowe: własności zmęczeniowe, *konstrukcje naczep*, *stale wysokowytrzymałe*, *analiza fraktograficzna*

DOI: 10.4467/2353737XCT.16.225.5974

* Ph.D. Eng. Magdalena Mazur, Institute of Production Engineering, Faculty of Management, Czestochowa University of Technology.

1. Introduction

In spite of progress and development in science and technology designers have a great deal of grades of materials with different service properties at their disposal, from which they can select depending on the demands on the elements being designed. Satisfying all technical and operational requirements is sometimes difficult, and even impossible. The durability of parts operated during driving and carrying cargoes is connected with complex fatigue and tribological processes resulting from the mode of operation of individual subassemblies and with complex energy interaction processes that occur between the semitrailer's suspension and construction, as well as the load itself. This gives rise to the issue of both appropriate optimization of the part's design and proper selection of its material (in terms of chemical composition and phase structure) in order to increase operational quality and durability [1–4]. The article presents the analysis of preliminary fatigue tests results of two structural steel grades used in structural components of trailers, wagons, farm devices, etc. Getting to know properties of the materials is meant to answer the question whether it is possible to substitute traditional steel with high strength steel, resistant to wear and easily cold-shaped fine-grained steel.

The strategy of companies manufacturing means of transport, including WIELTON S.A., is to design and produce more efficient transport units by using lighter constructions, exchangeable modules and increased specialization of transport semitrailers. The design departments of the company, in cooperation with their partners, are conducting work on the application of new materials for constructional elements of semitrailers with the aim of reducing unladen mass and fuel consumption, increasing the tonnage of transported cargo, and lengthening the safe operation period [5, 6]. The research results will provide a basis for determining new applications of these materials and using them for constructional elements of semitrailers in order to increase their reliability and decrease the complete vehicle kerb weigh.

2. Experimental material

Steels Hardox (400 and 450) and Strenx 700MC have been used for the tests. The samples taken from Hardox 400 and 450 steel plate (13 mm thick) and Strenx 700MC steel plate (10 mm thick) were subjected to chemical analysis. The steel sheets were obtained directly from the manufacturer (SSAB Oxelosund Steel Mill) and taken from the WIELTON S.A. company's storage. The chemical analysis was made by means of the emission spectrometry method on an ICP (JY38S) emission spectrometer using a fast recording system, IMAGE.

The chemical analysis results were compared with the data provided by the high-strength steel manufacturer. The comparative analysis of chemical composition has confirmed that the contents of chemical elements correspond to the parameters provided for by the manufacturer in the material card. The increase in hardenability of these steels is also caused by carbide--forming elements (Cr, Mo) retarding the tempering processes. This is due to the coagulation rate of chromium and molybdenum carbides being lower than that of cementite. The presence of molybdenum (at min. 0.20% Mo) is important, all the more so because chromium (just

like phosphorus and other trace admixtures) increases the susceptibility to temper brittleness. Also nickel and manganese in the presence of chromium are favourable to this process. A function similar to that of molybdenum in Hardox steel is performed by boron, which strongly increases hardenability in pro-eutectoid steels. This effect is the more intensive the finer the grain occurring in the steel and the lower the carbon content of the steel (steels of the Hardox group are produced as fine-grained) [7, 8].

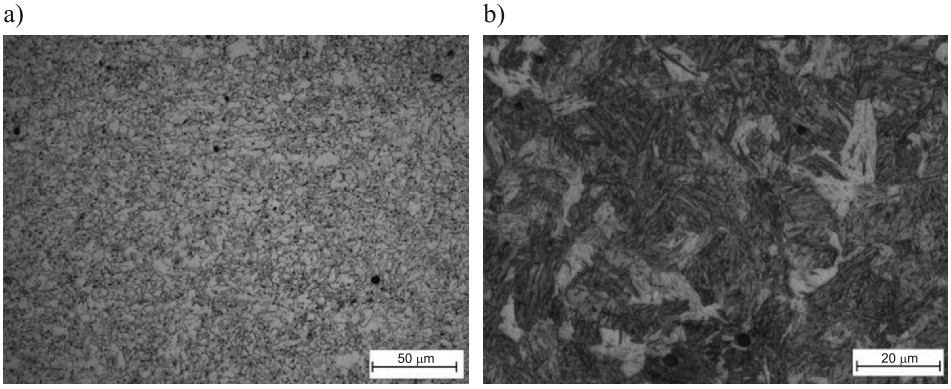

Fig. 1. Microstructure of the analyzed steel materials in the state as delivered, etched with 1% Nital: a) Strenx 700MC, b) Hardox 400

The observation of Strenx 700MC steel samples (Fig. 1a) showed that the steel was characterized by a fine-grained structure. The presented microstructure image revealed sparse titanium nitride particles with a regular geometric shape. The test material is also characterized by the occurrence of few inclusions in the form of black manganese sulphide (MnS) particles [3, 5]. The observations of the samples of Hardox 400 steel in the state as delivered (and etched with Nital) showed a structure of tempered martensite and retained austenite (Fig 1b). The structure of Hardox 400 steel exhibits high homogeneity over the entire cross-section; only few small inclusions were observed, which were unevenly distributed within the sample space. The analysis of the Hardox 450 steel microstructure also showed the occurrence of a martensitic structure.

The results of fatigue testing of specimens are strongly dependent on their surface. Therefore, the specimen working part must be prepared very carefully to have the surface roughness parameter of Ra – 0.32. During fatigue testing on the ROTOFLEX machine, the load cycle asymmetry factor was $R = -1$, and the specimens were loaded at the frequency of 30 Hz, at the ambient temperature of 20°C ± 10°C. The specimen working part was cooled during testing by means of fans. Based on the obtained results, the curve of the applied load amplitude versus the number of cycles to specimen fracture, $\sigma_a = f(N)$, was plotted. The results of the tests carried out are illustrated in Fig. 2.

Figure 3 represents the fatigue testing results of the materials analysis in a high-cycle range [9, 10]. The experimentally determined Whöler curve shows a decrease in the magnitude of specimen fracture stress with the increase in the number of load variation cycles up to the fatigue limit of Strenx 700MC steel (440 MPa). For the examined Hardox

steels, the occurrence of a fatigue limit can be clearly seen, which for Hardox 400 steel is at the level of 490 MPa, while for Hardox 450 steel at 460 MPa. The obtained results are similar; the difference is caused by the higher mechanical properties and hardness of Hardox 450 steel.

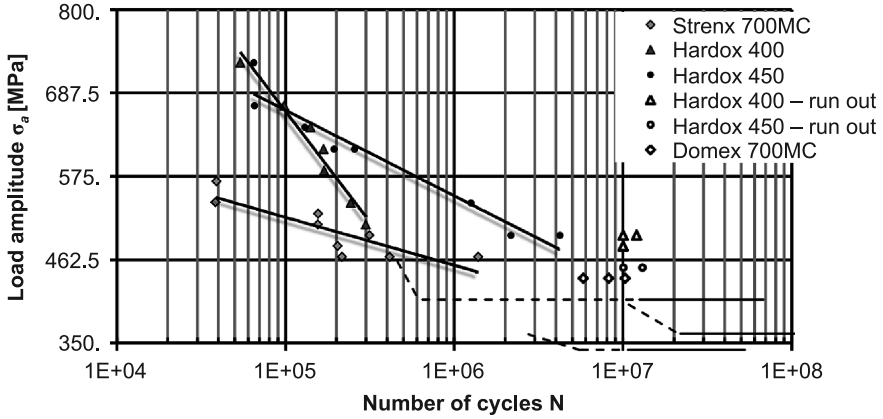

Fig. 2. The fatigue life of researched steels; fatigue test, rotary bending in the high--cycle interval [$f = 30$ Hz, $T = 20°C \pm 10°C$, $R = -1$]

3. Fractographic analysis of fatigue fractures

For the fractographic analysis, a VEGA 3 SB scanning electron microscope (SEM) was used. A fatigue fracture analysis was made for each series of Strenx 700MC, Hardox 450 and Hardox 400 steel specimens after fatigue testing [11, 12].

For almost all specimens, the initiation of fatigue cracks occurred on the specimen surface (Fig. 3), with the initiation location being dependent on the surface type (surface development degree), stress amplitude σ_a, as well as number of cycles to specimen failure,

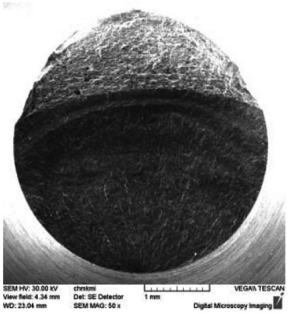

Fig. 3. Fatigue fracture of specimens on a macro scale: surface fatigue crack initiation for steel Hardox 450

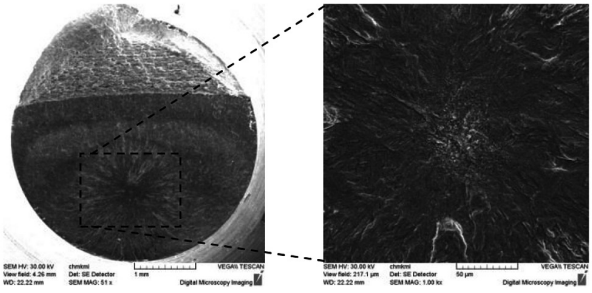

Fig. 4. A fracture of the Hardox 450 steel specimen on a macro scale; sub-surface fatigue crack initiation with a distinct crack initiation with a "fish-eye"

N. All the specimens except for 2 specimens from Hardox 450 steel were broken due to the initiation of fatigue cracks from the specimen surface as a result of formation of intrusions and extrusions. No more sub-surface fatigue crack initiation was observed.

The determination of the type of inclusion that was the point of stress concentration and the "fish-eye" mechanism initiation location for Hardox 450 steel was impossible (Fig. 4). The reason for this could be sought in the long-lasting fatigue effect (crack opening and closing), which resulted in the complete refinement of the inclusion particles.

On the surface of fatigue fractures of the test specimens made of Strenx steel, there occurs a transcrystalline fatigue fracture of a very fine morphology, which is characteristic for fine-grained steels. The character of the fatigue fracture for this steel in the unstable fatigue crack growth region before the final fracture region – radial steps and secondary cracks occur here. The final fracture region is characterized by a ductile fatigue fracture with a dimple morphology.

The examined fatigue fractures of Hardox 400 steel are characterized by a transcrystalline fracture of tempered martensite with a locally occurring intercrystalline fracture in the form of isolated intercrystalline facets, sometimes occurring on the surface of the fatigue fracture. The amount of intercrystalline failure on the fatigue fracture surface generally did not exceed 1%. In the stable fatigue crack propagation region, the propagation followed transcrystalline mechanisms, which was reflected in the **occurrence of striation** oriented perpendicularly to the fatigue crack propagation direction. The occurrence of fatigue striation is not typical for the fatigue fracture of high-strength materials. On the test specimen fracture, the increase in the distances between striations towards the final fracture regions can be seen.

4. Conclusions

High-strength steels of the Hardox type are distinguished by high sensibility to the occurrence of notches; this is associated with the presence of martensitic structure. During testing, particular attention should be given to inclusions, and particularly to their shape and size. The following rule applies: the harder and tougher the steel is the more it is prone to the occurrence of inclusions. In the case of Hardox 400 steel, whose matrix is by 50 HB softer than Hardox 450 steel, no impact of inclusions on fatigue failure was observed, and the initiation of all fatigue cracks took place on the specimen surface, following the same mechanism as for Strenx 700MC steels [13].

The results of fatigue tests of the investigated steels, carried out in the high-cycle range on a Rotoflex machine – the relationship $\sigma_a = f(N)$ assume the classic shape of the Wohler curve with a distinct fatigue limit. Determined from the experimental results, the curve showed a decrease in the magnitudes of stress amplitude σ_a with the increase in the number of load cycles N up to the fatigue limit level. The determination of the fatigue strength of new materials is crucial for assuring the reliability of designed equipment and extending its service life.

The obtained results have provided a basis for the development of new application capabilities of high-strength fine-grained steels to be used in the structural parts of machinery and equipment, as well as for the improvement of simulation models of automotive

semitrailer loading and operation. Research on fatigue testing in the high and ultra-high cycle fatigue is becoming increasingly important, taking into account the increased exploitation of constructed machines and devices, as well as their extended service life. Strength testing of high-strength steels has confirmed their high property declared by the manufacturer. New semi-Master series, which are manufactured by WIELTON S.A., represent new directions of development of the company. Possibilities of using the tested materials in the construction of semi-trailers manufactured by the company have been confirmed by the results of all the material research. Hardox has been used in parts of boxes semi-hoppers (such as: floor panels, side panels, front and rear wall flaps) in the parts in which high resistance to abrasion is an important feature. Steel Strenx 700MC can be used to make many items of chassis trailers discharge (chassis frame, the mounting plates and cross beams), a basic requirement in relation to this material in the first place being good weldability.

References

[1] Szataniak P., Novy F., Ulewicz R., *Fatigue Properties and Application Options of the Fine--Grained Steel of DOMEX Type*, Transcom Proc. of 11th Europ. Conf. of Young Researchers and Scientists. Sec. 5 – Material Engineering Mechanical Engineering Technologies, 2015, 309-314.

[2] Armigliato A., *Light Weighting in Commercial Transport*, Conference "Connecting Innovations. Wielton", Warsaw, 3–4 June 2014, presentation.

[3] Barani A.A., Ponge D., Raabe D., *Strong and Ductile Martensitic Steels for Automotive Applications*, Steel Research International, vol. **77** (9–10), 2006, 704-711.

[4] Sońta G., Dudek A., Selejdak J., Ulewicz R., *Analysis of Structure of Elements for Automotive Industry*, App. Mech. and Mat., vol. **712**, 2015, 81-86.

[5] Ulewicz R., Szataniak P., Novy F., *Fatigue Properties of Wear Resistant Martensitic Steel*, Proc. of 23rd Int. Conf. on Metallurgy and Materials METAL 2014, 21–23 May 2014, Brno, 784-789.

[6] Trško L., Bokůvka O., Nový F., Lago J., *Quality and fatigue characteristics relation*, Production Engineering Archives, vol. **10**, 2016, 9-12.

[7] Mroziński S., *Stabilizacja własności cyklicznych metali i jej wpływ na trwałość zmęczeniową*, Wydawnictwa Uczelniane Uniwersytetu Technologiczno-Przyrodniczego, Bydgoszcz 2008 [in Polish].

[8] Blicharski M., *Inżynieria materiałowa. Stal*, Wydawnictwa Naukowo-Techniczne, Warszawa 2004 [in Polish].

[9] Kokavec M., Konečná R., Nicoletto G., *Nodular cast iron fatigue lifetime in cyclic plane bending*, Materials Engineering – Materiálové inžinierstvo, vol. **19** (3), 2012, 104-109.

[10] Bokůvka O., Nový F., Mintach R., Činčala M., *Influence of Loading Type on the Shape of Lifetime Curve*, International Journal of Applied Mechanics and Engineering, vol. **15** (2), 2010, 321-328.

[11] Ulewicz R. Szataniak P., *Fatigue Cracks of Strenx Steel*, Materials Today: Proceedings, vol. **3** (4), 2016, 1195-1198.

[12] Szataniak P., Mazur M., Ulewicz R., Novy F., *Fractographic analysis of Hardox steels research in the field of high-cycle fatigue regime*, Communications Scientific Letters of the University of Žilina, **18**, 2016, 89-92.

[13] Mazur M., Ulewicz R., Bokůvka O., *Mechanical and Fatigue Properties of Hardox 400 and 450 Steels*, Advanced Manufacturing and Repairing Technologies in Vehicle Industry – 30th International Colloquium, Visegrád, Hungary 2013, 61-66.

TECHNICAL TRANSACTIONS | **CZASOPISMO TECHNICZNE**
MECHANICS | MECHANIKA
4-M/2016

RENATA FILIPOWSKA*

VARIATIONAL ITERATION TECHNIQUE FOR SOLVING HIGHER ORDER BOUNDARY VALUE PROBLEM WITH ADDITIONAL BOUNDARY CONDITION

ITERACYJNA TECHNIKA WARIACYJNA ZASTOSOWANA DO ZAGADNIENIA BRZEGOWEGO WYŻSZEGO RZĘDU Z DODATKOWYM WARUNKIEM BRZEGOWYM

A b s t r a c t

This paper treats a variational iteration technique, which is based on variational iteration method, for solving linear and non – linear two – point boundary value problems in the form of a fourth – order differential equation and five boundary conditions. The solution of this problem is possible only when the considered equation includes an unknown parameter. The presented method has been illustrated with a numerical example.

Keywords: *boundary value problem*, *variational iteration technique*, *approximate solution*, *system of integral equations*

S t r e s z c z e n i e

W artykule przedstawiono iteracyjną technikę wariacyjną opartą na iteracyjnej metodzie wariacyjnej, zastosowaną do rozwiązywania zarówno liniowego, jak i nieliniowego dwupunktowego zagadnienia brzegowego składającego się z równania różniczkowego czwartego rzędu oraz pięciu warunków brzegowych. Rozwiązanie tak postawionego problemu jest możliwe tylko wtedy, gdy rozpatrywane równanie zawiera nieznany parametr. Prezentowaną metodę zilustrowano przykładem obliczeniowym.

Słowa kluczowe: *zagadnienie brzegowe*, *iteracyjna technika wariacyjna*, *rozwiązanie przybliżone*, *układ równań całkowych*

DOI: 10.4467/2353737XCT.16.226.5975

* Ph.D. Eng. Renata Filipowska, Institute of Applied Informatics, Faculty of Mechanical Engineering, Cracow University of Technology.

1. Introduction

Boundary value problems (BVPs) play an important role in many fields, e.g. in mathematical modeling of viscoelastic and inelastic flows, physical and engineering sciences. There are different methods of solving these problems, e.g. the spectral Galerkin method [1], Adomian decomposition method [2], shooting method [3] or method with the use of B-spline functions [4]. In [5], the homotopy perturbation method was described, which is very efficient in finding analytical solutions. The variational iteration method (VIM) was developed by He [6], but it should be mentioned that this method was first considered by Inokuti and his colleagues [7]. It has proved to solve effectively and accurately a large class of differential equations with approximate solutions, which converge rapidly to accurate solutions. In [8], some useful iteration formulas about VIM were summarised. This method requires the determination of a convergent series by means of a correct functional. Describing the variational iteration technique (VIT), which is based on VIM [9], the authors [10] showed that higher-order BVPs are equivalent to the system of integral equations by using a suitable transformation. Next, this system can be solved efficiently by means of the VIM. This technique may be considered as an alternative method for solving BVPs.

In this paper the VIT [10] will be considered, but it will be modified and applied for solving non-standard fourth-order non-linear BVPs, where the number of boundary conditions exceeds the order of the differential equation. An example is given to illustrate this method.

2. Basic Concept of Variational Iteration Method

In order to present the VIM, we consider the following general differential equation:

$$Lu(x) + Nu(x) = g(x) \tag{1}$$

where L denotes a linear operator, N is a non-linear operator, $u(x)$ is a sought function and $g(x)$ is a given continuous function. We can construct a correct functional of the form [6, 7]:

$$u_{n+1}(x) = u_n(x) + \int_0^x \lambda(Lu_n(t) + N\tilde{u}_n(t) - g(t))\,dt \tag{2}$$

where λ denotes a general Lagrange multiplier, which can be identified optimally by the variational theory, the subscripts n denotes the n-th approximation, $\tilde{u}_n$ is a restricted variation, i.e., $\delta\tilde{u}_n = 0$.

The successive approximations $u(x)$, $n \geq 0$ of the solution $u(x)$ will be readily obtained upon using the obtained Lagrange multiplier and by using any selective function $u_0(x)$, which is an initial approximation with possible unknowns. In [8] authors wrote, that the main feature of this method is that the initial solution can be chosen with some unknown parameters in the form of the searched solution. Consequently, the solution may be obtained by using:

$$u(x) = \lim_{n\to\infty} u_n(x) \tag{3}$$

By applying the imposed boundary conditions, we obtain values of unknown parameters, which are included in a function $u_0(x)$, subsequently in $u_n(x)$ and consequently a solution in terms of convergent series.

3. Variational Iteration Technique – BVP with additional boundary condition

We consider the non-standard BVP, which consists of fourth–order differential equation:

$$u^{(\mathrm{IV})}(x) + f(x,u,u',u'',u''',p_1) = 0 \tag{4}$$

and five boundary conditions:

$$u(a) = u_a, \quad u'(a) = u_{1a}, \quad u''(a) = u_{2a}, \quad u(b) = u_b, \quad u'(b) = u_{1b} \tag{5}$$

A solution to equation (4) can fulfill five boundary conditions only when this equation contains one unknown parameter p_1. By means of the following transformation:

$$u_1 = u, \quad u_2 = u', \quad u_3 = u'', \quad u_4 = u''' \tag{6}$$

we can convert the BVP (4) and (5) to an initial value problem (IVP), which consists of a system of four first-order differential equations:

$$\frac{du_1}{dx} = u_2(x), \quad \frac{du_2}{dx} = u_3(x), \quad \frac{du_3}{dx} = u_4(x), \quad \frac{du_4}{dx} = f(x,u_1,u_2,u_3,p_1) \tag{7}$$

and initial conditions, that include a subsequent unknown parameter p_2:

$$u_1(0) = u_a, \quad u_2(0) = u_{1a}, \quad u_3(0) = u_{2a}, \quad u_4(0) = p_2 \tag{8}$$

According to the correct functional (2), we can rewrite system (7) as a system of four integral equations:

$$\begin{cases} u_1^{(k+1)}(x) = u_1^{(k)}(x) + \lambda \int_0^x u_2^{(k)}(t)dt \\ u_2^{(k+1)}(x) = u_2^{(k)}(x) + \lambda \int_0^x u_3^{(k)}(t)dt \\ u_4^{(k+1)}(x) = u_4^{(k)}(x) + \lambda \int_0^x f(t,u_1^{(k)}(t),u_2^{(k)}(t),u_3^{(k)}(t),p_1)dt \end{cases} \tag{9}$$

If we start with the initial approximations:

$$u_1^{(0)}(x) = u_a, \quad u_2^{(0)}(x) = u_{1a}, \quad u_3^{(0)}(x) = u_{2a}, \quad u_4^{(0)}(x) = p_2 \tag{10}$$

we obtain a subsequent approximations of $u_i(x)$, $i = 1\ldots4$ and finally the solution:

$$u(x) = \lim_{n\to\infty} u^{(n)}(x) \tag{11}$$

By applying the boundary conditions (5) at the right side of the domain, we obtain values of the unknown parameters p_1, p_2 and consequently, a solution in terms of convergent series.

4. Numerical Example

To apply VIT to BVP with additional boundary condition, an example will be presented that consists of the fourth–order differential equation which contains unknown p_1:

$$u^{(\mathrm{IV})}(x) = u^2(x) - x^{10} + 4x^9 - 4x^8 - 4x^7 + 8x^6 - 4x^4 + p_1 x - 48 \tag{12}$$

and five boundary conditions:

$$u(0) = 1, \quad u'(0) = 0, \quad u''(0) = 4, \quad u(1) = 1, \quad u'(1) = 1 \tag{13}$$

We know ([10]) that for $p_1 = 120$, equation (12) has the following exact solution:

$$u(x) = x^5 - 2x^4 + 2x^2 \tag{14}$$

which fulfills all boundary conditions (13). Taking into consideration (6), we rewrite the above BVP as a system of four first-order differential equations:

$$\begin{cases} \dfrac{du_1}{dx} = u_2(x), \\ \dfrac{du_2}{dx} = u_3(x), \\ \dfrac{du_3}{dx} = u_4(x), \\ \dfrac{du_4}{dx} = u_1^2(x) - x^{10} + 4x^9 - 4x^8 - 4x^7 + 8x^6 - 4x^4 + p_1 x - 48 \end{cases} \tag{15}$$

with initial conditions, which include a second unknown parameter p_2:

$$u_1(0) = 0, \quad u_2(0) = 0, \quad u_3(0) = 4, \quad u_4(0) = p_2 \tag{16}$$

By means of (2) we can rewrite the system of differential equations (15) as a system of four integral equations with $\lambda_i = 1$, $i = 1 \ldots 4$. The initial approximations are based on the initial conditions (16).

$$\begin{cases} u_1^{(k+1)}(x) = 0 + \displaystyle\int_0^x u_2^{(k)}(t)\,dt, \\ u_2^{(k+1)}(x) = 0 + \displaystyle\int_0^x u_3^{(k)}(t)\,dt, \\ u_3^{(k+1)}(x) = 4 + \displaystyle\int_0^x u_4^{(k)}(t)\,dt, \\ u_4^{(k+1)}(x) = p_2 + \displaystyle\int_0^x ((u_1^{(k)}(t))^2 - t^{10} + 4t^9 - 4t^8 - 4t^7 + 8t^6 - 4t^4 + p_1 t - 48)\,dt \end{cases} \tag{17}$$

The *Maple*™ program with accuracy *Digits* = 20 was used to solve this non-standard problem. Calculations have been completed after 12 approximations. Using the boundary conditions at $x = 1$, we obtain:

$$p_1 = 120.0000000048, \quad p_2 = 2.08 \cdot 10^{-10} \tag{18}$$

and the series solution is given by:

$$u(x) = 2x^2 - 3.46 \cdot 10^{-11} x^3 - 2x^4 + x^5 + \ldots - 5.61 \cdot 10^{-36} x^{67} \tag{19}$$

Table 1 exhibits the exact solutions (14), the errors obtained by using the modified VIT and iterative shooting method (ISM) used to the BVP with additional boundary conditions, which was described in [11].

Table 1

Error estimates

x	$u_{\text{exact}}(x)$	Errors* (VIT)	Errors* (ISM)
0.0	0.00000	0.0000	0.0000
0.1	0.01981	$3.4279\ 10^{-14}$	$9.8256\ 10^{-15}$
0.2	0.07712	$2.6465\ 10^{-13}$	$8.0465\ 10^{-14}$
0.3	0.16623	$8.3881\ 10^{-13}$	$8.4766\ 10^{-14}$
0.4	0.27904	$1.7599\ 10^{-12}$	$3.4477\ 10^{-14}$
0.5	0.40625	$1.4173\ 10^{-12}$	$1.0776\ 10^{-13}$
0.6	0.53856	$2.3855\ 10^{-11}$	$1.0341\ 10^{-13}$
0.7	0.66787	$2.9626\ 10^{-10}$	$4.0618\ 10^{-14}$
0.8	0.78848	$2.2899\ 10^{-9}$	$3.4080\ 10^{-14}$
0.9	0.89829	$1.3479\ 10^{-8}$	$5.9746\ 10^{-14}$
1.0	1.00000	$6.4569\ 10^{-8}$	$1.6930\ 10^{-13}$

* Error = abs (exact solution – series solution (VIT) or discreet solution (ISM))

5. Summary

There are many methods of solving the BVP, but most of them concern the standard BVP, where the order of equation and number of boundary conditions are the same. Taking into consideration methods for the non-standard BVP, the ISM [11], and the VIT described in this article, we can conclude that the differential equation must contain unknown components. Their number must correspond to the number of excessive boundary conditions. The values of these parameters can be calculated by applying additional boundary conditions. Due to the modification of the VIT, there is no need to do huge and time consuming computational work that is available in the ISM. Taking the VIT into consideration, we obtain a solution in the terms of convergent series with easy computable components. Higher

accuracy can be obtained by increasing the expansion order in series solution by means of a larger number of iterations.

References

[1] Davies A.R., Karageoghis A., Philips T. N., *Spectral Galerkin methods for the primary two-point boundary value problems in modeling viscoelastic flows*, Int. J. Numer. Methods. Eng., vol. **26**, 1988, 647-662.

[2] Wazwaz A.M., *The numerical solution of fifth-order boundary value problems by Adomian decomposition*, J. Comput. Appl. Math., vol. **136**, 2001, 259-270.

[3] Rao S.S., *Applied Numerical Methods for Engineers and Scientists*, Prentice Hall, Upper Saddle River 2002.

[4] Caglar H.N., Caglar S.H., Twizell E.E., *The numerical solution of fifth-order boundary value problems with sixth degree B-spline functions*, Appl. Math. Lett., vol. **12**, 1999, 25-30.

[5] Noor A.M., Mohyud-Din S.T., *An efficient algorithm for solving fifth-order boundary value problems*, Math. and Comp. Modelling, vol. **45**, 2007, 954-964.

[6] He J.H., *Variational iteration method – a kind of nonlinear analytical technique: some examples*, Int. J. Nonlinear Mech., vol. **34**, 1999, 699-708.

[7] Inokuti M., Sekine H., Mura T., *General use of the Lagrange multiplier in nonlinear mathematical physics*, Variational Method in the Mech. of Solids, Pergamon Press, New York 1978, 156-162.

[8] He J.H., Wu X.H., *Variational iteration method: New development and applications*, Computers and Mathematics with Applications, vol. **54**, 2007, 881-894.

[9] Zhang J., *The numerical solution of fifth-order boundary value problems by the variational iteration method*, Computers and Mathematics with Applications, vol. 58, 2009, 2347-2350.

[10] Noor A.M., Mohyud-Din S.T., *Variational iteration technique for solving higher-order boundary value problems*, App. Math. and Comp., vol. **189**, 2007, 1929-1942.

[11] Filipowska R., *An iterative shooting method for the solution of higher order boundary value problems with additional boundary conditions*, Solid State Phenom., vol. **235**, 2015, 31-36.

TECHNICAL TRANSACTIONS | CZASOPISMO TECHNICZNE
MECHANICS | MECHANIKA
4-M/2016

AGNIESZKA SZCZOTOK*

METALLOGRAPHIC STUDY OF POROSITY IN IN713C SUPERALLOY IN AS-CAST AND AFTER CREEP TEST

BADANIA METALOGRAFICZNE POROWATOŚCI W NADSTOPIE IN713C W STANIE LANYM I PO PRÓBIE PEŁZANIA

Abstract

The paper summarizes the results of observation and quantitative analysis of porosity in IN713C superalloy in as-cast and after the creep test. The sources of porosity in castings are shortly described and the methodology of pores measurement is circumscribed. The results of pores in as-cast and after the creep test were shown and, finally, the interpretation of the result was presented.

Keywords: *metallography*, *porosity*, *microstructure*, *map of pores distribution*, *image analysis*, *microstructure*

Streszczenie

W artykule przedstawiono wyniki obserwacji i badań ilościowych porowatości występującej w nadstopie IN713C w stanie lanym i po próbie pełzania. Scharakteryzowano pokrótce źródła powstawania porowatości w odlewach. Metodyka pomiaru porów opisano i przedstawiono uzyskane wyniki pomiarów wraz z ich interpretacją.

Słowa kluczowe: *metalografia*, *porowatość*, *mikrostruktura*, *mapa rozkładu porów*, *analiza statystyczna wyników*

DOI: 10.4467/2353737XCT.16.227.5976

* Ph.D. Eng. Agnieszka Szczotok, Institute of Materials Science, Faculty of Materials Science and Metallurgy, Silesian University of Technology.

1. Introduction

Porosity may be the most persistent and common complaint of casting users. Porosity in castings contributes directly to customer concerns about their reliability and quality. Controlling porosity depends on the understanding of its sources and causes [1]. The most well-known methods for the control of porosity are by means of X-Rays [2].

Formation of pores can have many sources. One of the pore sources is an air bubble trapped in a casting during the pouring process, which is unable to escape before solidification. Closely related to air bubbles trapped during filling are gas bubbles that are blown into the liquid from a core or mold. Much of the porosity in castings is not a result of excess gas pressure forming blowholes or gas solubility forming pinholes, but a result of oxides. In fact, most of the surface or subsurface porosity is likely due to oxide formation. Solidification shrinkage occurs as the liquid metal becomes a more dense solid. When feeding is cut off and metal continues to solidify, the pressure in the remaining metal pool decreases while segregation causes the gas content to increase [1].

Gas and shrinkage porosity is a cause of mechanical properties lowering turbine blades and vanes applied to a jet engine. These properties include: creep strength, durability, impact strength resistance, elongation and tensile strength [3, 4].

2. Methodology

Carrot-shape IN713C superalloy castings were produced in an investment casting cluster mould and creep test samples (Fig. 1) were then prepared from the castings.

Creep test cylindrical samples with a diameter and length of 6 and 100 mm, respectively, were prepared. The creep tests were conducted according to the requirements of the recipient.

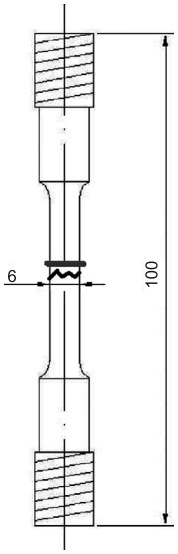

Fig. 1. Creep test sample scheme with a marked sampling way with red line

The tests were performed by means of a Zwick/Roell Kappa 50DS creep-testing machine, which placed each tensile specimen under a constant load of 151.7 MPa maintained at a constant temperature of 982°C up to fracture.

The resultant macro- and microstructures were observed and characterized after the creep tests by means of a light microscope (LM) and *Hitachi S-4200* scanning electron microscope (SEM) equipped with EDS.

The creep specimens were sectioned longitudinally along the gauge length and prepared for the microstructural examination. Firstly, the porosity was examined on the ground, polished, and the unetched metallographic samples by means of LM. Then, the specimens were lightly etched in a solution containing 3g MoO_3, 100 ml HNO_3, 100 ml HCl and 100 ml H_2O and observed by means of the SEM technique.

3. Microscopic observation

The metallographic observations have shown that the investigated Ni-based superalloy in as-cast state, as well as after the creep test, contain gas and shrinkage porosity (Fig. 2). The increased porosity observed in the specimens after the creep tests relative to that of the as-cast material indicates that porosity can result from cracking propagation along the pores.

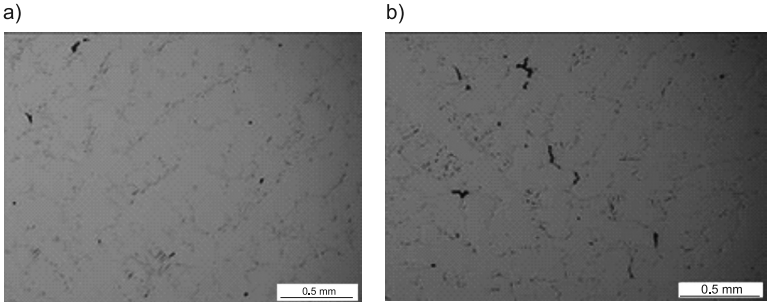

Fig. 2. Microstructure of IN713C Ni-based superalloy with pores visible on the unetched sample: a) as-cast state, b) after the creep test. LM, BF

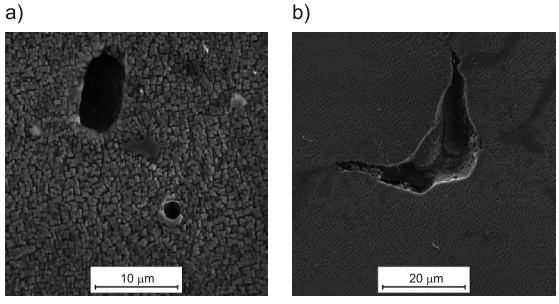

Fig. 3. Microstructure of IN713C with porosity on the etched samples: a) as-cast state, b) after the creep test. SEM, SE

Interdendritic areas are the places of privileged formation of shrinkage porosity. Gas porosity seems to be evenly distributed. It should be noted that propagation of microcracks from the initial casting pores is considered to be the critical life-limiting factor.

On the etched surface of sample using higher magnification (SEM) you can observe the morphology of pores and cracking propagation in consequence of pores presence in the case of the creep test sample (Fig. 3).

4. Measurement of porosity

A series of 15 images were taken by means of LM equipped with a digital camera to evaluate the area fraction of the pores and other parameters describing the pores. The most important part of the image analysis of the pores was performed by means of the Met-Ilo image analysis program to automate pore detection and their measurement. The measurements were carried out on the binary images of the pores (Fig. 4b). An example of pores detection is presented in Fig. 4.

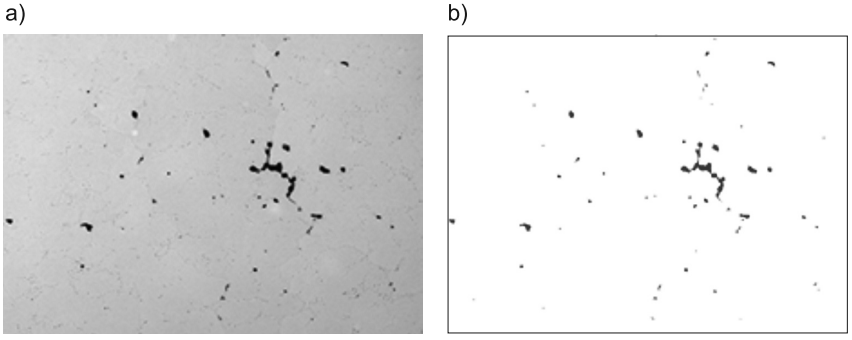

Fig. 4. Detection of pores on unetched sample in the Ni-based superalloy: a) grey initial image, LM, BF; b) and binarization of pores

The evaluation of the mean plane section area of pores and other parameters which describe their morphology was performed. In Table 1 the selected parameters are presented.

Table 1

Results of pores measurement in as-cast state and after creep test

Parameter	**After creep**	**As-cast**
Area fraction of pores A_A [%]	0.62	0.14
Mean plane section area of pores $\bar{A}$ [μm^2]	26.08	32.43
Coefficient of variation of plane section area v (A) [%]	242.6	128.9
Mean value of nondimentional shape factor	0.83	0.87
Coefficient of variation of nondimentional shape factor [%]	34.18	33.36

Fine pores predominate in both cases (Fig. 5). You can see that only small fraction of pores makes up pores with greater plane section area. The mean value of nondimentional shape factor could indicate that pores have a shape close to a circle (for a circle value equals 1), but it should be remembered that it is a mean value – in both cases there are gas as well as shrinkage pores.

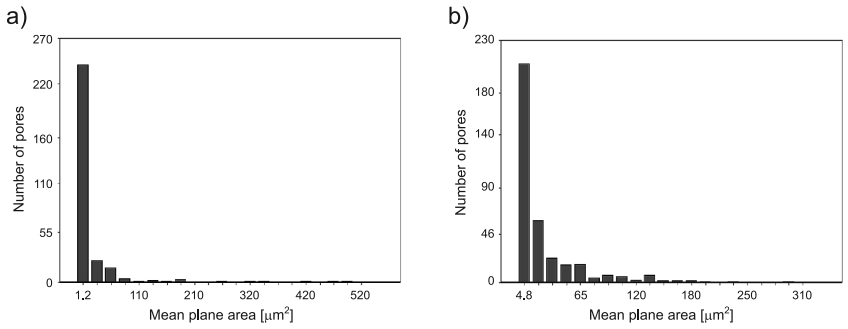

Fig. 5. Histograms of plane section area with the number of pores: a) after the creep test, b) as-cast

The comparison of two graphs in Fig. 5a, b and 5c, d indicates that after the creep test pores with greater plane section area are present. The maximum value after the creep test amounts to 525 μm^2, and for the as-cast maximum value is only 305 μm^2.

5. Summary

On the basis of the obtained results, the following observations were made:

- gas and shrinkage porosity are present in as-cast and after the creep test in IN713C superalloy;
- the area fraction of pores is higher in the case of material after the creep test (0.62 %) in comparison with as-cast state (0.14%);
- the mean plane section area of pores is smaller after the creep test than in the as-cast, but after the creep test greater pores have been noted (with higher plane section area – Fig. 5), and, moreover, the coefficient of variation of plane section area is higher after the creep test than the as-cast;
- the mean value of the nondimentional shape factor of the pores in both cases range from 0.83 to 0.87, simultaneously both gas and shrinkage pores are present in the as-cast and after the creep test.

Propagation of microcracks from the initial casting pores is observed in the material after the creep test and it can explain higher evaluation of area fraction of pores after the creep test than in the as-cast state. It is very hard to distinguish the difference between pores on 2D microstructure image and propagation of cracking from the initial pores, which is why the evaluation of pores after the creep test can be overestimated.

Acknowledgements: *Financial support from the Structural Funds in the Operational Programme – Innovative Economy (IE OP) financed from the European Regional Development Fund – Project No. POIG.0101.02-00-015/08 is gratefully acknowledged.*

References

[1] Monroe R., *Porosity in Castings*, American Foundry Society, Schaumburg, IL USA, 2005.
[2] Peti F., Grama L., *Analyze of the possible causes of porosity type deffects in aluminium high pressure diecast parts*, Scientific Bulletin of the "Petru Maior", University of Târgu Mureş, vol. **8** (1), 2011, 41-44.
[3] Rozkosz S., *Kompleksowa ocena porowatości odlewów precyzyjnych z żarowytrzymałych nadstopów niklu*, Wyd. Politechniki Śląskiej, Gliwice 2011 [in Polish].
[4] Yavorska M., Sieniawski J., Filip R., Krupa K., *Charakterystyka warstw aluminidkowych wytworzonych metodami CVD na nadstopach niklu Inconel 625 oraz Inconel 713 LC*, Inżynieria Materiałowa, vol. **4**, 2010, 1287-1290 [in Polish].

TECHNICAL TRANSACTIONS | **CZASOPISMO TECHNICZNE**
MECHANICS | MECHANIKA
4-M/2016

ŁUKASZ PASIECZYŃSKI*, NORBERT RADEK**

DEVELOPMENT OF POLYURETHANE PAINT WITH SPECIAL METALLIC EFFECT

OPRACOWANIE FARBY POLIURETANOWEJ O SPECJALNYM EFEKCIE METALICZNYM

Abstract

The article analyzed the problem of cloud defect in metallic paint, caused by grain arrangement during paint application on a structural element. Presents test results of coating system consist of a high solid corrosion protection primer and a two-component topcoat with a metallic gloss effect (RAL 9006) developed in our company. The paint system properties were examined after the conditioning period.

Keywords: *cloud defect*, *polyurethane metallic paint*, *metallic topcoat*, *polyurethane special effect*

Streszczenie

W artykule przedstawiono problem tworzenia się defektu chmurki w lakierach metalicznych spowodowanych nieodpowiednią dystrybucją pigmentu. W artykule przedstawiono wyniki systemu zawierającego podkład antykorozyjny oraz lakier nawierzchniowy z efektem metalicznym (RAL 9006) opracowany w firmie BARWA. Właściwości systemu malarskiego zostały określone po okresie kondycjonowania.

Słowa kluczowe: *defekt „chmurki”*, *lakier metaliczny*, *specjalny efekt farby poliuretanowej*

DOI: 10.4467/2353737XCT.16.228.5977

* M.Sc. Eng. Łukasz Pasieczyński, Firma Handlowa BARWA Jarosław Czajkowski.
** D.Sc. Ph.D. Eng. Norbert Radek, Assoc. Prof., Centre for Laser Technologies of Metals, Faculty of Mechatronics and Machine Design, Kielce University of Technology.

1. Introduction

In order to enhance the competitiveness of vehicle appearance and to attract customers, painting systems are used with special effects. One of them is the use of metallic pigments in paint topcoats. Such pigments glamorize appearance of coatings, as well as create a protective barrier against harmful elements of the environment. Metallic effect is obtained by dispersing metallic aluminum (aluminum flakes, aluminum grain) in a coating film. The process is difficult, because the final result of the achieved metallic coating is strongly dependent on many factors, such as pigment distribution and shape, surface smoothness, pigment orientation in relation to the surface of substrate or previous layer, pigment wet ability and grain size [1, 2].

Due to the shape, aluminum pigments are divided into two basic groups: irregular flakes (cornflakes) and lenticular flakes (silverdollar). The use of various shapes of metallic pigments causes differences in gloss of coatings as well as their visual appearance (surface smoothness, the absence of protruding pigment). Irregular flakes will scatter the light more than lenticular flakes (silverdollars) which have a more rounded shape. Lenticular flakes are commonly used in industrial and automotive paints.The size of particles dispersed in the system is yet another considerable factor. The larger particles are dispersed the greater metallic effect is obtained (brilliance, sparkle effect). Smaller particles give more homogenous effect with darker coating because of the better light scattering at the edges of the particles [3].

Distribution of aluminum pigments in a coating film on the surface or in the entire volume of a resin is as important as their shape. Every type of grain distribution has both its advantages and disadvantages. The way the grain is distributed in a resin depends on the technology of preparation. Leafing pigments of high surface tension do not get wet by a resin and float onto the surface of a wet film. This effect is obtained by the use of stearic acid in the pigment production. However, in high polar systems, pigment may get wet by a resin and "drown" inside the coating, turning into a non-leafing pigment. Addition of oleic acid or dispersing agents in the production process causes such an effect. Metallic effect is obtained by light reflection on the smooth surface of aluminum flakes [1].

Reflected light may, however, refract or scatter on the flakes' edges or micro-roughness of the pigment surface. In that case, metallic effect is the sum of light reflection and scattering. The higher the ratio of reflected light the greater and more intense effect is to be observed. Metallic effect depends on the grain distribution and therefore on the angle of reflection. Pigment orientation of pigment in a coating film is an important factor in the visual effect. The more parallel aluminum pigment flakes are arranged to the surface the greater light reflection is noticed. Poor orientation results in a cloudy appearance. The type of grain and the process of its introduction into a metallic paint have an influence on grain distribution in a resin and defects of coating appearance which may occur after application. Poor grain selection, its size and shape as well as improper mixing lead to the atrophy of metallic effect, the coating darkening or "cloud" effect which is caused by improper pigment particles distribution. A cloud is formed by agglomeration of aluminum pigment particles in a resin and is observed by darker and brighter spots or stripes on the coating.

To avoid such defect on coating, it is recommended to apply more paint layers and cross painting because each following paint layer reduces the cloud effect. However, it increases production costs.

2. Experimental

The designed paint system includes epoxy primer with a high solid content and a two--component polyurethane paint with a high metallic gloss effect. Epoxy provides very good adhesion to steel due to the multitude of functional groups in the polymer molecule and corrosion resistance. The topcoat paint RAL 9006 is designed by F.H. Barwa laboratory. The coating was applied with SATA spray guns with 1.3-1.4 nozzle on steel. Before the application, the surface of steel was polished with a 240-grit sandpaper. Next, the epoxy primer was applied and heated at 60° Celsius for 60 min. The two layers of topcoat paint were applied wet-on-wet with a good hiding power. There was a 10-minute break between painting of the two layers in order to let the thinners evaporate from the coating. The prepared samples were conditioned at 23 degrees Celsius and 50% humidity for minimum 7 days in order to perform tests on dry coating.

3. Results and discussion

The paint is easy applicable. It can be applied as simply as an ordinary polyurethane topcoat without the necessity of cross painting or spraying to minimize the cloud defect. Additionally, RAL 9006 topcoat has much thicker grain and its metallic effect is similar to the base coat system. This paint system also enables repair of a paint surface damaged by external factors (e.g. brushing, scratching) with low production cost and within a short period of time. As a proof, a part of the sample was polished with a P400-grit sandpaper and polyurethane coating was re-applied in the abrasion place. No defects were observed in the coating.

Metallic effect depends on many factors and each factor has a direct effect on the final coating. For this reason, metallic effect measurement requires several techniques: tint and color saturation, gloss, brightness and hiding power or DOI (distinctiveness of image). It causes improvement in gloss, brightness and color saturation. A flop is another measured parameter. It is a change in brightness depending on the observation angle. It is especially noticeable on a car mask and car bumper.

The DOI parameter is responsible for the clarity of reflecting objects that surround the coating (trees, buildings, other cars). Market dictates high demands on paint coatings with metallic effect. They should be high gloss, bright with visible metallic effect and have high DOI and flop coefficient at the same time. After the formulation, the properties of the product were examined. Table 1 shows the results of the following tests performed on the liquid paint: density, solid content, flow time, drying time. Values given in Table 1 were obtained on a ready to use product (with added hardener and thinner).

Cured coating was also tested for mechanical properties, corrosion and humidity resistance. After the conditioning period had finished, the thickness of dry coating was tested by the magnetic induction method and adhesion tests were performed by the cross cut method and pull-off test. The hardness of cured coating was measured by Koenig pendulum. The corrosion resistance test was performed in the salt spray chamber according to PN--EN ISO 9227 at 35°C using 5% saline solution. The tests in the humidity chamber were conducted according to PN-EN ISO 6270-2 with following parameters of the chamber inside: humidity 100% and temperature 40°C. The summary tests results are presented in Table 2.

Table 1

Properties of liquid product ready to use

Test	**Standard**	**Result**
Density [g/cm^3]	PN-EN ISO 2811-1	0,95
Solid content by mass [%]	PN-EN ISO 3251	57
Solid content by volume [%] (calculation method)	Technical procedure	54
Flow time cup Ford4 [s]	PN-EN ISO 2431	26
Drying time at 60°C [h]	–	2
Color RAL	–	9006

Table 2

Selected properties of dry coating applied on steel

Test	**Standard**	**Result**	
Thickness [µm]	PN-EN ISO 2808	121,9	
Cross cut	PN-EN ISO 2409	No change	
Adhesion [MPa]	PN-EN ISO 4624	4,96	
Hardness, Koenig pendulum [s]	PN-EN ISO 1522	105	
Corrosion resistance test [1000 h]	PN-EN ISO 9227	No change	
Humidity resistance test [1000 h]	PN-EN ISO 6270-2	No change	
Gloss [gloss unit]	PN-EN ISO 2813	20°	67,2
		60°	94,2
		85°	90,9

The next test of resistance to aggressive environmental conditions (corrosion and moisture) were finished and assessed after 1000 hours of exposure. The result revealed no changes in the tested coatings (no blistering, cracking, corrosion or thread-like corrosion). 1000 hours is a minimum time for a coating to be resistant to environmental effects. However, this time could be extended when aluminum is used as a substrate instead of steel.

The paint could be applied by the wet on wet method or on the surface of a dry sanded primer. Two layers should be applied to obtain entire paint coverage. Our product does not cause a cloud effect but creates an uniform varnish layer on the element. During the

evaporation of solvents we can observe the grain which spreads across the entire surface within the next two or three minutes. In the next test, the two samples were prepared with and without a cloud defect. Each sample had a grid with a similar surface area. The surface of the samples was examined by a spectrophotometer (with six different angles –15°, 15°, 25°, 45°, 75°, 110°) to determine the change of the color by measuring $L^*a^*b^*$ parameter. The results are shown in Figs. 1 and 2.

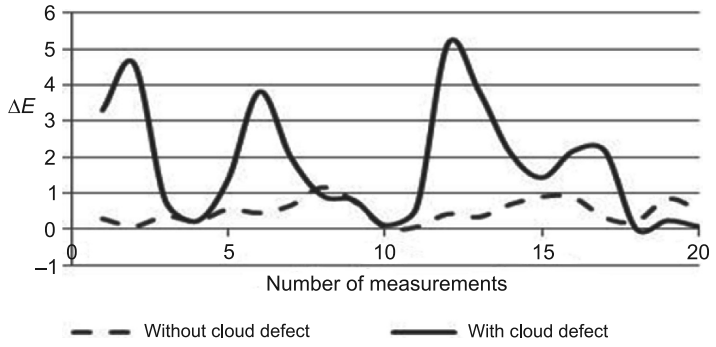

Fig. 1. Color difference for angle 25°

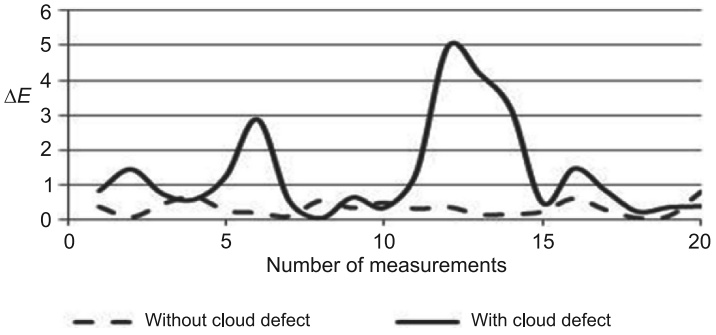

Fig. 2. Color difference for angle 45°

Figures 1 and 2 present a comparison of color difference (ΔE) for samples with and without a cloud defect in the two of six selected angles (25° and 45°). The sample with a cloud defect has a significantly higher value of the ΔE parameter than the sample without such a defect.

ΔE (1) parameter equals:

$$\Delta E^*_{ab} = \sqrt{(\Delta L^*)^2 + (\Delta a^*)^2 + (\Delta b^*)^2} \tag{1}$$

The values of Δa and Δb parameters do not exceed 0.5 for the sample with a cloud defect, although the change in color is well observed. In this case, the ΔL parameter (brightness parameter) explains the effect. The ΔL parameter gives some information about brightness in a given point and its fluctuations are caused by a cloud defect that is irregular

distribution of grains in the resin. The study on spectrophotometer for 8° angle deviation from the perpendicular axis to the tested surface was finished with the ΔE parameter not exceeding 1.0 for the sample without the cloud defect. A scratch test was conducted to test the adhesion of the coatings. Adhesion tests were conducted by means of the REVETEST instrument (CSEM, Switzerland). The measurements were performed at the load increase rate of 49 N/min, table feed rate of 10 mm/min and scratch length of 10 mm. A special

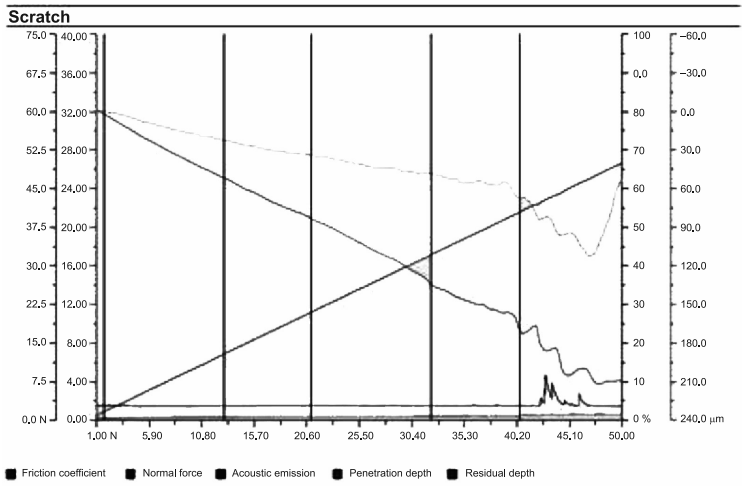

Fig. 3. Result of scratch tests of metallic coating adhesion

Rockwell diamond cone indenter with a corner radius of 50 µm, was used to scratch the samples at a gradually increasing normal load. The information about cracking or peeling of the layers was obtained based on the measurements of material resistance (tangential force) and the registration of acoustic emission signals. The lowest normal force causing a loss of adhesion of the coating to the substrate is called a critical force and is assumed to be the measure of adhesion. The value of critical force was 42 N, the result of the scratch test is shown in Fig. 3.

4. Summary

Low production costs due to an easy application, the same as for ordinary polyurethane varnish. Cross painting or application of a thin finishing layer is not required. Metallic effect is obtained without losing high gloss. It is comparable to double layer systems.

No cloud defect and the entire coverage of primer is achieved when the paint is applied in two layers.

Good resistance of a finished product to aggressive environmental factors and good adhesion to steel.

Possibility to repair local damaged areas (scratches) without losing the surface appearance and metallic effect.

References

[1] Hryniewicz T., *Surface technology and coatings*, Wyd. Politechniki Koszalińskiej, Koszalin 2004 [in Polish].
[2] *Coatings painting and varnishing*, ed. Orzelowski S., Guide edition, No. III, WNT, Warszawa 1983 [in Polish].
[3] Carl Schlenk AG Metal Foils, http://www.schlenk.com [date of acc. 2016-08-17].
[4] Metallic Pigments, http://www.eckart.net [date of acc. 2016-08-17].
[5] Radek N., *Welding technologies in surface engineering*, Wyd. Politechniki Świętokrzyskiej, Kielce 2013.

TECHNICAL TRANSACTIONS | CZASOPISMO TECHNICZNE
MECHANICS | MECHANIKA
4-M/2016

MANUELA INGALDI*

MANAGEMENT OF PACKAGING WASTE

GOSPODAROWANIE ODPADAMI OPAKOWANIOWYMI

A b s t r a c t

Most of the products available on the market are sold together with different types of packaging. Information about the product, manufacturers etc., is placed on these packages but their main function is to protect the product during transport. After the product is removed, the packaging becomes waste which, according to Polish law, should be managed in an appropriate way. Recycling and recovery of the material are the most important issues. Basic statistics on recycling of packaging waste showed that paper, cardboard and aluminum packaging are recycled to the greatest extent in Poland. In the article, definitions of packaging and packaging waste according to Polish law are presented, together with legal acts on waste management. The main statistics connected with the management of packaging waste are also presented.

Keywords: waste, *packaging waste*, *waste management*

S t r e s z c z e n i e

Większość wyrobów dostępnych na rynku sprzedawana jest łącznie z opakowaniami. Na opakowaniach tych umieszczane są informacje o produkcie, producencie itd., ale główną ich funkcją jest ochrona wyrobu w trakcie transportu. Po wyjęciu produktu opakowania staja się odpadem opakowaniowych, z którym – według polskiego prawa – powinno się postępować w odpowiedni sposób. Najważniejszy jest odzysk materiałów. Podstawowe statystyki dotyczące recyklingu odpadów opakowaniowych pokazują, że opakowania papierowe, kartony oraz opakowania aluminiowe są odzyskiwane w największym stopniu w Polsce. W artykule przedstawiono definicje opakowań oraz odpadów opakowaniowych według polskiego prawa oraz podstawowe akty prawne związane z gospodarowaniem odpadami opakowaniowymi. Pokazano również podstawowe statystyki związane z gospodarowaniem odpadami opakowaniowymi.

Słowa kluczowe: odpady, *odpady opakowaniowe*, *gospodarowanie odpadami*

DOI: 10.4467/2353737XCT.16.229.5978

* Ph.D. Eng. Manuela Ingaldi, Institute of Production Engineering, Faculty of Management, Czestochowa University of Technology.

1. Introduction

During everyday purchases customers acquire both products and packaging in which these products are supplied. Information about the producer, composition of the product or expiration date is placed on the packaging which is designed to protect products from damage and facilitate their transport.

Unfortunately, after unpacking the product, the packaging becomes unnecessary and useless. It can be used by the customer for a chosen purpose, but in most cases it becomes waste.

In Poland and European Union there are many acts which regulate the management of packaging and packaging waste. The main problem of waste packaging management is recycling of such type of waste. Limited access to raw materials and a large amount of such type of waste create the need for waste recycling. At the beginning, a suitable segregation of packaging waste is required. People's attitudes to separate packaging waste is also slowly changing. Variety of advertising campaigns, frequent publications, packaging collection actions lead people to change their behavior for the better [1, 2].

The purpose of this article is to define packaging and packaging waste according to Polish law and to present the main acts which describe the management of packaging waste. The main statistics connected with the management of packaging waste are also presented.

2. Definition of packaging and packaging waste

Packaging and packaging waste are defined in the available literature, but the most important definitions were included in the legislation. At the beginning, packaging should be defined. According to the Act on packaging and packaging waste, packagings are "products placed on the market, made of any materials, intended for the storage, protection, transport, delivery or presentation of any product, from raw materials to already processed goods" [3]. Packaging in the understanding of this Act includes [3]:

- packaging units, for transmitting the product to the user in the place of purchase, including also consumption product, such as disposable dishes;
- multipacks containing multiple unit packages of products, regardless of whether they are transmitted to users or to selling points, which can be removed from the product without compromising its features;
- transport packagings, used to transport products in packaging units or multipacks in order to prevent damage, with the exception of containers for transport by road, rail, water or air.

The aim of product packaging is to encourage potential customer to buy the product. It contains information about the name of the product, its composition, producer and expiration date. It protects the product from damage and helps the customer to transport this product home. Due to the need to protect the environment, and thus the need to use recycled materials, also product packaging should be recycled and reused [4].

Packaging, like other products, must meet many requirements. Only then can they be treated as fully valuable products and used for its planned purpose. The packaging

quality was defined in the standard ISO 8402, where quality packaging is defined as a "set of characteristics, parameters characterizing the packaging associated with its ability to meet the needs of buyers and users" [5].

Materials like glass, paper and board, plastics, wood and metals such as aluminium and steel are mainly used for packaging. Some types of packaging can be used repeatedly, such as glass bottles and wooden pallets. However, it should be remembered that, according to the Act on packaging and packaging waste, the packaging or product shall be presumed placed on the market only once [3]. Additionally, no matter what material was used for the production of packaging, over time it becomes packaging waste.

The definition of packaging waste was included in the Act on packaging management and packaging waste, where it can be understood as "all packaging including reusable packaging withdrawn from the re-use, constitute waste within the meaning of the waste legislation, with the exception of waste generated in the production of packaging" [3].

The same Act defines the activities that help in the management of such waste. According to the Act, the manufacturer should remember about a few rules to reduce the impact of packaging on the environment [3]:

- the volume and weight of packaging should be limited to the minimum required to fulfill the functions of the packaging;
- packaging should be designed and executed in a way that allows their re-use and recycling later, and if this is not possible, at least recycling, and if this is not possible, another form of recovery;
- packaging should contain the smallest possible amount of the substance posing threat to the life or health of humans and the environment.

The Act amending the Act on maintaining cleanliness and order in municipalities introduces, together with other acts, the need to segregate the municipal waste, including packaging of products purchased by residents of the municipality [7]. Thanks to this Act, more and more people are separating waste, including packaging waste. It should also be emphasized that the overall waste management is based on the Act of 14 December 2012 on waste and Act of 27 April 2001 in the Environmental Protection Law [8, 9].

In addition to the already mentioned laws in Poland and European Union, other provisions on packaging waste are applied. Current legislation stipulates the following [10]:

- Summary of EU Waste Legislation on Packaging and Packaging Waste (short information on objectives, scope and main elements of the Packaging and Packaging Waste Directive, as well as related acts);
- Directive 94/62/EC on Packaging and Packaging Waste (consolidated version).

Also, some amending acts should be followed. These are [10]:

- Directive 2004/12/EC amending Directive 94/62/EC on packaging and packaging waste;
- Directive 2005/20/EC amending Directive 94/62/EC on packaging and packaging waste (extension of deadlines for the attainment of the recycling and recovery targets for the Member States acceding the EU in 2004);
- Regulation (EC) No 219/2009 adapting a number of instruments subject to the procedure referred to in Article 251 of the Treaty to Council Decision 1999/468/EC with regard to the regulatory procedure with scrutiny;

– Commission Directive 2013/2/EU amending Annex I to Directive 94/61/EC on packaging and packaging waste;
– Directive (EU) 2015/720 of the European Parliament and of the Council of 29 April 2015 amending Directive 94/62/EC as regards the consumption of lightweight plastic carrier bags.

The packaging waste is one type of basic groups of waste included in the waste catalogue. The waste catalogue was presented in the Regulation of the Minister of Environment of 27 September 2001 on the waste catalogue. This regulation specifies the catalogue with a list of hazardous waste and stipulates how to classify them. In the catalogue, the types of the waste are divided into 20 groups according to their source (with some exceptions) [11]. According to the waste catalogue, packaging waste should be marked with code 15 01.

3. Main statistics of packaging waste

In 2013, 156.9 kg of packaging waste was generated per inhabitant in the EU-28. This quantity varied between 46.7 kg per inhabitant in Croatia and 210.4 kg per inhabitant in Germany [12]. In Fig. 1 the shares of packaging waste generated by weight by all countries of the UE in 2013 were presented.

According to Eurostat, (Fig. 1) paper and cardboard were the largest group of packaging waste generated in 2013. It should be remembered that cardboards are used as bulk packaging for the products already packaged in other packagings, so this can be the reason of their large percentage of the total amount of packaging waste generated. Cardboards are those packagings which are usually not suitable for re-use, but can be recycled. Paper and cardboards are packagings that can be subjected to the fastest biodegradation.

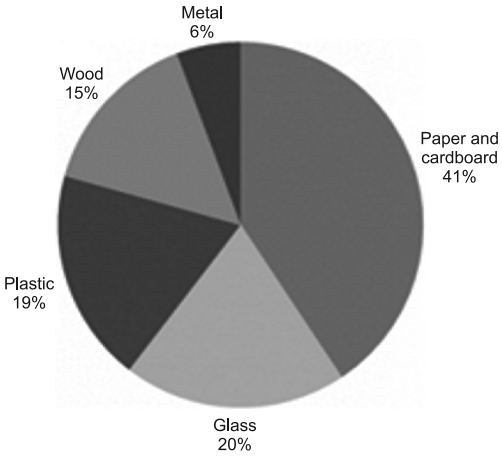

Fig. 1. Shares of packaging waste generated by weight, 2013 [12]

One ton of recycled paper is equal to 17 trees, which results in saving plants that are still able to produce the oxygen needed for life. Recycling of 1 ton of paper saves 2–7 m^3 of

landfill space, 26.5 thousand liters of water, 1,476 liters of oil and 4.2 thousand kWh, which is what is needed to heat an average apartment for half a year [13].

Packaging should follow the 3R's hierarchy. The first R stands for „reduce". Packaging should be reduced prior to the manufacturing stage, by designing and marketing products for the first "R". This means reducing the number of layers, materials and toxins at source. The second R stands for "reuse". Packaging should be designed to be reusable, refillable, returnable and durable to the greatest extent possible. The third R stands for "recycle". Packaging should be designed to be recyclable and/or made with recycled content [14].

In Table 1, the recycling of packaging waste in 2009–2014 in Poland was shown.

Table 1

Recycling of packaging waste in 2009–2014 in Poland [15]

Specification	Achieved level of recycling					
	2009	2010	2011	2012	2013	2014
Plastic packaging	21.5	20.2	22.6	22.2	20.0	28.6
Aluminium packaging	64.5	60.5	54.2	46.7	34.0	48.1
Steel packaging, of which steel sheet packaging	33.6	39.5	40.4	47.1	34.8	55.5
Paper and cardboard packaging	50.9	57.2	58.7	53.2	49.7	72.9
Household glass packaging excluding ampoules	41.9	45.6	45.1	51.3	43.4	60.2
Packaging made of natural materials (wood and textiles)	23.1	21.0	27.3	28.3	21.9	48.6

In Poland, recycling of the packaging waste was very diverse. The highest percentage of the recycling was noted in case of paper and cardboard packaging and aluminium packaging. In Poland, since 1th July 2013 a new Act amending the Act on maintaining cleanliness and order in municipalities and some other acts has been in force [16]. Under the Act, local governments have taken control of waste, including packaging waste. It is worth noting that Poland has changed the regulations on waste management as one of the two last European Union countries. According to the act, all waste should be divided into paper, plastic, metal and glass. However, a simplified division into dry waste (recyclable), wet waste and glass is also accepted and used in many municipalities. Changes concerning the act which forced residents to change their behavior, could have caused a large decrease in the recovery of various materials in 2013. Residents needed some time to get used to the new rules and new requirements for the segregation of waste.

4. Conclusions

The concept of sustainable development and global environmental regulations have forced also Poland to change legislation in this area. It should be remembered that the success of these changes depends primarily on the attitude of the people and their willingness to

change their behavior. During purchasing a variety of products everyday different types of the packaging waste are produced. Some part of this waste can be easily reused. But in order to do this, their prior segregation is needed. Therefore, adequate awareness of people who produce such type of waste is the most important.

In Poland, a large part of packaging waste is recycled. Some variations in this trend can be noticed, but Poland is still behind in comparison with other European countries when it comes to the packaging waste recycling. However, in the case of paper, cardboard and aluminum packaging, recycling in Poland is quite high. Maybe in 20–30 years, when the present generation of children who are brought up in the spirit of nature grows, they will improve this situation.

References

[1] Konstanciak A., Brozova S., Pustejovska P., *Wykorzystanie alternatywnych źródeł energii w Polsce i Republice Czeskiej*, Rynek Energii, **107** (4), 2013, 33-36 [in Polish].

[2] Kardas E., *Analiza jakości wytwarzania opakowań szklanych*, Logistyka, **5**, 2011, 106-110 [in Polish].

[3] Act of 13th June 2013 on packaging management and packaging waste (Journal of Laws of 2013, item 888) [in Polish].

[4] Dziuba S.T., Ingaldi M., *Segregation and recycling of packaging waste by individual consumers in Poland*, 15th International Multidisciplinary Scientific GeoConference SGEM 2015, SGEM2015, Conference Proceedings, June 18–24, 2015, Book 5, Vol. 3, 545-552.

[5] PN-ISO 8402:1996 Zarządzanie jakością i zapewnienie jakości – Terminologia [in Polish].

[6] Żakowska H., *Recykling odpadów opakowaniowych*, Warszawa 2005 [in Polish].

[7] Act of 11th July 2011 on maintaining cleanliness and order in municipalities and other acts (OJ 2011, No. 152, item. 897) [in Polish].

[8] Act of 14th December 2012 on waste (OJ 2013 item. 21) [in Polish].

[9] Act of 27th April 2001 the Environmental Protection Law (OJ 2001, No. 62 item. 627) [in Polish].

[10] *Packaging and Packaging Waste*, http://ec.europa.eu/environment/waste/packaging/legis.htm [date of acc.: 2016-05-22].

[11] Regulation of the Minister of the Environment of 27th September 2001 on the waste catalogue (OJ 2001, No. 112, item. 1206) [in Polish].

[12] Eurostat, http://appsso.eurostat.ec.europa.eu/nui/show.do (date of acc.: 2016-05-22).

[13] *European waste catalogue and hazardous waste list*, Valid from 1 January 2002, Environmental Protection Agency.

[14] Ingaldi M., *Management of the packaging waste in companies in Poland*, International Multidisciplinary Scientific GeoConference SGEM 2015, SGEM2015 Conference Proceedings, June 18–24, 2015, Book 5, Vol. 3, 385-392.

[15] http://stat.gov.pl/obszary-tematyczne/srodowisko-energia/ [date of acc.: 20160522].

[16] Act of 1st July 2011 on amending the Act on maintaining cleanliness and order in municipalities and some other acts (OJ 2011, No, 152, item. 897) [in Polish].

TECHNICAL TRANSACTIONS | **CZASOPISMO TECHNICZNE**
MECHANICS | MECHANIKA
4-M/2016

LESZEK WOJNAR*

APPLICATION OF ASTM STANDARDS IN QUANTITATIVE MICROSTRUCTURE EVALUATION

WYKORZYSTANIE NORM ASTM DO ILOŚCIOWEJ OCENY MIKROSTURKTURY

Abstract

Quantitative microstructure characterization is currently required in R&D as well as in routine quality control of materials and products. Every step: preparation of the laboratory and specimens, measurements and interpretation of the results etc. can be a source of serious errors. Application of the ASTM guidelines can minimize these problems and improve international circulation of the results. The paper characterizes selected ASTM standards devoted to laboratory practice and analyses the complexity of microstructural materials characterization.

Keywords: ASTM, *image analysis*, *metallography*, *microstructure*, *standardization*

Streszczenie

Ilościowa ocena mikrostruktury jest obecnie powszechnie wymagana zarówno w działalności R&D, jak i podczas rutynowej kontroli jakości materiałów i wyrobów. Każdy krok: przygotowanie laboratorium i próbek, pomiary oraz interpretacja wyników etc. może być źródłem poważnych błędów. Wykorzystanie zaleceń ASTM może zminimalizować te problemy i ułatwić międzynarodową wymianę wyników. W artykule scharakteryzowano wybrane normy ASTM poświęcone praktyce laboratoryjnej oraz przeanalizowano złożoność problemu ilościowej charakterystyki mikrostruktury materiałów.

Słowa kluczowe: ASTM, *analiza obrazu*, *metalografia*, *mikrostruktura*, *normalizacja*

DOI: 10.4467/2353737XCT.16.230.5979

* Prof. D.Sc. Ph.D., Eng. Leszek Wojnar, Institute of Applied Informatics, Faculty of Mechanical Engineering, Cracow University of Technology.

1. Introduction

The question: *Why should we quantify materials microstructure?* is neither simple not naïve. One can define two major groups dealing with materials: producers and customers. The producer supplies materials to the customer, often in the form of semi products, and is interested mainly in production costs, technology and properties required by the customer. The customer, on the other hand, (the one who can use a given material for further production of several goods) is interested in the price and properties of the materials offered by producers. Please, note that nobody is interested in microstructure. The above demonstrated discussion is usually very surprising for students who devote a lot of time to study microstructures of different materials and methods of how to test them. The importance of materials microstructure becomes quite obvious if we discover that materials engineering is based on a simple theorem that in fact cannot be found even in advanced textbooks:

Two materials with ***identical microstructure*** *have* ***identical properties*** *irrespective of their technological history.*

If one considers the above rule it will be clear that quantitative parameters of the microstructure can be successfully used in quality control and assessment of structure-property relationships. Basic rules of microstructure quantification have been defined and well known for decades [1]. Unfortunately, only a very limited number of structure-property relationships has been fixed and verified [2]. Some of them are presented in Table 1. It is noteworthy that even if the relation is well known, we often have no precise, quantitative formula which describes it.

Table 1

Well defined structure-property relationships

Structure-property relationship	Quantitative relation
Effect of grain size on yield point (Hall-Petch relation)	Yes
Effect of pearlite content on properties of annealed carbon steel	Yes
Effect of hard phase content on wear resistance	Yes
Effect of porosity on mechanical properties of sintered materials	No
Effect of graphite shape on mechanical properties of cast iron	No
Effect of non-metallic inclusions on mechanical properties of steel	Partially
Effect of dislocation density on plastic deformation	No
Effect of nonhomogeneity of wear resistance on cast alloys	No

The above analysis demonstrates that the problem of practical application of microstructural data is still far from final solving. In most cases, one uses these data for quality control. The de facto world standards in this area are set by ASTM and therefore the possibility of building a complete set of procedures based on ASTM documents is analysed in the subsequent part of this paper.

2. Laboratory preparation

In this template, styles are created to facilitate writing. Depending on what you want to write, you have to choose the right style.

Table 2

Selected standards for laboratory preparation

Number of the standard	Title of the standard
ASTM E7 – 15	Standard Terminology Relating to Metallography
ASTM E3 – 11	Standard Guide for Preparation of Metallographic Specimens
ASTM E768 – 99(2010)e1	Standard Guide for Preparing and Evaluating Specimens for Automatic Inclusion Assessment of Steel
ASTM E883 – 11	Standard Guide for Reflected–Light Photomicrography
ASTM E1951 – 14	Standard Guide for Calibrating Reticles and Light Microscope Magnifications
ASTM E2014 – 11	Standard Guide on Metallographic Laboratory Safety
ASTM E691 – 15	Standard Practice for Conducting an Interlaboratory Study to Determine the Precision of a Test Method

To ensure precise communication, standard terminology related to metallography (ASTM E7) and preparation of metallographic specimens (ASTM E3) are standardized. For automatic image analysis, which allows for much more effective microstructure quantification, one needs specimens prepared with higher precision. These requirements emerged later and therefore instead of thorough revision of the previous standard, a completely new procedure has been prepared (ASTM E768). Most of the test is performed with the use of reflected light microscopy. Guidelines concerning the proper choice of microscopes and their calibration can be found in the ASTM E883 and ASTM E1951 standards. There are also some standards, not listed here, which are devoted to macro and micro etching leading to better appearance of the microstructural features tested.

Ensuring safety work conditions is of the highest importance in a metallographic laboratory due to the machining of specimens made of hard materials and the presence of hazardous chemicals. When organizing a laboratory, one can find some help in the appropriate AST standard (E2014).

Subtle differences in specimen preparation, etching, image acquisition and subsequent analysis often lead to significant scatter in the results obtained in different laboratories. Objective validation of test procedures used in metallography is very limited and in many cases even impossible. This is caused by the lack of alternative source of microstructural information. For example, fine precipitations can be observed only by means of advanced methods of transmission electron microscopy (TEM), and one has no other possibility to observe these precipitations. Consequently, we cannot verify correctness of shape and size characteristics evaluated with the help of TEM. Comparative measurements performed during interlaboratory tests are the best and sometimes the only possible solution. This methodology is also standardized (ASTM E691).

3. Application of image analysis

ASTM standards are prepared in a form similar to a scientific paper. The contents describe the scope and terminology, apparatus and specimen preparation, the measurement procedure, interpretation of the results and report as well as appendixes with exemplary case histories etc. Usually, the standards are based on well known and possibly simple methods. At the end one can find a list of references. The structure of ASTM standards is flexible and can differ in some elements from one standard to another.

Table 3

Selected standards for determining microstructure characteristics

Number of the standard	Title of the standard
ASTM E112 – 13	Standard Test Methods for Determining Average Grain Size (image analysis methods described in E1382)
ASTM E1382 – 97(2015)	Standard Test Methods for Determining Average Grain Size Using Semiautomatic and Automatic Image Analysis
ASTM E562 – 11	Standard Test Method for Determining Volume Fraction by Systematic Manual Point Count (image analysis methods described in E1245)
ASTM E45 – 13	Standard Test Methods for Determining the Inclusion Content of Steel (image analysis in E1245)
ASTM E1245 – 03(2016)	Standard Practice for Determining the Inclusion or Second-Phase Constituent Content of Metals by Automatic Image Analysis
ASTM E2109 – 01(2014)	Standard Test Methods for Determining Area Percentage Porosity in Thermal Sprayed Coatings
ASTM E1268 – 01(2016)	Standard Practice for Assessing the Degree of Banding or Orientation of Microstructures
ASTM E2283 – 08(2014)	Standard Practice for Extreme Value Analysis of Nonmetallic Inclusions in Steel and Other Microstructural Features
ASTM E1181 – 02(2015)	Standard Test Methods for Characterizing Duplex Grain Sizes
ASTM E930 – 99(2015)	Standard Test Methods for Estimating the Largest Grain Observed in a Metallographic Section (ALA Grain Size)
ASTM E2627 – 13	Standard Practice for Determining Average Grain Size Using Electron Backscatter Diffraction (EBSD) in Fully Recrystallized Polycrystalline Materials
ASTM A247 – 16a	Standard Test Method for Evaluating the Microstructure of Graphite in Iron Castings (image analysis methods described in E2567)
ASTM E2567 – 16a	Standard Test Method for Determining Nodularity and Nodule Count in Ductile Iron Using Image Analysis

It is obvious that automated methods are newer than manual ones. Similarly, standards devoted to image analysis were introduced later and, consequently, their numbers are higher, as can be seen in Table 3 (for example, E112 and E1382). However, this is not always

the case. In some standards, for example E1181 or E1268, both types of measurements: manual and automatic are defined.

As shown in Table 3, most standard methods are devoted to analysis of grain size and nonmetallic inclusions. Quantification of other microstructural features is only partially covered by standard procedures or one observes a complete lack of standardization. In such a case, it is necessary to develop a new procedure that can be later added as a new standard. New procedures, usually apply image analysis and some guidelines for practice in this field can be found in dedicated literature [3, 4].

Metallurgy seems to be the most advanced in the standardization of microstructure characterization. However, other areas of application, like medicine, textiles or cement industry can be found among the standards (Table 4).

Table 4

Selected standards for microstructure characterization in areas different than metallurgy

Number of the standard	Title of the standard
ASTM D7879 – 13	Standard Test Method for Determining Flax Fiber Widths Using Image Analysis
ASTM E1695 – 95(2013)	Standard Test Method for Measurement of Computed Tomography (CT) System Performance
ASTM F1854 – 15	Standard Test Method for Stereological Evaluation of Porous Coatings on Medical Implants
ASTM C1356 – 07(2012)	Standard Test Method for Quantitative Determination of Phases in Portland Cement Clinker by Microscopical Point-Count Procedure

Test procedures in the ASTM standards are based on well-known and documented methods. Such a solution is safe; however, it can petrify small errors or uncertainties that have been corrected in more recent works. Fortunately, the ASTM standards are revised every few years and there is a possibility to significantly upgrade the procedure. The year of last revision is always a part of number of a given standard (see Tables 2–4).

4. Discussion

ASTM provides a very large set of 25,338 standards and publications devoted to materials. The subset related to test methods consists of 13,628 items. Such a huge collection makes finding the appropriate document difficult, even with the help of an electronic search system. When looking for a suitable document, one should keep in mind that access to full text documents is always paid. Nevertheless, ASTM provides the largest collection of documents related to microstructure evaluation. Moreover, many of them constitute a de facto world standard.

24 ASTM standards listed in this paper demonstrate the above mentioned wide range of documents that allow for the organisation of a laboratory that will be internationally accepted as a source of microstructural information.

In spite of enormous progress in image analysis methods, laborious and time consuming methods are still widely represented within the standard procedures. Within the automated methods, processing of the image leading to a binary image suitable for measurements is the weakest and practically not fixed point. The user has to evaluate their own procedures for feature detection and this step lies outside the standard. On the other hand, it is decisive for the final results. Therefore, it is recommended to perform interlaboratory tests in order to verify and fix the correctness of the elaborated procedure.

The ASTM standards give guidelines for test procedures but it is the user's responsibility to fix details and evaluate the whole procedure. Many details, especially concerning specimen preparation cannot be standardized due to the practically countless number of alloys, ceramics, plastics or composites. Fortunately, there are other sources of information which give answers to practical problems [5].

To summarize, the ASTM standards provide a huge set of information and rules suitable for microstructures evaluation. However, not all the problems are covered by these standards and many details have to be fixed on the basis of other sources of information or the user's own experience.

Miscellaneous

Numbers, names and basic information cocerning the contents of the ASTM Standards are available free of charge on the ASTM web site at www.astm.org.

References

[1] Underwood E.E., *Quantitative stereology*, Addison-Wesley, Reading 1970.
[2] Dobrzański L., *Materiały inżynierskie i projektowanie materiałowe*, WNT, Warsaw 2006.
[3] Practical guide to image analysis, ASM International, Materials Park, 2000.
[4] Wojnar L., *Image analysis. Applications in materials engineering*, CRC Press, Boca Raton 1998.
[5] ASM Handbook, Vol. 9, Metallography and Microstructures, ASM International, Materials Park, 2004.

TECHNICAL TRANSACTIONS | CZASOPISMO TECHNICZNE
MECHANICS | MECHANIKA
4-M/2016

NORBERT RADEK*, MIECZYSŁAW SCENDO**

LASER BEAM WELDING OF DC04 STEEL

LASEROWE SPAWANIE STALI DC04

Abstract

This paper discusses the effect of selected parameters of laser welding on mechanical properties of welds. Two parameters were analysed: the welding speed and the laser power. The properties of the material in the fusion zone and the heat affected zone were determined by hardness tests and microscopic analysis. The results indicate welds produced at different welding parameters have similar properties.

Keywords: laser welding, *fusion zone*, *properties*

Streszczenie

W artykule przestawiono badania wpływu wybranych parametrów spawania laserowego na własności mechaniczne spoiny. Badano wpływ dwóch parametrów: prędkość posuw oraz moc wiązki. Na badania własności spoiny oraz stref do nich przyległych składały się pomiary twardości oraz obserwacje mikroskopowe. Przeprowadzone badania wykazują, że spoiny otrzymane przy różnych parametrach spawania charakteryzują się zbliżonymi własnościami.

Słowa kluczowe: spawanie laserowe, *spoina*, *własności*

DOI: 10.4467/2353737XCT.16.231.5980

* D.Sc. Ph.D. Eng. Norbert Radek, Assoc. Prof., Centre for Laser Technologies of Metals, Faculty of Mechatronics and Machine Design, Kielce University of Technology.

** D.Sc. Ph.D. Mieczysław Scendo, prof. UJK, Institute of Chemistry, Faculty of Mathematics and Natural Sciences, Jan Kochanowski University in Kielce.

1. Introduction

The process of laser beam welding involves melting the edges of metals to be joined with a focused beam of radiation at a power density of $10^4 \div 10^6$ W/mm^2 [1]. The development of lasers with a high input power made it possible to join thick plates by directly melting the adjacent edges with no need to chamfer them or use time-consuming filling of the bevel groove. This method of fusion is also used in electron beam welding but the process has numerous disadvantages, for example, the necessity to place the elements to be welded in vacuum, the necessity to remove random magnetic fields as well as the necessity to protect the workpiece against X-ray radiation occurring during high-voltage electron beam welding [2].

The process of laser welding has the following advantages:

- high purity of the process (dependent on the surface preparation and gas purity),
- joining difficult to weld materials,
- easy automation,
- welding with high precision (e.g. joining thin and thick elements),
- high speed of the welding process,
- one source of radiation for several welding stations,
- welding performed under atmospheric pressure (by contrast, electron beam welding is performed in vacuum),
- high power density (in the case of deep welding), and as a result, small distortions,
- narrow heat affected zone.

2. Materials and methods

The specimens to be tested were cut from a steel sheet 0.8 mm in thickness. As a material resistant to aging, DC04 steel is used extensively in high-performance applications including deep drawing and drawing, and in the transport industry. DC04 steel is characterised by good weldability which means that no special preparation of the work is needed. Table 1 shows the chemical composition of DC04 steel, respectively.

Table 1

Chemical composition of DC04 steel [3]

Steel grade	Maximum content [%]				
	C	Mn	P	S	Ti
DC04	0.08	0.40	0.030	0.030	0

The analysis of the properties of the joints produced by laser welding involved examining their microstructure and measuring their hardness.

The microstructural observations were conducted using a Joel JSM-5400 scanning electron microscope. The hardness was measured with a NEXUS 4304 tester at a load of 1 kG applied for 10 s.

3. Selection of laser welding parameters

The welding tests were conducted by changing two parameters: the laser power and the welding speed. According to the literature [4, 7], these two parameters have the greatest influence on the quality of welds.

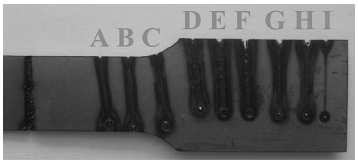

Fig. 1. View of the reference specimen with laser pass lines imitating welds

Figure 1 shows a specimen with laser pass lines imitating welds, whereas Table 2 provides the parameters of laser welding used during the tests. The macroscopic analysis of the laser pass lines and the phenomena accompanying the welding process helped select the main parameters of laser welding: the laser power and the welding speed.

Table 2

Values of the main process parameters

Number of the laser pass line	Laser power P [kW]	Welding speed v [m/min]
A	1.5	3
B	1.8	3
C	2	3
D	2.5	3
E	2	2
F	2	2.5
G	2	3.5
H	2	4
I	2	5

The laser pass lines A-D were formed at a welding speed of 3 m/min and the initial power of 1.5 kW gradually increased to 2.5 kW. When the pass line was produced at a power of 1.5 kW, plasma was not present. At a power of 1.8 kW, a small plasma cloud was observed, but its influence on the welding process was negligible. When the laser pass line was formed at a power of 2 kW or 2.5 kW, a positive effect of the plasma cloud was observed. After the macroscopic examinations of the laser pass lines, it was assumed that the tests would be conducted at a laser power of 2 kW. During the next five tests, the laser pass lines E-I were produced by changing the welding speed from 2 m/min to 5 m/min, with the laser power being constant (P = 2 kW). It was found that when the welding speed was 5 m/min, the weld penetration was incomplete (pass line I). The experimental data was analysed to select the laser welding parameters:

– laser power $P = 2$ kW;
– welding speed v: 2 m/min; 2.5 m/min; 3 m/min; 3.5 m/min; 4 m/min;
– shielding gas: argon $Q = 10$ l/min.
– preheat time $t = 5$ s;
– pulse repetition rate $f = 30\,000$ Hz;
– nozzle-workpiece distance $\otimes f = 0$ mm.

The tests were conducted for five series of laser welded specimens and one series of unwelded specimens, where the base metal was DC04 steel. There were three specimens in each series numbered from 0 (base metal) to 5 (where $v = 4$ m/min).

4. Results and discussion

The microstructure of the welded joints was analysed using a Joel JSM-5400 scanning electron microscope.

The microscopic examinations of the welded joints were performed on polished metallographic specimens in the plane perpendicular to the weld, which enabled observation of the fusion zone and the heat affected zone. It was also possible to analyse the structures formed and to measure the width of the heat affected zone (HAZ).

The aim of the analysis was to compare the resulting microstructures of the welded joints and to determine how variable values of the welding speed affect the shape of the weld.

The laser welding process is characterised by very high heating and cooling rates, which leads to the narrowing of the width of both the fusion zone and the heat-affected zone.

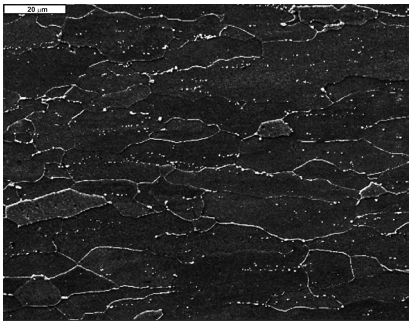

Fig. 2. Ferritic-pearlitic microstructure of the base metal (×1000 magnification)

Figure 2 shows an image of the microstructure of the base metal. The results suggest that the base metal had a coarse-grained ferrite-pearlite structure. From Fig. 2 it is clear that the grains are arranged in bands, which indicates that the production of steel sheets (DC04 steel) involved rolling. The analysis of a specimen of series 1 showed that the material in the HAZ had a fine-grained ferritic-pearlitic microstructure with visible metallic precipitates in the pearlite grains.

For a specimen of series 1, a Widmanstätten pattern was observed in the fusion zone (Fig. 3). It contains plate-shaped ferrite precipitates running at 60° and 120°. The occurrence

of the Widmanstätten structure indicates that the steel was overheated, which caused a decrease in the mechanical properties of the weld.

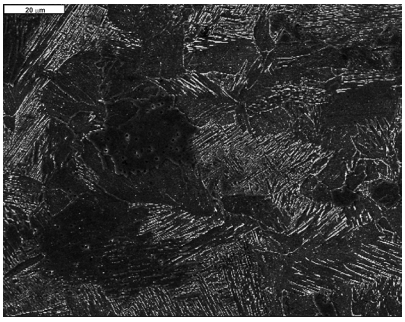

Fig. 3. Widmanstätten structure in the fusion zone (×1000 magnification)

The microscopic examinations were performed to determine the influence of different welding speeds on the microstructure and shape of the welds. It was found that the welding speed affected the weld shape and the penetration depth. The higher the welding speed the smaller the penetration depth and the more narrow the fusion zone; there was also a change in the direction of the fusion line resulting from a change in the weld shape from mushroom--like to triangular (Fig. 4). When the welding speed was too low, the width of the fusion zone and the width of the heat affected zone increased.

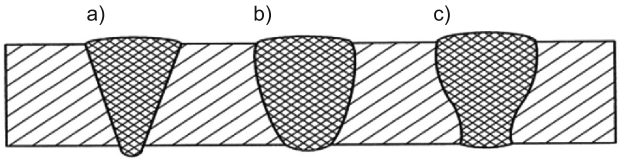

Fig. 4. Weld shapes after laser welding: a) triangular, b) and c) mushroom-shaped

The hardness of the material was measured by means of the Vickers method. The indentations were made in all the specimens of series 1–5 prepared as metallographic specimens. The measurements were taken on surfaces perpendicular to the three zones: the fusion zone (at the face), the heat affected zone and the base metal.

The values of the hardness in the base metal zone obtained for all the specimens were comparable. It can be assumed that the specimens had a similar structure with no microdefects that would contribute to the weakening of the material. The average hardness in the base metal zone for all the specimens of series 1–5 was 105 HV1.

The analysis of the hardness of the material in the heat affected zone indicates that the highest values were reported for a welding speed of 3.5 m/min (a series 4 specimen). The average hardness in the HAZ obtained for that specimen was 184 HV1. For the specimens of series 1–5, the average hardness in the HAZ was 38% higher than the average hardness in the base metal zone.

The highest hardness at the weld face was reported for a specimen of series 4; the average value was 256 HV1. The lowest hardness in the fusion zone was reported for a specimen of series 3 (v = 3 m/min); the average hardness for that specimen was 236 HV1. The phase transitions that occurred in the heated material during its rapid cooling contributed to material hardening both in the fusion zone and the heat affected zone. The phase transitions were responsible for the formation of martensite-like and ferrite-bainite structures, which improved material hardness. The average hardness in the fusion zone was 31% higher than that in the heat affected zone.

5. Summary

The following are the conclusions drawn from the experimental data:

1. The shape and thickness of the welds as well as the width of the heat affected zone are dependent on the welding speed.
2. The hardness measurement results confirm that the welded specimens are not homogeneous but very complex in structure.
3. An increase in the welding speed caused visible, irreversible structural changes in the fusion zone and the heat affected zone, which were attributable to high heating and cooling rates. The changes included refinement of the grain structure and higher hardness.

References

[1] Radek N., *Laboratorium wiązkowych technologii obróbki materiałów*, Wyd. Politechniki Świętokrzyskiej, Skrypt, Nr 456, Kielce 2013 [in Polish].
[2] Szczeciński Z., *Spawanie wiązką promieniowania laserowego*, Przegląd Spawalnictwa, vol. 9–10, 1985, 12-17 [in Polish].
[3] Ruukki catalogue, http://www1.ruukki.pl/~/media/Poland/Files/metals-coldrolled/karty-produkty/Ruukki-zimnowalcowane-Stale-przeznaczone-do-formowania.pdf [date of acc. 10.06.2016].
[4] Chen S., Huanga J., Xiaa J., Zhaoa X., Lin S., *Influence of processing parameters on the characteristics of stainless steel/copper laser welding*, J Mat. Proc. Tech., vol. 222, 2015, 43-51.
[5] Kuryntsev S.V., Gilmutdinov A.Kh., *Welding of stainless steel using defocused laser beam*, J. Constructional Steel Res., vol. 114, 2015, 305-313.
[6] Hayashi T., Matsubayashi K., Katayama S., Abe N., Matsunawa A., Ohmori A., *Reduction mechanism of porosity in tandem twin-spot laser welding of stainless steel*, Weld. Int., vol. 17, 2003, 12-19.
[7] Torkamany M.J., Ghaini F.M., Poursalehi R., *An insight to the mechanism of weld penetration in dissimilar pulsed laser welding of niobium and Ti–6Al–4V*, Optics & Laser Technology, vol. 79, 2016, 100-107.

TECHNICAL TRANSACTIONS | **CZASOPISMO TECHNICZNE**
MECHANICS | MECHANIKA
4-M/2016

PIOTR SYGUT*

CLEANER PRODUCTION STRATEGY AS POSSIBILITY OF WASTE REDUCTION IN WOOD SAWING

STRATEGIA CZYSTSZEJ PRODUKCJI MOŻLIWOŚCIĄ REDUKCJI ODPADÓW PRZY PRZECIERANIU DREWNA

A b s t r a c t

Cleaner production is a management strategy aimed at reducing the losses associated with waste of energy and raw materials which focuses on waste prevention and not the way of its utilization. Cleaner Production can also reduce company's costs incurred during the processes taking place within the organization. In the case of companies involved in wood processing (sawmills, carpenters, etc.)a lot of waste in the form of sawdust, shavings or edgings is created. These are materials that can be used as an alternative fuel for firing furnaces and boilers. Good sales management of this type of waste after production allows companies to obtain additional income and minimize environmental risks.

Keywords: clean production, *pellet production*, *protection of the environment*

S t r e s z c z e n i e

Czystsza produkcja jest to strategia zarządzania przedsiębiorstwem mająca na celu ograniczenie strat związanych z marnotrawstwem energii i surowców, skupiająca się na zapobieganiu powstawania odpadów, a nie sposobów ich utylizacji. Czystsza Produkcja pozwala też na redukcję kosztów przedsiębiorstwa ponoszonych podczas procesów zachodzących wewnątrz organizacji. W przypadku przedsiębiorstw zajmujących się obróbką drewna (tartaki, stolarnie itp.) powstaje bardzo dużo odpadów w postaci trocin, wiór czy też zrzyn. Są to materiały, które można wykorzystać jako paliwa alternatywne do opalania pieców i kotłów grzewczych. Dobre zarządzanie sprzedażą tego typu odpadami poprodukcyjnymi pozwala przedsiębiorstwom na uzyskanie dodatkowych dochodów i zminimalizowanie zagrożeń dla środowiska naturalnego.

Słowa kluczowe: czystsza produkcja, *produkcja pelletu*, *ochrona środowiska*

DOI: 10.4467/2353737XCT.16.232.5981

* Ph.D. Eng. Piotr Sygut, Institute of Production Engineering, Faculty of Management, Czestochowa University of Technology.

1. Introduction

Cleaner Production (CP) is a continuous use of processes and products integrated into a preventive environmental strategy to reduce the risk to humans and the environment. Cleaner Production uses a system which, when appropriate procedures are used, becomes a voluntary and not formalized environmental management system. UNEP defines Cleaner Production as follows: Cleaner Production is a strategy for environmental protection involving a continuous, integrated, preventive action in relation to processes, products and services, aimed at increasing the efficiency of production and services, and reduce the risk to humans and the environment [1]. Fig. 1 shows the use of Cleaner Production in practice.

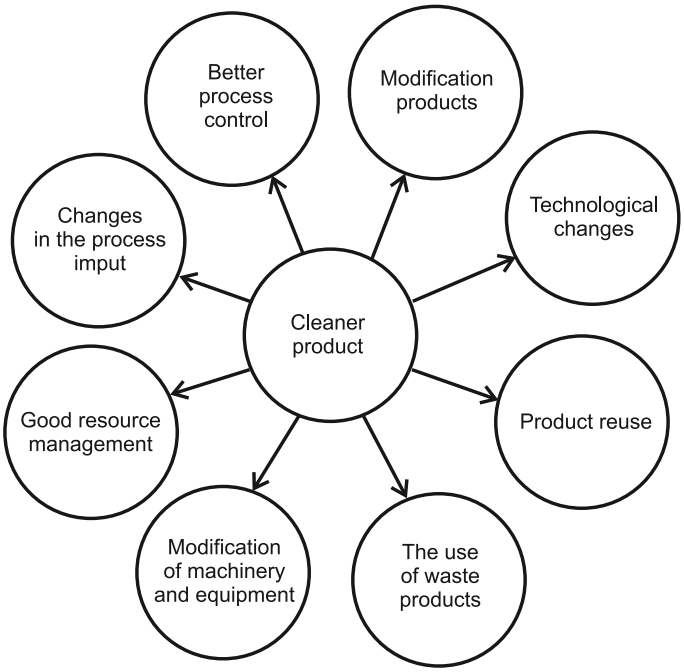

Fig. 1. Use of Cleaner Production in practice

Cleaner Production program is achieved by technical and organizational measures aimed at eliminating or reducing the short-term and long-term adverse impacts of production processes and products on people and the environment. Cleaner production process refers to both manufacturing processes and the environmental characteristics of an article throughout its life cycle. With regard to the course of manufacturing process, this means the elimination of harmful materials and emissions and rational use of living labor, materials and energy [2]. In the Cleaner Production program, we can distinguish four main principles [3]:

– the precautionary principle – advocates the necessity of proving a potential poisoner that its activities or products will bring harm to the environment, shifting the burden of proof to the manufacturer instead of the local community which had already existed to

prove damages. The rejection of this approach is the use of quantitative computed degree of risk as the sole factor in deciding whether to use a chemical or the introduction of new technology. In this case, science is not ignored, but notes that if industrial production is also a huge social influence besides scientists, also other people should have influence over those decisions;

- the preventive approach – the process of preventing damage to the environment is cheaper and more effective than trying to "heal" the same environment after its destruction. Prevention requires going "against the tide" of the production process to remove the source and cause of the problems, instead of trying to control the outcome or damage. Pollution prevention should replace preventive pollution control. For example, prevention requires changes in the production process, allowing to stop a huge waste stream, while the lack of a "precautionary approach" produces more and more sophisticated models of incinerators. The increase in energy efficiency should suppress the appetite to consume fossil energy sources;
- democratic control – clean production involves all the affected by industrial activity, and thus workers, consumers and local communities. The information available on the production and involvement in decision-making supports democratic control. The community must have information concerning production company and minimum access to information on industrial emissions, pollution registers and plans for the reduction of toxic substances in the course of production as well as data on the composition of products;
- the integrated and holistic approach – people need to adopt an integrated approach for the use of natural resources and consumption. Ignorance of contemporary approach, interrelationships and dependence of the production allows for the movement of pollutants between air, water and soil. Reducing the resulting emissions associated with the production does not lead by itself to reducing harmfulness of the product. Minimization of risks can be obtained by taking into account the entire product life cycle, paying attention to the materials used, the flow of water and energy and economic impact of switching to cleaner production. Life Cycle Analysis is one of the tools in maintaining a holistic, comprehensive approach [4].

2. Characteristics of waste produced in wood sawing

During the process of wood sawing, a large amount of waste in the form bark, sawdust, edgings, blocks manipulation, etc. is produced. This amount of wastes needs a lot of space for warehousing or storage. In the case of sawdust shavings, you often need extra space or storage in the form of silos. Storage of such waste is associated with many risks for humans and the environment. There is a danger of spontaneous combustion of wood waste, if there is no control of the temperature and density of biomass. Sparks, heating of the machines working on these landfills, lightnings and biochemical processes can also cause biological hazards (viral and fungal diseases). They can cause skin and respiratory diseases. Because of the way these wastes are stored, disease can spread through the air and wild animals, birds and rodents. In the case of transport of sawdust and wood dust, explosions can occur

mixing the waste with atmospheric air, which can become an ignition source. In storage areas waste, wood can acidify the soil. Inadequate protection of sawdust stored in dumps may cause its spread to the surrounding areas under the influence of winds. These dumps can become habitat for rodents and wild animals.

3. Characteristics of pellets

In the analyzed company waste from primary production (sawing of wood raw material), pellets are partially processed in plants and sold to contracted customers. Bark is sold to companies engaged in the horticultural industry. Shavings and sawdust are used for firing furnaces in plants and sold to biomass power plants. With shavings, also wood pellets are produced. Edgings from production lines are crushed in special machines adapted to this (wood chippers), processed and used for the production of wood pellets.

Wood pellets organic fuel is produced from the sawmill wood and intended for heat generation in boilers allocated to combustion of the pellets used to produce heat. Pellet can be used for heating purposes in houses, hotels, industrial buildings, warehouses, public buildings, and wherever there is a demand for heat. Fig. 2 shows wood pellets.

Fig. 2. Wood pellets with 6 mm in diameter

Characteristics – pellet has high energy properties and low moisture content. 1 ton of pellets is created after burning up to 3 kg of organic ash, which can be used as a natural garden fertilizer. It is environmentally friendly-production of pellets does not cause any additional cutting of trees in the forest. Its use gives comfort, cleanliness and comfort during transportation and handling. Low CO_2 emissions during combustion. Pellet is a renewable energy source. Combustion may be in a maintenance-free boiler. Availability of purchase and ease of transport. It is not harmful to humans and does not cause allergies.

Specifications: 6 mm diameter [+/–1 mm]; length 3.15–12 mm; humidity 10%; ash content 0.7%; caloric content in the range 14–19 GJ/Mg; bulk density above 600 kg/m^3.

Packaging – pellets are packed in bags of 15 kg or big-bag packagings of 1000 kg or 1200 kg. Pellets can also be stored in bulk, but you should fulfill the following conditions: storage - pellets should be stored dry, free from moisture and condensed from the roof surface without insulation. Wood material is characterized by high absorption of moisture from the air. Therefore, you should pay special attention to whether pellets are stored in conditions of low natural humidity.

Transport – pellets must be transported by cars having tarpaulins or be otherwise protected against the weather. Pellets should be protected against humidity and protected during transport to prevent overturning pallets. Pellets transported in bulk must also be protected by tarpaulin or otherwise. Due to their shape and construction, they can also be transported in bulk tankers suitable for transport in a loose and granulated form.

4. The pellet manufacturing process in terms of technology

Pellet is produced from the sawmilling waste. It is processed in a number of operations before it can be packaged and sent to the recipient. Production is continuous stoppages during the production process due to failure or planned review. The manufacturing process in terms of technology is a description of all the operations occurring in the pellet production process represented by the specific symbols (Fig. 3).

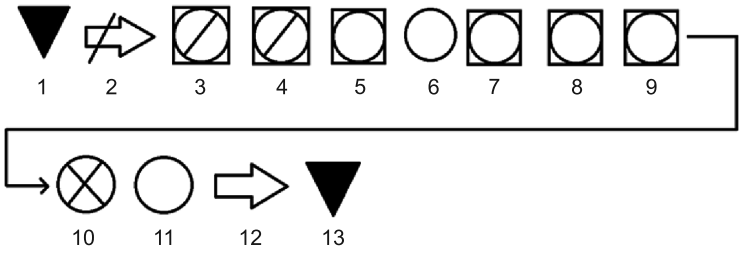

Legend:

1. Storage – raw material for the production of pellets in the form of shavings and waste after production from sawmill is stored in a designated and prepared place on a raw material storage yard.
2. Transport – is done using a wheel loader.
3. Drying the sawdust - using a belt dryer equipped with heat exchangers which generate the appropriate drying temperature. Sawdust humidity after drying should be less than 10%.
4. Purification – involves the removal of foreign bodies from the shavings, such as sand and metals using a solenoid mounted on the belt and screens.
5. Milling – is the process of homogenization of sawdust pieces, which takes place in hammer mills equipped with the ankle to shredding material.
6. Filtering – in this phase of the production process dust resulting from the previous grinding operation is removed and retained in filter bags.
7. Pressing – at this stage raw materials are added 1 to 2% of water in the form vapor, dust is heated to the temperature of 70°C for easier formation of granules and then compressed by a piston through a die.
8. Granulation – a process in which the raw material is subjected to high pressure and molded into granules of a fixed size depending on the diameter of the holes in the die and is cut off to the desired length using a knife.
9. Cooling – the process of cooling pellets to ambient temperature takes place in a cooling device which uses compressed air to enhance the stability of granules.
10. Dust removal – is done by means of screens on which there are separated dust and small particles from the finished product. The waste from this operation is returned to the beginning of the recyclable production process.
11. Packaging – this process takes place on the automated line where pellet is packed and weighed.
12. Transport – transport of pellets into a warehouse for finished products.
13. Storage – finished product packed in bags is stored in the warehouse or in the open air under the protection foil so that moisture does not get into it. Pellet is stored in bulk in large siloses at 15 to 30°C and proper humidity.

Fig. 3. The wood pellets manufacturing process in terms of technology

5. Conclusion

Pellet production is a very good ecological solution, which allows companies to minimize the risks arising from the storage of wood biomass. This is due to processing of waste heat in the pellets production process which minimizes biological hazards. Storage space is reduced by compacting waste pellets and protecting the surrounding area against pollution resulting from the conditions in which the pellets are stored. Apart from minimizing fire hazards, there are also financial benefits for businesses arising from processing wood waste in the main production of pellets. Pellet is a solid fuel alternative to coal and is quite popular fuel compared to sawdust or edgings. Additional costs associated with the pellets production are compensated by their price and revenues they bring.

References

[1] Nowak Z., *Polski ruch czystszej produkcji – wczoraj, dziś, jutro*, Czystsza Produkcja i Eko-Zarzadzanie, maj 2015, nr 1–2, 2015 [in Polish].
[2] Adamczyk W., *Ekologia wyrobów – jakość, cykl życia, projektowanie*, PWE, Warszawa 2004 [in Polish].
[3] Nowak Z., *Zarządzanie środowiskiem*, cz. II, Wydawnictwo Politechniki Śląskiej, Gliwice 2001 [in Polish].
[4] Kruszewska I., Thorpe B., *Strategies to Promote Clean Production*, Briefing, Greenpeace International, 1995.

TECHNICAL TRANSACTIONS | **CZASOPISMO TECHNICZNE**
MECHANICS | MECHANIKA
4-M/2016

EWA KOZIEŃ*, MAREK S. KOZIEŃ**

THE ESTIMATION OF DIVERSIFICATION SCALE OF PRODUCTION IN MACHINERY INDUSTRY BY APPLICATION OF THE ENTROPY NOTION

OCENA STOPNIA DYWERSYFIKACJI PRODUKCJI W PRZEMYŚLE MASZYNOWYM Z WYKORZYSTANIEM POJĘCIA ENTROPII

Abstract

Diversification strategy is currently used by enterprises to increase their stability and economic condition. It is not easy to realize the measurement of the process. The application of the parameter of entropy, which is well-known is physics, is one idea of parametrization. In the machinery industry, product diversification is connected with different consumers representing factories from different machinery sectors: mining, steel, building, agricultural and food. The possibility of estimation of the production diversification in the machinery industry by the application of the entropy-based parameters is discussed in the paper.

Keywords: diversification, *machinery industry*, *production engineering*, *strategy*

Streszczenie

Strategia dywersyfikacji jest stosowana przez przedsiębiorstwa do zwiększenia ich stabilności oraz kondycji ekonomicznej. Ilościowe określenie procesu dywersyfikacji jest trudne. Jednym ze sposobów parametryzacji opisu jest zastosowanie znanego w fizyce pojęcia entropii. W przemyśle maszynowym dywersyfikacja produktu jest związana z różnymi przedsiębiorstwami z różnych sektorów: górniczego, hutniczego itp. Pokazana jest możliwość estymacji dywersyfikacji produkcji w przemyśle maszynowym z zastosowaniem parametrów zdefiniowanych.

Słowa kluczowe: dywersyfikacja, *przemysł maszynowy*, *inżynieria produkcji*, *strategia*

DOI: 10.4467/2353737XCT.16.233.5982

* Ph.D. Ewa Kozień, Department of Management Strategy and Organization, Faculty of Economics and International Relations, Cracow University of Economics.

** D.Sc. Ph.D. Eng. Marek S. Kozień, Assoc. Prof., Institute of Applied Mechanics, Faculty of Mechanical Engineering, Cracow University of Technology.

1. Introduction

Among different strategies of firm growth, these two are opposite in the idea and generally commonly used. The first one is concentration strategy, when the action of a firm is connected with single business or product in a single market with a single dominant technology [10]. The opposite one is diversification strategy, when a firm acquires businesses outside its current products and markets [6]. Choosing types of strategy growth of enterprise by diversification depends on its potential. The enterprise management makes a decision about the initialization of production projects: changing the existing ones, starting new innovative ones (connected with enterprise profile or not connected with the existing profile, enhancing the area of interest by merger or takeover of another firm, especially from another sector). Operations for the diversification of production profile are determined be external causes defined by environment or internal ones connected with enterprises reserves.

The possibility of estimation of the production diversification in the machinery industry by application of the entropy-based parameters is discussed in the paper.

2. Definition and types of diversification

The definition of diversification is connected with changing priorities from production specialization to a broader one and differentiating it. Ansoff was one of the pioneers of research of the strategy in firms. For him, diversification strategy denotes enterprise growth by introducing new products, different than those produced until now and their sales in new markets [1].

The importance of diversification process is discussed by Chandler [2, 3], based on empirical studies of growth strategies and management structures done for American enterprises. Chandler presented a model of enterprises growth according to historical stages of economic growth. One of the stages is diversification, which is starting of enterprise activity in new markets for the realization of new client requirements and taking into account market competition. Diversification is a kind of protection from fluctuation of demand, which is dangerous for specialized enterprises. Diversification often requires changes in organization and management structure [11].

The measurement of diversification process is an interesting problem in production engineering and management. Ramanujam and Varadaajam identify about sixty different parameters, which can be applied to classify firms to extent of diversification [12].

Rumelt [14] classified firms, from the diversification point of view, based on the percent of revenue obtained from different products. His definition includes: single-product firms, dominant-product ones, related-product ones and unrelated-product ones. The related-product firms (related diversified firm) derive less than 70 percent of their revenue from a single product domain, and rest of their revenue is from a related product domain. The unrelated product firms (unrelated diversified firm) derive less than 70 percent of their revenue from a single product domain, but the rest of their revenue is from unrelated product domain.

An interesting idea, suitably defined parameter of entropy, which is well-known in physics and engineering, is used in the quantitative classification of diversification process.

Its application is discussed by Palepu [9] and Rangunathan [13]. Thompson, Strickland and Gamble [16] identified the following diversification types:

– Horizontal diversification, when activity is extended on products from the area of current activity of enterprises. Products are based on familiar technologies and are sold on similar markets by its own chain of sales offices. These actions are the reason of technological and market synergy. Horizontal diversification is a source of positive effects in the use of reserves, growth and financial safety.
– Concentric diversification is going to new areas of activity, which have something in common with the current activity (e.g. technology, distributions). A new activity connected with old production generates the product-market synergy, which makes it possible to increase sale and/or decreasing costs.
– Conglomerate diversification is the idea of starting activities in completely new areas. It is often connected with the use of new technologies or finding new markets. This type of diversification is one of growth directions of contemporary, big enterprises from the high technology countries. The source of positive finance effects is finance synergy, which comes from the finance policy of the conglomerate. Moreover, the costs of management are relatively low. When it succeeds, it triggers possible fast growth of enterprise.

3. Entropy in economics and management

The entropy was previously defined in physics (statistical thermodynamics) by Clausis at the end of the XIX century. The realistic physical process decreases the order in a system and makes the entropy higher. In the XX century, analogous parameters were defined in the theory of information by Shannon and then in the theory of chaos by Kolmogorov.

The beginnings of application of the entropy-based parameters in economics and management started in 1967 and are connected with activities of Theil [15]. Since then, some authors have applied this idea to determine the level of diversification and to determine its type. A review of these methods was done by Raghunathan [13]. In quantitative analyses, the following parameters are used [13]: total diversification (TD), relative entropy (RE), distribution scale (DS), total diversification score (TDS), related scale (RS), related diversification score (RDS), unrelated scale (US), unrelated diversification score (UDS). The definition of these parameters are collected by Raghunathan [13] and are discussed by the authors [7].

Three estimators of entropy of a diversified firm will be applied in performed analysis – total diversification, diversification score and total diversification score.

The formula for total diversification is based on two classic formulations: weighed average of diversification between sectors [5] or weighted average of share between sectors [4]. The natural logarithm of reciprocal of part of share in each of segment is assumed as a weight [4]. The formal definition of entropy has the form of (1) [13], where P_i is a share for the i-th segment/sector, and n is the total number of segments. It is a useful parameter, which takes into account the number of segments/sectors and relative share each of segments. Unfortunately the same value of TD may be obtained for firms diversified in a different way.

$$TD = \sum_{i=1}^{n} P_i \ln\left(\frac{1}{P_i}\right) \qquad P_i \neq 0 \tag{1}$$

If the maximal value of entropy is assumed to be equal ln(n), the value of TD may be given in relation to this value, defined the distribution scale (2) [13]. The value of DS varies from zero to one. The zero value is obtained for activity in only one segment. Value one is obtained for the same distribution of shares for each sector, whose number is more than one.

$$DS = \frac{1}{\ln(n)} \sum_{i=1}^{n} P_i \ln\left(\frac{1}{P_i}\right) \qquad P_i \neq 0 \tag{2}$$

The total diversification score (3), which is the multiplication of DS by the number of segments [13], is another useful parameter.

$$TDS = \frac{n}{\ln(n)} \sum_{i=1}^{n} P_i \ln\left(\frac{1}{P_i}\right) \qquad P_i \neq 0 \tag{3}$$

4. Example of estimations

In the machinery industry, product diversification is connected with different consumers, representing factories from different machinery sectors: mining, steel, building, agricultural and food. In the machinery sector, the products include machines of general application, factory machines, their elements and parts of mechanisms. Product diversification in the machinery industry is connected with a broad spectrum of the production offer, from the point of view of innovation and quality.

As an example of estimation of distribution scale of machinery type firms, let us consider five enterprises who may working maximally in three segments. Not so high number of segments is typical for machinery industry. Some of them work in two segments and action of others is diversified in segments on sectors (related diversification). The characteristics of their activities are given in Table 1.

Table 1

Characteristics of diversified enterprises

ENTERPRISE	SEGMENT 1		SEGMENT 2	SEGMENT 3
	SECTOR 1	SECTOR 2		
I	1	0	0	0
II	0	0	1	0
III	0.3	0.2	0.5	0
IV	0.4	0	0.6	0
V	1/6	1/6	1/3	1/3

In Table 2, calculated values of entropies TD, DS and TDS for the analyzed enterprises are given. The actions of enterprises I and II are connected only with one sector of one segment. Therefore, the value of DS is equal to zero. The action of enterprise V is evenly distributed in three segments, and in segment 1 in two sectors. Therefore, the value of DS is maximal and equals one. The actions of enterprises III and IV are diversified in two active sectors. Hence, the values of DS for them are relatively high. However, the value of DS for enterprise IV is higher than for enterprise III, the values of TDS are in opposite order for them. It is due to the fact that firm III is active in two sectors of segment 1.

Parameter TD cannot be so easily interpreted as parameters DS and TDS.

Table 2

Estimated parameters of diversification of enterprises

ENTERPRISE	TD	DS	TDS
I	0	0	0
II	0	0	0
III	0.447	0.937	2.812
IV	0.292	0.971	1.942
V	0.602	1	4

5. Conclusions

Application of the entropy is a useful form of quantitative analysis of diversification level of firm or production process. The well-known different parameters based on entropy concept makes possible application for different types of firms/diversifications.

Activities of firms can be compared each other. Moreover dynamics of diversification can be analyzed quantitatively for the given firm. Scale of distribution can be compared with parameters of economic growth of firm in considered country/region or area of activity.

Product diversification for machinery industry increase range of activity of enterprise and leads to change technology, create new knowledge, growth co-operation between suppliers and consumers and open a new markets.

Analysis of process of diversification by applying the entropy parameters show, that if analyzed enterprises makes decisions of diversification, it is reduced to two or maximal three segments. Due to characteristics of machinery industry, enterprises usually applied horizontal diversification, which is good for stability and growth of firm and concentric diversification. These two types of diversifications are not so high in risk than the conglomerate one, when effects coming from finance synergy may be not enough. Realization of innovation projects, which realize the market requirements may has positive influence of growth of machinery industry.

The advantage of diversification of production in machinery industry is distribution of risk of firm activity. It is very important for enterprise to define the main area (product/products) of activity, and then start process of diversification.

References

[1] Ansoff H.I., *Strategic managament*, Palgrave Macmillan, New York 2007.

[2] Chandler A.D. Jr, *Strategy and structure: Chapters in the history of American Industrial Enterprises*, MIT Press, Cambridge, Massachusetts 1962.

[3] Chandler A.D. Jr, *The visible hand: The managerial revolution in American Business*, Harvard University Press, Cambridge, Massachusetts 1977.

[4] Chatterjee S., Blocher J.D., *The Continuous measurement of firm divessification: Is it robust?*, Journal of the Academy of Management, vol. **35** (4), 1992, 874-888.

[5] Jacquemin A.P., Berry C.H., *Entropy measure of diversification and corporate growth*, Journal of Industrial Economics, vol. **27** (4), 1979, 359-369.

[6] Kotler P., Armstrong G., *Marketing: Can Introduction*, Prentice-Hall International Inc., New Yersey 2008.

[7] Kozień E., Kozień M.S., *Wybrane modele fizyki matematycznej w zarządzaniu*, Wyd. PK, Kraków 2014 [in Polish].

[8] Oyedijo A., *Effects of product – market diversification strategy on corporate financial performance and growth: an empirical study of some companies in Nigeria*, American International Journal of Contemporary Research, vol. **2** (3), 2012, 199-210.

[9] Palepu K., *Diversification strategy, profit performance and entropy measure*, Strategic Management Journal, vol. **6**, 1985, 239-255.

[10] Pearce J.A., Robinson R.B., *Strategic management*, McGraw-Hill, New York 2007.

[11] Pierścionek Z., *Strategie rozwoju firmy*, PWN, Warszawa 1996 [in Polish].

[12] Ramanujam V., Varadarajam, Robinson R.B., *Research on corporate diversification: A synthesis*, Strategic Management Journal, vol. **10** (6), 1989, 523-551.

[13] Rangunathan S.P., *A refinement of the entropy measure of firm diversification: toward definitional and computational accurancy*, Journal of Management, vol. **21** (5), 1995, 989-1002.

[14] Rumelt R.P., *Divesification strategy and profitability*, Strategic Management Journal, vol. **3**, 1977, 359-369.

[15] Theil H., *Economics and information theory*, North-Holland, Amsterdam 1967.

[16] Thompson A.A., Strickland A.J., Gamble P., *Strategic management. Crafting and executing strategy*, John Wiley & Sons, London 2008.

TECHNICAL TRANSACTIONS | **CZASOPISMO TECHNICZNE**
MECHANICS | MECHANIKA
4-M/2016

MARIUSZ PIETRASZEK*, TOMASZ KLEMBA*, JOANNA LUBIENIECKA*,
JERZY ŁUKASIEWICZ*, JACEK PIETRASZEK**

COMPARATIVE STUDY OF AN ADDITIONAL OXIDIZER CHARGE EFFECT ON SELECTED OPERATIONAL CHARACTERISTICS OF A SOLID-FUEL ROCKET ENGINE

BADANIA PORÓWNAWCZE WPŁYWU ŁADUNKU DODATKOWEGO UTLENIACZA NA WYBRANE PARAMETRY PRACY SILNIKA RAKIETOWEGO NA PALIWO STAŁE

Abstract

This paper describes a part of research related to the elimination of adverse phenomenon involving the occurrence of a negative oxygen balance of combustion products of missile engines during their firing from aircrafts. It also presents the results of comparative tests of rocket engines equipped with an additional oxidizer charge.

Keywords: oxygen balance, *rocket engine*, *aircraft*, *oxidizer charge*

Streszczenie

Artykuł opisuje fragment badań związanych z eliminowaniem niekorzystnego zjawiska polegającego na występowaniu ujemnego bilansu tlenowego produktów spalania silników pocisków rakietowych podczas ich odpalania ze statków powietrznych. Przedstawiono również wyniki porównawcze badań silników rakietowych wyposażonych w dodatkowy ładunek utleniacza.

Słowa kluczowe: bilans tlenowy, *silnik rakietowy*, *statek powietrzny*, *utleniacz*

DOI: 10.4467/2353737XCT.16.234.5983

* Ph.D. Eng. Mariusz Pietraszek, M.Sc. Eng. Tomasz Klemba, M.Sc. Eng. Joanna Lubieniecka, M.Sc. Eng. Jerzy Łukasiewicz, Air Force Institute of Technology.

** D.Sc. Ph.D. Eng. Jacek Pietraszek, Assoc. Prof., Department of Software Engineering and Applied Statistics, Faculty of Mechanical Engineering, Cracow University of Technology.

1. Introduction

Intensive development of air force weapons technology forces the integration of the newly formed systems with the systems already used on aircrafts. This involves conducting a series of tests designed to confirm the efficiency and safety of use of a given armament system [15].

One of the many tested aircraft characteristics of missiles is their impact on the carrier. It is required that fired missiles do not hinder the flight of the aircraft which carries them and do not negatively affect the work of other on-board systems [5, 8, 9]. One of the cases of adverse effects of the fired rocket on the carrier is the impact of the powder gas stream of the rocket engine on the operation of aircraft turbine engines, which can lead to, among others, the engine's compressor stall [4, 13].

This phenomenon was encountered in the case of rockets with engines powered with high--energy solid fuel with a negative oxygen balance. The products of such fuels combustion are rich in unburned carbon and hydrogen molecules. Moreover, their temperature is around 1200 K [3]. The result is their immediate secondary burning out in the atmosphere behind an engine jet, which causes the lack of oxygen behind the flying rocket [2]. In the case of the firing of missiles series in flight, a zone of heated air deprived of oxygen propagates. Its effect on the aircraft may cause compressor stall, which may lead to the carrier's engine stall [6, 14].

In order to prevent the compressor stall, works on the engine missile modification were undertaken. However, due to economic reasons, minor design changes that would not alter significantly aerodynamic and ballistic characteristics of the missile were allowed. Therefore, it was decided to undertake works aimed at changing the oxygen balance of powder gases of the rocket engine without modifications to the powder pulp composition.

2. Theoretical analysis

The introduction of the oxidizer charge into the combustion chamber changes the oxygen balance of rocket fuel products. This method allows for changing the energy characteristics of the rocket engine combustion products (mainly temperature) without modifying the structure of the essential engine units and components like a chamber, a jet, an igniter and does not substantially modify the characteristics of internal ballistics (operating pressure and unit pulse).

The comparison of the after-combustion reaction using an oxygen from the air, without an additional oxidizer

$$2CO + 3H_2 + 2OH + 2\left(O_2 + \frac{0.79}{0.21}N_2\right) \Rightarrow 2CO_2 + 4H_2O + 2\frac{0.79}{0.21}N_2 \tag{1}$$

with the after-combustion reaction using the additional oxidiser in a form of the salt charge K_2SO_4

$$K_2SO_4 + 2CO + 3H_2 + 2OH + 2\left(O_2 + \frac{0.79}{0.21}N\right) \Rightarrow$$
$$2CO_2 + 3H_2O + H_2S + K_2O + 2O_2 + 2\frac{0.79}{0.21}N_2 \quad (2)$$

gives a qualitative picture of the oxygen balance improvement for rocket engine after--combustion reaction products. These stoichiometric dependencies do not reflect the entire complexity of the actual combustion with after-combustion reaction but they enable conducting the qualitative analysis.

Taking into account the characteristics of nitro-polymer fuel used in the rocket engine, potassium salts were analyzed as an oxidizer charge material since they are inhibitors of spontaneous ignition initiation of hot hydrocarbons formed from mixing with the atmospheric air. Decomposition reactions of potassium salts are endothermic, which makes it possible to use them as after-combustion flame dampers. In practice, these salts may be introduced into the composition of the fuel charge as an additive or as a separate, external charge placed in the rocket engine's combustion chamber. The literature data show that the use of the oxidizer additive as a component of the rocket engine fuel will completely extinguish the after-combustion flame for the entire engine operation time, using potassium nitrate in an amount of 1.14% of fuel weight or 4% of potassium sulphate charge.

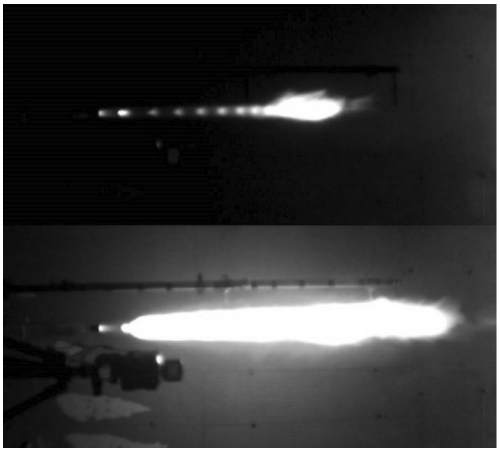

Fig. 1. Comparison of thermograms with corresponding moments of engine operation with the K_2SO_4 oxidiser charge (above) and without one (below)

In the case when an oxidant was used as the external load placed in the combustion chamber, the effect of complete extinguishment lasts for a time comprising 20% of the rocket engine's total operation time. In this latter solution, the much shorter extinguishment time is due to the fact that it is placed in front of the fuel combustion zone, where the temperature of gases is about 2700 K, which is much higher than the K_2SO_4 decomposition temperature (1962 K acc. to [1]). Under such conditions, this distribution can be very intense and its duration will be a function of the radial thickness of the potassium sulphate

charge. The comparison of the fuel charge thickness to the thickness of K_2SO_4 charge ratio amounting to 2.75 shows that the rate of movement of the K_2SO_4 charge combustion front is higher than the fuel burning rate [12].

Figure 1 shows the effect of the developed after-combustion flame damper of the operating rocket engine for the same times from the moment of starting the engine [16].

3. Materials and methods

The research conducted by the authors involved determining:

- ballistic characteristics of rocket engines; it was conducted on a horizontal dynamometer (Fig. 2);
- changes in the exhaust gas temperature of the engines using the FLIR SC6000 HSDR thermographic system;
- changes in the initial and maximum speed on a flight path using a Doppler radar.

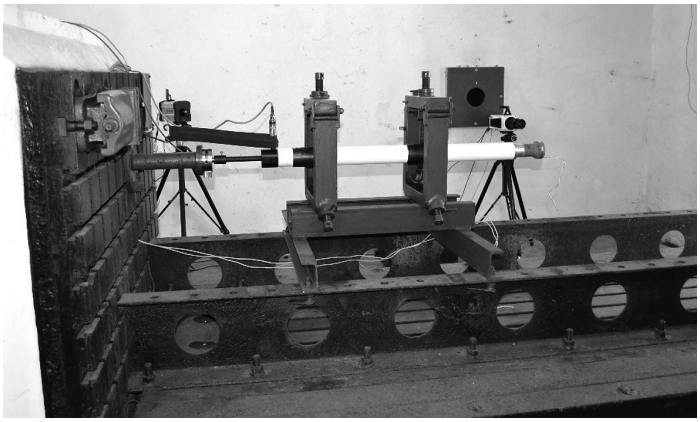

Fig. 2. Test stand with a mounted powder charge

The salts of potassium sulphate (K_2SO_4) were selected for ballistic characteristics tests and the process of their execution was developed [17]. In the developed process, the potassium sulphate charge is a glue of mouldings in the form of bushings embedded on a stainless steel rod. The mouldings were made of granulate, in which potassium sulphate grains were coated with a binding substance. The granulate structure was developed on the basis of trials. At the same time, minimizing the content of binding agents and obtaining appropriate physical properties of the moulding were aimed at [10]. In the course of comparative tests, two types of charges and various engine powder charge grindings were used, which aimed at reducing the maximum pressure in the combustion chamber by increasing its volume.

The placement of the K_2SO_4 charge in the rocket engine is shown in Fig. 3. The exact configuration of five rocket engines for tests is as follows:

a) powder charge no. 1: batch of 2015, grinding 3.50, K_2SO_4 rod weight: 133.39 g;
b) powder charge no. 2: batch of 2015, grinding 3.50, K_2SO_4 rod weight: 133.75 g;

c) powder charge no. 3: batch of 2009, grinding 3.50, K_2SO_4 rod weight: 133.70 g;
d) powder charge no. 4: batch of 2015, grinding 100, K_2SO_4 rod weight: 74.58 g;
e) powder charge no. 5: batch of 2015, grinding 60, K_2SO_4 rod weight: 74.42 g.

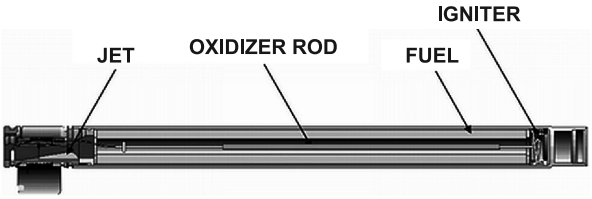

Fig. 3. Cross-section of the rocket engine with the K_2SO_4 charge

During measurements, the following parameters were studied:

– $P_{(t)}$ [MPa] – pressure course in time;
– $R_{(t)}$ [kN] – R draught force course in a function of time;
– t_p [s] – product operation time;
– I_c [kNs] – total draught force impulse;
– $R_{śr}$ [N] – average draught force;
– $\Delta R/R_m$ – draught force moment deviation;
– T_g [°C] – exhaust gases temperature;
– t_g [s] – K_2SO_4 rod operation time.

The results of tests of powder charges' ballistic parameters are shown in Table 1.

Table 1

Ballistic parameters tests results (source: [7])

Item	P_{max}	I_c	$R_{śr}$	t_p	Ratio R	Ratio t	Comments
	[MPa]	[kNs]	[KN]	[s]			
	15.5	min. 6.7	6 ± 0.25 kN	min. 0.9	min. 1.1	min. 1.1	Values required in TC
1	11.22	5.6	5.30	0.97	1.87	0.95	Chamber's tear
2	11.79	6.8	6.61	1.00	1.74	1.10	
3	11.18	6.8	6.07	1.05	1.67	1.17	
4	12.96	7.0	6.86	0.97	1.87	1.08	
5	11.58	7.0	6.83	1.00	1.85	1.10	

The results, except for the first case when the engine chamber was torn, are consistent with the values specified in the Technical Conditions. However, it is clear that the ballistic characteristics of the engines equipped with K_2SO_4 charges with lower mass are better. This is because, in order to eliminate the occurrence of maximum pressures above permissible values in the case of K_2SO_4 charges with higher mass, a flow cross sectional area was enlarged

by greater graining of an engine charge in the jet area. At the same time, greater engine charge mass decrease occurred.

Thermal-imaging tests results show that the exhaust gas temperatures at an outlet cone zone are virtually identical for each engine and are 500°C–600°C (Fig. 4), while the exhaust gas temperatures during operation of the inhibitor for the engines 1, 2, 3 are similar and oscillate about the temperature of 600°C for 0.3 sec, then rise to 900°C.

For the engines 4 and 5 (both of reduced rod mass), inhibitor working time (temperature 600°C) is shorter and is 0.18 sec (Fig. 5).

During the ground field tests, two missiles equipped with the K_2SO_4 charges with greater mass were fired. The tests, during which the Doppler radar was used, showed that the

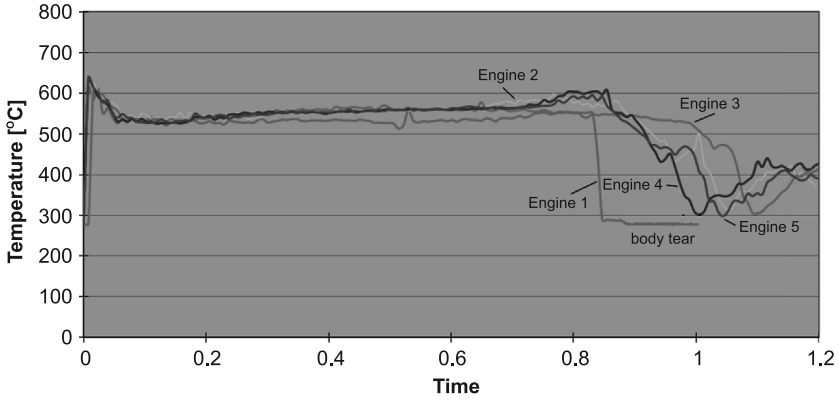

Fig. 4. Exhaust gas temperature changes course in the outlet cone zone

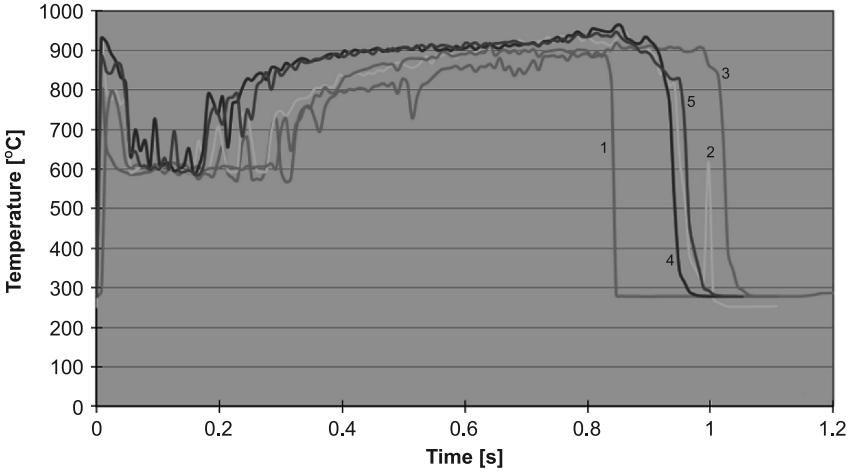

Fig. 5. Exhaust gas temperature changes course in the secondary flame zone: 1 – Engine 1 (grinding 3.5º); 2 – Engine 2 (grinding 3.5º); 3 – Engine 3 (grinding 3.5º); 4 – Engine 4 (grinding 10º); 5 – Engine 5 (grinding 6º)

missile's required initial velocity of not less than 45 m/s decreased to 39.1 and 34.7 m/s, while the maximum velocity of the required value of 650 m/s decreased to the value of 634.1 and 637.8 m/s when using potassium salt charges.

4. Conclusions

The experience gained during the operation of missiles of the same type but different production batches (made on the basis of the same technological documentation) shows that, due to the difference in the quality of the ingredients used in the rocket fuel production process, the threat level of aircraft engine's compressor stall from which the missiles are fired changes. The currently used acceptance tests and the apparatus do not allow to detect the threat at the production stage. For this reason, the authors undertook the task to solve the problem in a global manner using potassium salt charges. The introduction of an additional element in the form of an oxidiser rod into the combustion chamber of a rocket engine powered with rocket fuel results in a significant reduction in the exhaust gases temperature and limiting the degree of rocket engine's gaseous products after-combustion, in particular carbon monoxide.

However, the conducted research shows that this method of limiting flame after-combustion causes changes in the rocket engine's mechanical, dynamic and ballistic parameters. The greater the mass of the used K_2SO_4 charge, and hence the lighter engine powder charge mass (by increasing the combustion chamber's volume), the worse missile's ballistic parameters. Because of this, actions aimed at developing the salt charge with lower mass, hence lower effect on the ballistic parameters, which was confirmed with laboratory tests, were undertaken. The authors plan to conduct supplementary ground field tests using salt charges with lower mass, and then to conduct field tests in flight aimed at confirming finally the K_2SO_4 potassium salt charges' operation efficiency.

References

[1] Yang V., Brill T., Ren W., *Solid propellant chemistry, combustion, and motor interior ballistics*, American Institute of Aeronautics and Astronautics, Virginia 2000.

[2] Torecki S., *Balistyka wewnętrzna silników rakietowych na paliwo stałe*, Wojskowa Akademia Techniczna, 1989 [in Polish].

[3] Leciejewski Z., *Analiza i ocena poprawności metod badań pirostatycznych prochów jedno- i dwubazowych*, Wojskowa Akademia Techniczna, 2010 [in Polish].

[4] Gajewski S.A., Morozow F.N., Tichomirow J.P., *Awtomatika awiacjonnych gazoturbinnych silowych ustanowok*, Wojennoje Izdatielstwo Ministerstwa Oborony SSSR, Moskwa, 1980 [in Russian].

[5] Kurow W., Dołżański J., *Zasady projektowania pocisków rakietowych na paliwo stałe*, MON, Warszawa 1964 [in Polish].

[6] Nieczajew J.N., Fiedorow R.M. et al., *Teoria awiacjonnych dwigatielej*, Wojennoje Izdatielstwo Ministerstwa Oborony SSSR, Moskwa 1980 [in Russian].

[7] Lubieniecka J., Łukasiewicz J., Pietraszek M., Sosnowski M., Tchórznicki K., *Sprawozdanie nr S-14-27/15 z badań układów napędowych pocisków NLPR-70 z ładunkiem soli K_2SO_4*, Instytut Techniczny Wojsk Lotniczych, 2015 [in Polish].
[8] Lubieniecka J., Łukasiewicz J., Pietraszek M., Sosnowski M., *Sprawozdanie nr S-14-13/16 z badań układów napędowych pocisków NLPR-70 z ładunkiem soli K_2SO_4*, Instytut Techniczny Wojsk Lotniczych, 2016 [in Polish].
[9] Żyluk A., *Badania symulacyjne balistyki zewnętrznej lotniczych środków bojowych*, Wyd. ITWL, Warszawa 2009 [in Polish].
[10] Bagrowski J., Kamiński R., *Opracowanie technologii wytwarzania ładunku soli K_2SO_4 do silników rakietowych*, Instytut Techniczny Wojsk Lotniczych, 2011 [in Polish].
[11] Lubieniecka J., Łukasiewicz J., *Sprawozdanie nr S-1/16/2011 z badań układów napędowych 02.000"R1" niekierowanych lotniczych pocisków rakietowych (NLPR70)*, Instytut Techniczny Wojsk Lotniczych, 2011 [in Polish].
[12] Bagrowski J., Kamiński R., Klemba T., *Analiza wpływu stopnia znitrowania nitrocelulozy na bilans tlenowy paliwa rakietowego i określenie parametrów fizyko-chemicznych produktów spalania*, Instytut Techniczny Wojsk Lotniczych, 2011 [in Polish].
[13] Kowalski M., Pietraszek M., Szymczak J., Winczura Z., *Analiza wystąpienia pompażu podczas odpalania pocisków NLPR-70 ze śmigłowca W-3W*, Instytut Techniczny Wojsk Lotniczych, 2011 [in Polish].
[14] Instrukcje użytkowania śmigłowców [in Polish]: *Śmigłowiec Mi-24A, Mi-24D*, Praktyczna aerodynamika, Lo 2011/80, Poznań 1980; *Turbinowy silnik lotniczy TW3-117MT serii 3, Opis techniczny i eksploatacja*, Lot 2855/90, Poznań 1991; *Silnik turbinowy TWD-10B, Instrukcja Eksploatacji Technicznej*, Nr dok 19.0.646, WSK-Rzeszów, 1984.
[15] NO-10-A232:2009 Uzbrojenie lotnicze. Balistyka wewnętrzna silników rakietowych. Badania naziemne [in Polish].
[16] Lubieniecka J., Łukasiewicz J., Tchórznicki K., *Sprawozdanie nr S-14-01/13 z badań układów napędowych pocisków NLPR-70 z ładunkiem soli K_2SO_4*, Instytut Techniczny Wojsk Lotniczych, 2013 [in Polish].
[17] Hawley E., *MK66 Rocket Motor/Helicopter Compatibility Program*, Indian Head Division, 2003.

TECHNICAL TRANSACTIONS | CZASOPISMO TECHNICZNE
MECHANICS | MECHANIKA
4-M/2016

WŁADIMIR ANTONIUK*, JERZY JAROSZEWICZ**, LESZEK RADZISZEWSKI***, ŁUKASZ DRAGUN**

THEORETICAL STRESS ANALYSIS-BASED IMPROVEMENT OF FRICTION CLUTCH DISC MANUFACTURING PROCESS

UDOSKONALANIE PROCESU TECHNOLOGICZNEGO WYTWARZANIA TARCZ SPRZĘGIEŁ CIERNYCH NA BAZIE ANALIZY TEORETYCZNEJ STANU ODKSZTAŁCEŃ I NAPRĘŻEŃ

Abstract

Basic requirements for modern machine elements include the improvement of durability alongside the reduction of the cost of materials. This entails the need for the manufacturing process to ensure a stable geometric form of those elements. This analysis aims at developing loading schemes for the dynamic stabilization stand designed for the straightening of the discs buckled as a result of hardening heat treatment [1, 2].

Keywords: disc manufacturing process, *clutch disc*, *spring ring*, *friction linings*

Streszczenie

Podstawowe wymagania do współczesnych elementów maszyn to zwiększenie trwałości i obniżenie wydatku materiałowego. Wymaga to zapewnienia stabilnej formy geometrycznej elementów w trakcie procesu wytwórczego. Poniższa analiza ma na celu opracowanie schematów obciążenia dla stanowiska do dynamicznej stabilizacji prostowania tarcz, które zostały zwichrowane w wyniku obróbki cieplnej hartowania.

Słowa kluczowe: proces wytwarzania tarczy, *tarcza sprzęgła*, *pierścień sprężysty*, *okładziny cierne*

DOI: 10.4467/2353737XCT.16.235.5984

* D.Sc. Ph.D. Eng. Władimir Antoniuk, Laboratory of Metallurgy in Mechanical Engineering, Joint Institute of Mechanical Engineering of the NAS of Belarus, Minsk.

** D.Sc. Ph.D. Eng. Jerzy Jaroszewicz, M.Sc. Eng. Łukasz Dragun, Chair of Production Management, Faculty of Management, Bialystok University of Technology.

*** D.Sc. Ph.D. Eng. Leszek Radziszewski, Chair of Mechanics, Faculty of Mechatronics and Machine Design, Kielce University of Technology.

1. Theoretical analysis of strains in clutch discs

Maximum ring stresses in the spring result from maximum hub rotation. Figure 1 shows a diagram of a deformed spring.

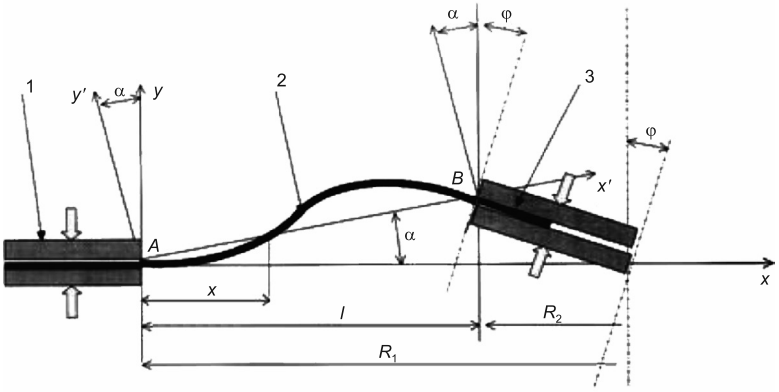

Fig. 1. Disc deformation in the maximum hub rotation plane [1]

The proposed method for stress calculation helps determine stress in any section of the disc. Here, we are interested in the value of maximum stress in the sections of maximum hub rotation and therefore a simplified stress calculation procedure can be used. Fig. 1 shows a diagram of a deformed spring in the section of the maximum angle of rotation φ. From the diagram it follows that with the hub rotation by angle φ, the spring rotates by angle α with respect to point *A*, and at point *B*, the spring rotates with respect to the hub by angle α + φ. The relationships between angles α and φ are the following:

$$\mathrm{tg}\alpha = \frac{R_2}{l}\,\mathrm{tg}\varphi, \tag{1}$$

where:

R_2 – is the inner radius of the spring,

l – is the length of the spring.

Thus, maximum stress in the spring of the clutch disc occurs in the section of maximum hub angle and therefore stress calculation can be conducted only for this section. At the opposite side of the spring, stress will also occur but opposite in sign. In the section perpendicular to that under consideration, the angle of hub rotation is equal to zero and respectively all stresses are equal to zero. With one rotation of the clutch hub, the stresses on one side of the spring change direction into opposite and on the opposite side of the spring they take the value of zero twice [4].

2. Computational load scheme for the disc with a rectangular cross-section

The differential equation of the elastic surface of an annular plate in polar coordinates can have the following form [5]:

$$\left(\frac{\partial^2}{\partial r^2}+\frac{1}{r}\cdot\frac{\partial}{\partial r}+\frac{1}{r^2}\cdot\frac{\partial^2}{\partial\alpha^2}\right)\left(\frac{\partial^2 W}{\partial r^2}+\frac{1}{r}\cdot\frac{\partial W}{\partial r}+\frac{1}{r^2}\cdot\frac{\partial^2 W}{\partial\alpha^2}\right)=\frac{p}{D}, \tag{2}$$

where:

$W = W(r, \alpha)$ – the deflection of the average plane of the plate,
r, α – polar coordinates defining the position of the design point on the average plane,
p – normal pressure on the plate surface,
$D=\frac{Eh^3}{12(1-\mu^2)}$ – cylindrical rigidity of the plate,
h – thickness of the disc,
E – the elastic modulus of the disc material
μ – Poisson's ratio.

Deflection W and pressure p were assumed to be positive in the downward direction. Inner moments – radial moment M_r and turning moment M_t as well as M_{rt} – the moment acting simultaneously in the radial and circumferential directions have the following forms:

$$M_r=-D\left[\frac{\partial^2 W}{\partial r^2}+\mu\left(\frac{\partial W}{r\cdot\partial r}+\frac{\partial^2 W}{r^2\cdot\partial\alpha^2}\right)\right], \tag{3}$$

$$M_t=-D\left[\frac{\partial^2 W}{r\cdot\partial r^2}+\frac{\partial^2 W}{r^2\cdot\partial\alpha^2}+\mu\frac{\partial^2 W}{\partial r^2}\right], \tag{4}$$

$$M_{rt}=-D(1-\mu)\left[\frac{\partial^2 W}{r\cdot\partial\alpha\cdot\partial r}-\frac{\partial W}{r^2\cdot\partial\alpha}\right]. \tag{5}$$

To define boundary conditions we take the condition that the plate is rigidly clamped on the boundary – then deflection W and the inclination angle of the average plane of the maximum angle φ is equal to zero.

$$W=0; \qquad \frac{\partial W}{\partial r}=0. \tag{6}$$

The general solution to homogeneous equation (5) can be expressed as a sum of general W^0 and particular W^-. The general solution of the homogeneous differential equation has the following form:

$$W^0=F_0(r)+\sum_1^\infty F_m(r)\cos m\alpha+\sum_1^\infty f_m(r)\sin m\alpha, \tag{7}$$

Functions will be determined in accordance with the equations analogous to (8). The particular solution W^- of equation (5) is determined in each specific case according to the set law of pressure distribution on the disc surface p.

$$\left.\begin{aligned} F_0(r) &= C_{10} + C_{20}r^2 + C_{30}\ln\frac{r}{R_1} + C_{40}r^2\ln\frac{r}{R_1} \\ F_m(r) &= C_{1m}r^m + C_{2m}r^{-m} + C_{3m}r^{m+2} + C_{4m}r^{-m+2} \quad (m \neq 1) \\ F_1(r) &= C_{11}r + C_{21}r^{-1} + C_{31}r^3 C_{41}r\ln\frac{r}{R_1} \quad (m = 1) \end{aligned}\right\} \tag{8}$$

where:

R_1 – the outer radius of the plate.

3. Equilibrium of the disc center of symmetry

To determine the relationship between the rotation angle of the center of symmetry, φ, and the magnitude of M, the equilibrium of the disc symmetry center is considered in accordance with Figure 2.

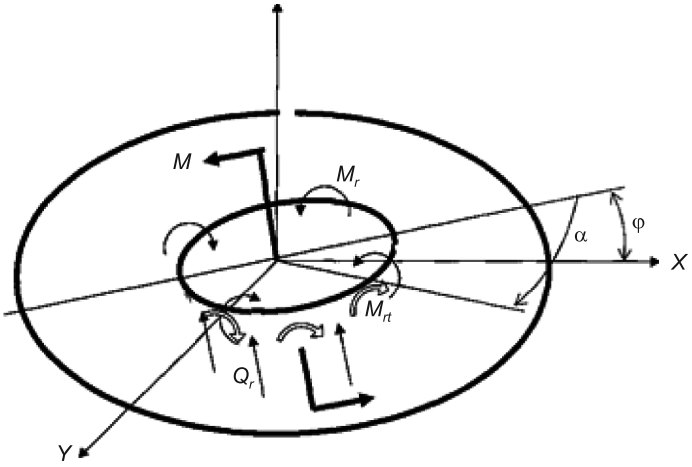

Fig. 2. Moments and forces acting on the rigid center of symmetry [1]

The rigid center is affected by the external moment M, the bending moment M_r distributed along the circumference of the radius R_2, the torsional moment M_{rt} and the transverse force Q_r. On this basis we can write the equation of the moment with respect to axis Y [3].

$$M + \int_0^{2\pi} M_r \cdot R_2 \cdot \cos\alpha \cdot d\alpha - \int_0^{2\pi} M_{rt} \cdot R_2 \cdot \sin\alpha \cdot d\alpha + \int_0^{2\pi} Q_r \cdot R_2^2 \cdot \cos\alpha \cdot d\alpha = 0. \tag{9}$$

Quantities M_r, $M_{rt} = 0$, Q_r are defined based on (3–4). Substituting to equation (9) and taking into account that we obtain $r = R_2$ in the following way:

$$M_r = -\frac{2\varphi \cdot D \cdot (a^2 - 1) \cdot \cos\alpha}{R_2 \cdot [(a^2 + 1) \cdot \ln a - (a^2 - 1)]}, \qquad Q_r = -\frac{2\varphi \cdot D \cdot (a^2 + 3) \cdot \cos\alpha}{R_2 \cdot [(a^2 + 1) \cdot \ln a - (a^2 - 1)]}. \tag{10}$$

Substituting formulas (9) in equation (10), after integration we obtain the formula for the angle of rotation necessary to attain the moment M.

$$\varphi = \frac{M[(a^2 + 1) \cdot \ln a - (a^2 - 1)]}{4\pi \cdot D \cdot (a^2 + 1)}. \tag{11}$$

The analysis indicated that the maximum value of the bending moment is (13) and occurs for coordinates $\alpha = 0$ and $r = R_2$.

$$M_{r\max} = +\frac{M(a^2 - 1)}{2\pi \cdot R_2 \cdot (a^2 + 1)}. \tag{12}$$

Respective maximum stresses occur at the same point of the plate and are equal to:

$$\sigma_{\max} = +\frac{6M(a^2 - 1)}{2\pi \cdot R_2 \cdot h^2 \cdot (a^2 + 1)}. \tag{13}$$

To simplify the calculation, expressions (11), (12), (13) are written:

$$\varphi = \beta_1 \frac{M}{Eh^3}, \quad \sigma_{\max} = \beta_2 \frac{M}{R_2 \cdot h^2}, \quad M = \frac{R_2 \cdot h^2}{\sigma_{\max} \cdot \beta_2},$$

$$\beta_1 = \frac{3[(a^2 + 1) \cdot \ln a - (a^2 - 1)] \cdot (1 - \mu^2)}{\pi \cdot (a^2 + 1)}, \quad \beta_2 = \frac{3 \cdot (a^2 - 1)}{\pi \cdot (a^2 + 1)}.$$

In real service conditions, the coupling between the hub and the friction lining can have certain sensitivity and therefore expressions (11) and (13) must be supplemented with corrective factors, taking into account the sensitivity at those points. Hence, expressions (11) and (13) take the following forms [5]:

$$\varphi = \beta_1 \frac{k_3 \cdot M}{Eh^3}, \quad \sigma_{\max} = \beta_2 \frac{k_3 \cdot M}{R_2 \cdot h^2}, \tag{14}$$

where:

$k_3 = k_{\text{out}} + k_{\text{in}}$, k_{out} – the factor of decreased restraint of the disc on the outside boundary,

k_{in} – the analogous factor on the inside boundary.

We define the value of radius $r = r^*$ at which the stress in the disc is 0. This radius value corresponds to the inflection point of $W(r, \varphi)$, which can be attained using condition (15).

$$\frac{\partial^2 W(r, \varphi)}{\partial r^2} = 0. \tag{15}$$

Substituting (9) into condition (15) we obtain

$$\frac{\varphi}{a[(a^2+1)\cdot\ln a-(a^2-1)]}\left[\frac{2R_2^2\cdot a^2}{r^3}-\frac{6r}{R_2^2}+2(a^2+1)\frac{1}{r}\right]\cdot\cos\alpha=0. \tag{16}$$

Hence, at a random angle α, condition (17) below should be satisfied:

$$\frac{R_2^2\cdot a^3}{r^3}+\frac{a^2+1}{r}-\frac{3r}{R_2^2}=0, \tag{17}$$

which can be converted into the form of the following biquadratic equation:

$$x^4-\frac{1}{3}(a^2+1)\cdot x^2-\frac{1}{3}a^2=0, \tag{18}$$

By solving equation (18), we find the root x corresponding to condition (15):

$$x=\sqrt{\frac{1}{6}\left[1+a^2+\sqrt{(a^2+1)^2+12a^2}\right]}, \tag{19}$$

where the searched radius value of zero stress in the disc is equal to:

$$r^*=R_2\cdot\sqrt{\left\{\frac{1}{6}\left[1+a^2+\sqrt{[(a^2+1)^2+12a^2]}\right]\right\}}. \tag{20}$$

4. Evaluation of the dynamic stabilization results

Table 1 summarizes the basic parameters of clutch discs on which dynamic stabilization was performed and for which the following results were obtained.

Table 1

Test results

Geometric parameters [mm]				Spring ring material	Accuracy of work surface [mm]			
					Before modification		After modification	
D	D1	D2	b		Flatness deviations	Runout	Flatness deviations	Runout
350	126	210	2	steel 45	up to 1.7	up to 2.5	0.4…0.5	0.6…0.8
340	136	210	2	steel 50	up to 1.7	up to 2.5	0.4…0.5	0.6…0.8
445	215	240	2.4	steel 45	up to 2.0	up to 3.2	0.4…0.6	0.6…0.9
316	137	156	2	steel 65H	up to 1.7	up to 2.5	0.4…0.5	0.6…0.8

5. Summary

In order to improve the geometry of clutch discs in which after heat treatment and assembly with the hub and friction linings, the spring ring exhibited considerable flatness deviations and runout of the friction surfaces, measured on the working surface, normalization of the final assembly operation is proposed – dynamic stabilization. The results of the tests indicate that the runout is reduced from 3 mm to 1 mm, which results in the decrease in the friction moment from 10 Nm to 3.5 Nm, and which occurs despite complete disengagement of the disc linings from the flywheel. Operation tests at the Tractor Factory in Minsk (Belarus) confirm that the clutch discs subjected to dynamic stabilization yield 30% higher durability and consequently, smaller number of failures.

References

[1] Antonjuk V.E., *Dynamic stabilization of geometrical parameters of details with alternating*, Minsk: «Technoptint», 2004, 184 s.
[2] Sandomirski S., *Primeneniye polyusnogo namagnichivaniya v magnitnom strukturnom analize (obzor)*, Defektoskopiya, vol. 9, 2006, 36-64.
[3] Timoshenko G., Woinowsky-Krieger S., *Teoria płyt i powłok*, Arkady, Warszawa 1963.
[4] Antonjuk V.E., Sandomirski S., Jaroszewicz J., *Issledovaniye vozmozhnostey otsenki ostotochnykh napryazheniy po gradiyentu polya ostotochnoy namagnichennosti*, Energia w Nauce i Technice, Oficyna Wydawnicza Politechniki Białostockiej, Białystok 2014.
[5] Hoerbiger Lamellenhandbuch – A5K113/HOERBIGER Antriebstechnik GmbH // www.hoerbiger.com/ Publikationen.255.0.html?&L=6 [date of access: 07.10.2010].

TECHNICAL TRANSACTIONS | **CZASOPISMO TECHNICZNE**
MECHANICS | MECHANIKA
4-M/2016

DARIUSZ KARPISZ*

THE QUALITY OF IMPLEMENTATION OF MANUFACTURING ICT – SELECTED PROBLEMS

JAKOŚĆ IMPLEMENTACJI PRZEMYSŁOWYCH SYSTEMÓW INFORMACYJNYCH – WYBRANE PROBLEMY

A b s t r a c t

The paper presents models for designing of information systems for manufacturing. Chosen model of system implementation has a significant impact on the quality and performance of the target solution. Special focus is on the data model layer and the possibility of changing the standard three-tiered model of information systems through increased utilisation of resources of database server.

Keywords: manufacturing ICT, *databases*, *n-tier models*, *database-centric architecture*

S t r e s z c z e n i e

W artykule przedstawiono modele projektowania systemów informatycznych do zastosowań przemysłowych. Wybrany model implementacyjny ma istotny wpływ na jakość i wydajność docelowego rozwiązania. Szczególnie skupiono się na warstwie modelu danych i możliwości zmiany standardowego modelu trójwarstwowego systemów informacyjnych przez większe wykorzystanie zasobów serwera baz danych.

Słowa kluczowe: przemysłowe systemy informacyjne, *bazy danych*, *model wielowarstwowy*, *architektura zorientowana na dane*

DOI: 10.4467/2353737XCT.16.236.5985

* Ph.D. Eng. Dariusz Karpisz, Institute of Applied Informatics, Faculty of Mechanical Engineering, Cracow University of Technology.

1. Introduction

The specific conditions for using information systems in industrial applications should generate the appropriate design and implementation patterns. The variety of software such as CAD/CAM/CAE causes many difficulties in cooperation among themselves and with other systems such as ERP or CRM. It would seem that over the years of progress of computer science, in the domain such as ICT (Information and Communication Technologies) [1, 2] there were made the right choices in the areas of hardware, software and its integration. The fact is that IT corporations use the standardized models to deliver products to market as soon as possible in order to maximize the ROI (Return of Investment) regardless of different industry requirements. These standard models are correct, however, maximization of performance for targeted ICT solutions is not applicable to them. Presented in article multilayered models of systems are used for rapid software developing for IT companies. This can be achieved due to the possibility of segregating of work and partial code generation, mainly resulting from the application templates and data models without consideration of the specific needs in industry.

2. Methods of implementation ICT in Manufacturing

The main aspect in the ICT systems designing, both single application and composed of separate cooperating programs are multi-layer models.

2.1. *n*-Tier Architecture

Due to solutions for logical separation of information systems there are set single-, two-, three- and multi-tiered models known as *n*-Tier Architecture [3]. All of these models consist of three types of functional modules:

– *presentation module* – translation, presentation of tasks and results to the user (called also as User Interface – UI),
– *logic module* – control of an application functionality and process flow (called as Business Logic),
– *data module* – data persistence mechanisms and data access layer.

Within the single-tier model all tasks associated with storing data and data manipulation, business logic, data presentation and user interface generating are supported on a single computer.

Within the two-tier model, presentation layer and business logic are executed on the client's workstation, and the data is stored in a separate, dedicated database server. In this mode data can be shared by many customers as opposite to single-tier model.

Within the three-tier model there is performed only presentation layer at the Client Machine (usually in the form of access via a Web browser or Java application) while the main functionality is supported by the Application Server. In this mid-range layer there is implemented full business logic along with application layer access to data stored on a dedicated server – Database Server with Database Management System (DBMS).

Progress in Object-Oriented Programming (OOP) drove a significant acceleration of the development of applications as well as expansion of business logic and design of application based on functional model. An integral part in this approach implemented in ntiers model is Object-Relational Mapping (ORM) mechanism to connect classic relational data model [4] (or other data models [5]) with class structure of OOP application. Using ORM and OOP moved data oriented design to the business logic design.

2.2. Architecture of Manufacturing Systems

Manufacturing Systems are most expanded domain of ICT. In fact, most of the software and hardware is part of a Three-tiered model however much more advanced. On Fig. 1 is a model example of ICT used in the preparation of production. Classic CAM software can be treated as One-tired model excluding license servers. In more advanced systems there is often used Product Lifecycle Management software (PLM) which acts as an intermediate layer in access to detailed data that is available on the Database Server. There are also used specialized databases such as materials databases used in Simulation-Based Engineering [6]. Additional software to support the design and production planning [7] and quality management [8] are used in specific areas of manufacturing. Such software use normally the same shared database server to support thematic databases.

Local or central databases are used in all of the modules of complex industrial systems. Despite this fact, the designing of systems following the bottom-up concept from data model to UI is not popular.

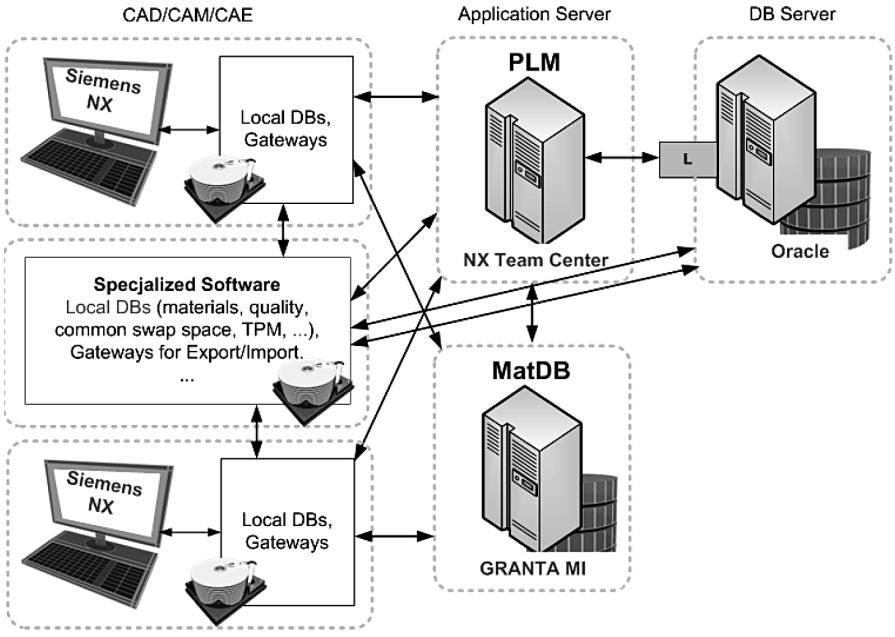

Fig. 1. Example application model using in CAM/CAE systems

2.3. The Problem: Fast Implementation or Quality/Performance

Figure 2 provides an overview on the design, implementation and application of information systems. In the three-tier model the highest investments are incurred for database servers and high-speed dedicated storage. It is therefore always a layer with the highest efficiency. The presentation layer in the form of hardware and software supporting e.g. WWW interface is the cheapest part of the investment and potentially of the smallest performance.

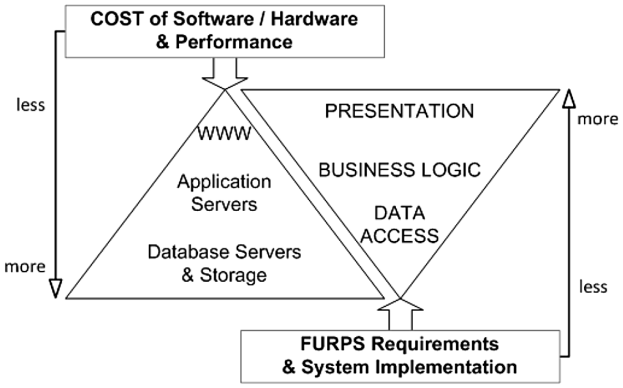

Fig. 2. Dependencies between Architecture of ICT and Implementation Process

Fast alignment of the product compliance with client's expectations, usually defined as a set of functional requirements (Functionality in FURPS Method) is delivered due to enhanced UI and advanced business logic. The extensive use of OOP and ORM techniques results in insufficiency within the definition of the data model. The vast majority of requirements is then moved to the presentation services with low performance hardware instead of using User Defined Functions (UDFs) which are executed in more powerful servers and storage systems. It seems obvious that such an approach is incorrect.

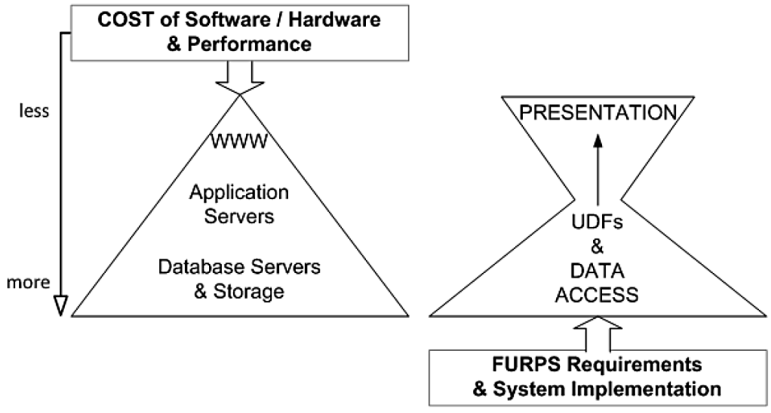

Fig. 3. Database-centric Architecture used for enhanced utilization of resources

Due to use of solutions such as trigerrs and UDFs it is possible to move a number of mechanisms implemented in the presentation layer and the business logic directly to database servers for execution (Fig. 3). Given approach is known as Database-centric Architecture [9] allowing better utilization of resources.

3. Solutions and Results

Based on materials database example (Fig. 4) consisting of a standard set of tables Materials and Factors remaining in the multi-value relationships self-organizing database can be built. As previously mentioned, software such as CAD/CAM/CAE use a local databases e.g. tools, tooling systems, materials, configurations. Below is sample description of material in the local database for Siemens NX:

DATA|MAT0_00266|7050|ALUMINUM|75-150 HB|ALUMINUM ALLOYS, WROUGHT -

Normally, in order to supply the system CAM with real data, it is required to manually edit the database files, use the GUI or use PLM. Additional software layer is also used within the application server to synchronize data. On the other angle, having ability to use specialised systems for production support [5] it may be worth considering adding to the data model procedures, which will automatically generate code row for CAM.

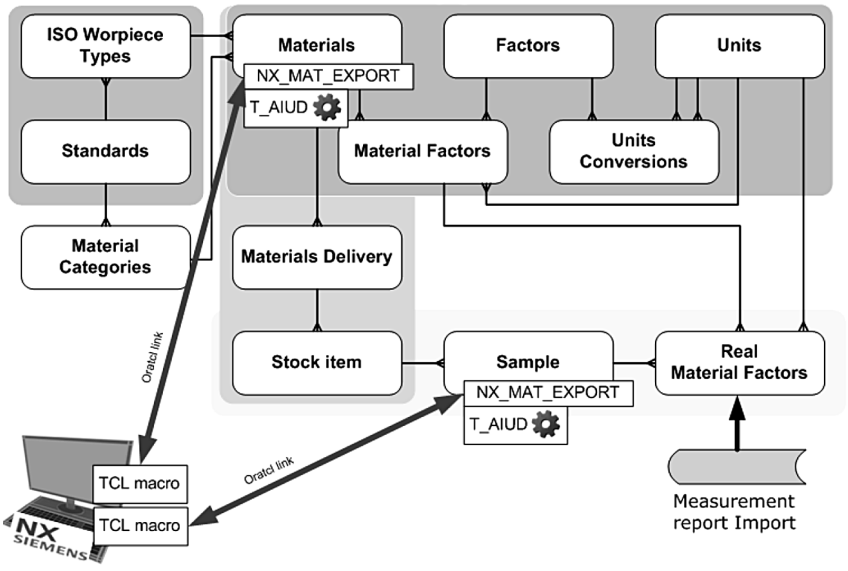

Fig. 4. Example of materials database using to auto-generate CAM material database row

Fig. 4 presents a table with *Materials* and *Samples* (of materials) with added column *NX_MAT_EXPORT* to store Siemens NX row with material description. The *T_AIUD* is a trigger of After Insert or Update, or Delete type which automatically responds to data editing and inserts text for *NX_MAT_EXPORT* column. It is the most advanced model for

data preparation which is to be exported to other systems outside the database server. Data prepared in this way does not require any additional software to its translation, but only macroprocedures within CAM workstation (e.g. as a script in Tool Command Language – TCL). In this case, the database connection can be implemented directly by the Oratcl library and is invisible to the user.

In this paragraph there will be presentation of transition from the classical approach to Database-centric Architecture base on advanced triggers and UDFs mechanisms. The base query is a request from Application Server for a preparation of specific material row for the NX System:

```
select * form MATERIAL where MAT_NX_MATCODE = 'MAT9_00500';
```

The most powerful solutions of this problem is the use of UDF:

```
select NX_MAT_EXPORT('MAT9_00500') from dual;
```

or the specific trigger *T_AIUD* executed in *NX_MAT_EXPORT* column:

```
select NX_MAT_EXPORT from NX_MAT_EXPORT
where MAT_NX_MATCODE = 'MAT9_00500';
```

The final result:

```
DATA|MAT9_00500|500T|ARMOX STEEL|480-540|High Hardness Armor Alloing Steel
```

The last solution requires only reading of the final row for export to the CAM workstation. Data preparation can be several times faster than in the case of translating raw data on the application server. In all cases presented applications use standard request of data – SQL query. There is no need for any additional techniques for calling functions type of UDFs from the applications connecting to the database. In fact, every procedure or function can be requested in form of query in advanced database servers like Oracle so the transfer of part of the functionality associated with parsing, checking whether the translation of data for export to a variety of systems that do not require changes in the way the programming and data retrieval.

References

[1] U.S. Access Board, *Information and Communication Technology (ICT) Standards and Guidelines*, Notice of Proposed Rulemaking, 36 CFR Parts 1193&1194, United States Access Board, 2015.

[2] Tongia R., Subrahmanian E., Arunachalam V. S., *Information and Communications Technology for Sustainable Development, Defining a Global Research Agenda*, Allied Publishers, Bangalore, 2005, 19-41.

[3] Fowler M., *Patterns of Enterprise Application Architecture*, Addison Wesley, 2002.

[4] Codd E.F., *A Relational Model of Data for Large Shared Data Banks*, Communications of the ACM, Vol. 13, No. 6, 1970.

[5] Karpisz D., *Relational Data Model is Not Only One*, Technical Transactions, Vol. 4-M1, 2011, 187-194.

[6] Stojek M., Pietraszek J., *Simulation-Based Engineering Science Challenges of the 21st Century*, Applied Mechanics and Materials, Vol. 712, 2015, 3-8.

[7] Gawlik J., Kiełbus A., Karpisz D., *Application of an Integrated Database System for Processing Difficult Materials*, Solid State Phenomena, Vol. 223, 2015, 35-45.

[8] Gawlik J., Kiełbus A., *Application of artificial intelligence in supervising the technological equipments and quality of products*, The Practice of Quality Management of the 21st, Wydawnictwo Naukowe PTTŻ, Kraków 2012.
[9] Babers C., *The enterprise architecture sourcebook*, Vol. 2, Data-Centric Architectures, El Paso 2006.

TECHNICAL TRANSACTIONS | CZASOPISMO TECHNICZNE
MECHANICS | MECHANIKA
4-M/2016

MAREK KRYNKE*

NUMERICAL ANALYSIS OF BOLTS LOADING IN SLEWING BEARING

ANALIZA NUMERYCZNA OBCIĄŻENIA ŚRUB W ŁOŻYSKU WIEŃCOWYM

A b s t r a c t

This article analyzes screw connection of slewing bearings to various structures of support elements. The susceptibility of support elements to the load distribution in particular bearing screws was examined by means of the Finite Element Method. The load values of screws and their distribution around the perimeter of the combined bearing rings were also specified.

Keywords: slewing bearings, *bolt connections*, *load capacity bearings*

S t r e s z c z e n i e

W niniejszym artykule dokonano analizy połączenia śrubowego mocującego łożysko wieńcowe do różnych struktur jego zabudowy. Korzystając z metody elementów skończonych, zbadano wpływ podatności podzespołów wsporczych na rozkład sił przypadających na poszczególne śruby mocujące łożysko. Określono wartości obciążenia śrub i ich rozkład po obwodzie łączonych pierścieni łożyska.

Słowa kluczowe: łożyska wieńcowe, *połączenia śrubowe*, *nośność łożysk*

DOI: 10.4467/2353737XCT.16.237.5986

* Ph.D. Eng. Marek Krynke, Institute of Production Engineering, Faculty of Management, Czestochowa University of Technology.

1. Introduction

In the construction of heavy machinery, large-size bearings called slewing bearings are used to embed the body performing the rotation motion on the chassis. These bearings are connected to the seats of a work machine with a pre-tight bolted joints. Fastening the screws of slewing bearing rings to supporting structures is an important piece of the entire mechanism of rotation which to a large extent affects the rigidity of bearing rings, while bolts strength often determines the carrying capacity of the entire working system [8, 10].

Methods which are available in the literature for determining the slewing bearings load capacity often do not include the impact of susceptibility of supporting components and the bearing mounting bolts [1, 6]. These factors can only be taken into account by using numerical methods.

The main cause of screw connections failure during the life of slewing bearings is believed to be, besides material cause, insufficient rigidity of load-bearing elements in substantial warping of the contact surface of the flange. In fact, a lot of devices, because of the limitation of the height of the rotary node, fails to construct a sufficiently rigid framework stiffness which does not change by leaps and bounds, which is the cause of the distribution forces occurrence in the bearings considerably different from the projected. This is confirmed by a series of experimental and simulative research presented in the works [2, 3, 5, 9].

In this chapter, distributions of forces in each slewing bearing fastening screws which are built in different support components have been presented and compared (Fig. 1). Also, points of excessive load carried by bearing which is working in components that do not provide adequate support for the slewing bearing have been indicated.

2. Subassembly support and slewing bearing

There are several constructions of support subassemblies which have a differentiated structure, shaped by reason of the load carried, type of installation, etc. This analysis focuses on three different support components (Fig. 1). The supporting structures are different from each other in the fitting of slewing bearing. The first and second support component consists of a plate mounted on stringers which are made of plates welded together to form a closed cross section box (Fig. 1a, b). In the third subassembly, a ring girder in the form of a thick--walled sleeve with a flange for mounting the bearing is used instead of a plate. All the three support frame substructures have two planes of symmetry.

For the calculation, a catalog of single row slewing ball bearing of four-point contact is assumed (Fig. 2) [7]. In this bearing, there is one row of balls and each ball cooperates with two pairs of raceways.

The study analyzed bearings with the following parameters:

- rolling diameter d_t = 1400 mm,
- balls diameter d = 40 mm,
- balls number z = 84,
- coefficient of balls to the raceway adhesion k_p = 0,96,
- nominal contact angle $\alpha_0 = 45°$,

– raceway hardness – 54 HRC,
– number of fastening screws – 36 screws M24-10.9 in each ring.

In addition, it was assumed that:

– raceway surfaces and the rolling elements have an ideal shape, and all parts of the roller have the same diameter,
– materials of rings and rolling elements are homogeneous and isotropic.

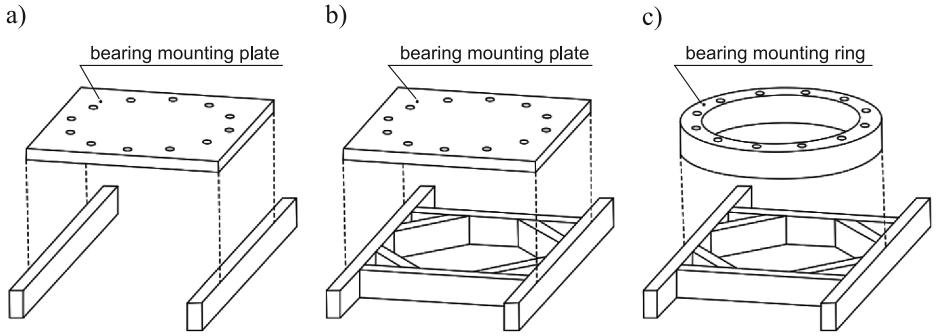

Fig. 1. Frame without gussets near mounting holes requires thicker plate1 – model (a), Gussets added near bearing mounting holes increase rigidity – model V2 (b), Gussets added near mounting holes and ring replace plate for additional rigidity – model V3 (c)

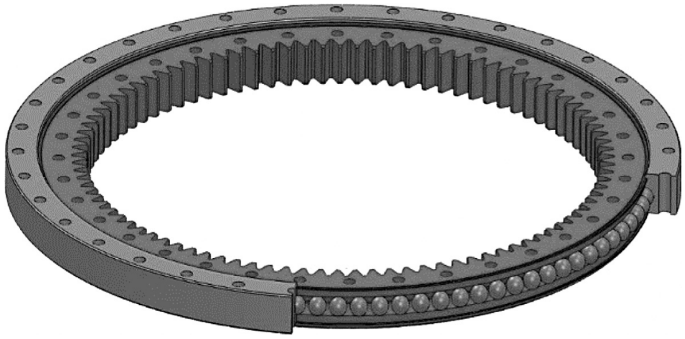

Fig. 2. Four-point contact ball slewing bearing

3. Numerical computations

Slewing bearing is a complex structure. The computational model of the bearing was made by means of the Finite Element Method (Fig. 3) [4]. The slewing bearing uses a large number of contact zones (sometimes hundreds). To avoid an undesired increase tin he size of the numerical model, a part of the rolling bearing is replaced by the so-called super--elements introduced, among others, in [8]. The main portion of the super-element is a rod element with a nonlinear characteristic which is determined on the basis of a substitute characteristics of contact zone [2].

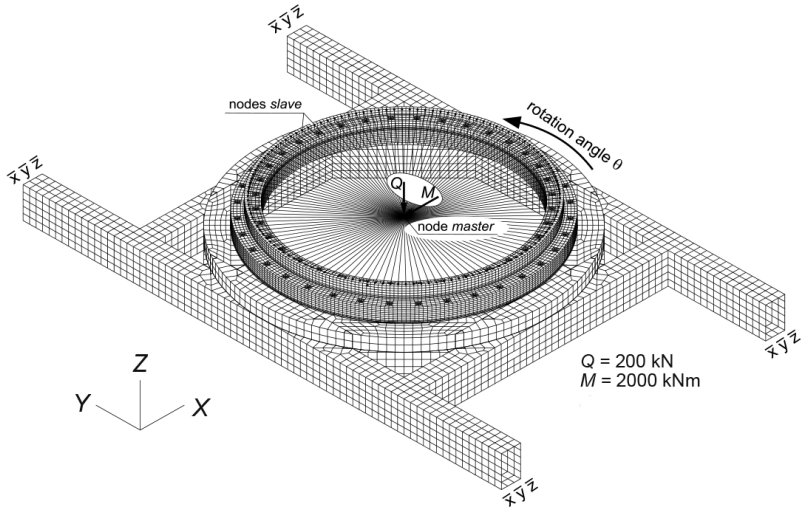

Fig. 3. FEM model of the subassembly support and slewing bearing with boundary conditions marked

For the discretization of bearing rings, plate and girder ring gear, 8-node type components 3D-SOLID were used. The discretization of stringers components in subassembly support was made by means of shell elements such as SHELL. In the geometric models, only the most important elements that affect the rigidity of load-bearing frames were included. In this study, it was assumed that the bolts are modeled by means of special beam elements, which can be attributed to founded preload [4]. In addition, the following simplifications were introduced:

– all walls and ribs were decided to be considered as the surfaces,
– gear of bearing rings was omitted,
– minor construction details, such as sealing grooves, lubricants holes, etc. were omitted.

One of the bearing construction girders, which is associated with the support component, is called the support girder. The load is applied to the second grider called the load girder. Conditions were defined between the respective surfaces of the bearing rings and the surfaces of his mounting contact.

4. Analysis of the obtained results

Calculations were performed for all the three computational models designated as V1, V2 and V3. The purpose of the calculations was to determine the forces acting on individual parts of rolling bearing and bolts that attach the bearing to the support structures. This chapter focuses on the analysis of the screw connection, while the load range of the rolling elements was addressed in work [4]. In the analyzed types of supporting structures (V1, V2, V3), different positions of the body during its rotation angle θ are included. With the use of the symmetry of tested models, analyzes were performed for the angle $\theta = 0 – 90°$. The load

which was adopted for the calculation was the axial force Q = 200 kN, and a cranky moment amounted to M = 2000 kNm. This is the limit load resulting from the sheet characteristic of load ratings [7].

Figure 4 shows the maximum load of the bearing mounting screws as a function of the position of the load girder.

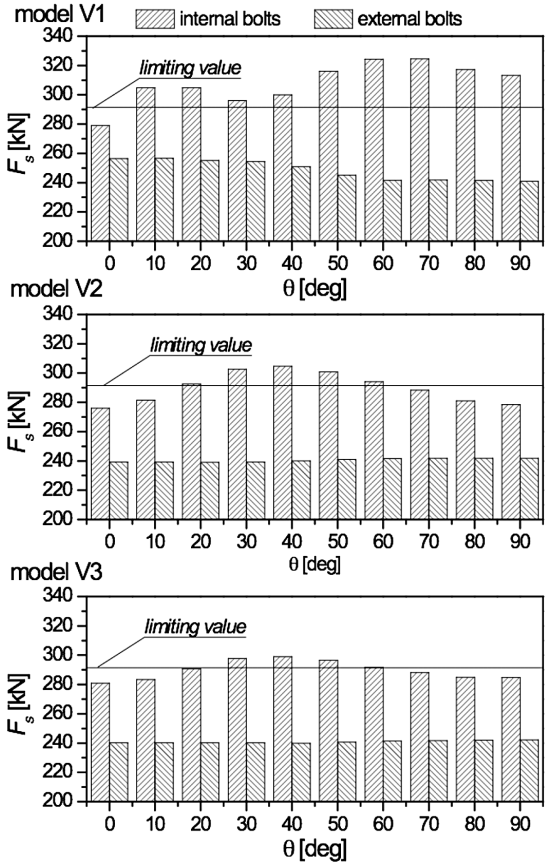

Fig. 4. The maximum force in the bearing fixing bolts for the different positions of the support subassembly (θ = 0 – 90°)

The presented results show that in the case of all the types of analyzed support structures, the limit bolt load was exceeded (Fig. 4), which could result in damage of the bearing raceway. In the accompanying drawings it can also be seen that in the case of models V2 and V3, the largest load of bearing raceways exists for the body position of angle of approximately 40°.

5. Conclusions

The study indicates how important in the design of slewing bearings is the appropriate design of bolted joints. It has been shown that in the analyzed screw connection, significant changes occur in the load of each bolt connecting the bearing rings with the supporting structures. This is important because often a carrying capacity of the whole unit determines the strength of the bolts. The results of the mentioned analyzes indicate that the screw connections of slewing bearing rings carry uneven loads, particularly in cases where it does not have a sufficient rigidity of the supporting structure. If the limit values are exceeded in any of the mounting screws, we need to change the design of the connection, i.e. select bolts of a larger diameter or higher strength class, increase the number of screws or change the design of the connection (to increase rigidity). Breaking of even one bolt in the connection quickly leads to severing of the remaining screws, which ends with a serious failure of the whole unit.

The analysis demonstrates the validity of numerical methods in practical engineering calculations. It allows for the precise distribution of forces transmitted byeach bearing rolling elements. Such modeling allows for the quick verification of all technological design changes introduced to both bearing geometry and building structure.

References

[1] Kania L., Krynke M., *Computation of the general carrying capacity of slewing bearings*, Engineering Computations, vol. **30** (7), 2013, 1011-1028.

[2] Kania L., Krynke M., Mazanek E., *A catalogue capacity of slewing bearings*, Mechanism and machine theory, vol. **58**, 2012, 29-45.

[3] Kania L., Śpiewak S., *Influence of radial forces on change of friction torque in twin slewing bearing*, Machine Dynamics Research, vol. **38**, 2014, 121-131.

[4] Krynke M., Borkowski S., *Wpływ postaci konstrukcyjnej podzespołu wsporczego na dystrybucję obciążeń w łożysku wieńcowym*, Przegląd Mechaniczny, vol. **7–8**, 2014, 23-29 [in Polish].

[5] Krynke M., *The dynamic state monitoring of bearings system*, Production Engineering Archives, vol. **6** (1), 2015, 35-38.

[6] Mazanek E., Krynke M., *Możliwości modelowania śrub mocujących łożysko wieńcowe*, Transport Przemysłowy i Maszyny Robocze, vol. **2** (8), 2010, 53-57 [in Polish].

[7] ROTHER ERDE – Slewing Bering, Catalog 2008.

[8] Smolnicki T., *Wielkogabarytowe toczne węzły obrotowe. Zagadnienia globalne i lokalne*, Oficyna Wydawnicza Politechniki Wrocławskiej, Wrocław 2013 [in Polish].

[9] Szataniak P., Mazur M., Ulewicz R., Novy F., *Fractographic analysis of hardox steels research in the field of high-cycle fatigue regime*, Communications Scientific Letters of the University of Žilina, vol. **18**, 2016, 89-92.

[10] Ulewicz R., Jelonek D., Mazur M., *Implementation of logic flow in planning and production control*, Management and Production Engineering Review, vol. **7** (1), 2016, 89-94.

TECHNICAL TRANSACTIONS | **CZASOPISMO TECHNICZNE**
MECHANICS | MECHANIKA
4-M/2016

JACEK PIETRASZEK*, MARIUSZ KRAWCZYK**, ANDRZEJ SOBCZYK**,
EWA SKRZYPCZAK-PIETRASZEK***

THE DOMINANT FACTOR DETECTION IN THE SHAININ'S APPROACH

WYKRYWANIE DOMINUJĄCEGO CZYNNIKA ZA POMOCĄ PODEJŚCIA SHAININA

Abstract

Shainin's approach is a specific sequential heuristic aimed at finding and ranking the most important factors which impact the investigated process. The sequential aspect of the approach is simultaneously its strongest and weakest side, because just after detection of the most important factor, the further analysis is stopped without any additional cost. However, such a detection may take place at the end of the whole sequence. This paper tries to answer the question if the dominant factor may be hidden by interactions with other factors.

Keywords: Shainin's approach, *Red X*, *design of experiment*

Streszczenie

Podejście Shainina jest specyficzną heurystyką sekwencyjną nakierowaną na wykrywanie i rangowanie najważniejszych czynników wpływających na badany proces. Sekwencyjność podejścia jest jednocześnie jego najmocniejszą i najsłabszą stroną, gdyż po wykryciu najważniejszego czynnika cała dalsza analiza jest przerywana bez ponoszenia dodatkowych kosztów, ale wykrycie tego czynnika może nastąpić dopiero przy końcu całej sekwencji. Artykuł poszukuje odpowiedzi na pytanie, czy istnieje ryzyko maskowania istnienia czynnika dominującego wskutek działania interakcji.

Słowa kluczowe: podejście Shainina, *Red X*, *planowanie doświadczeń*

DOI: 10.4467/2353737XCT.16.238.5987

* D.Sc. Ph.D. Eng. Jacek Pietraszek, Assoc Prof., M.Sc. Eng. Mariusz Krawczyk, Institute of Applied Informatics, Faculty of Mechanical Engineering, Cracow University of Technology.

** D.Sc. Ph.D. Eng. Andrzej Sobczyk, Assoc Prof., Institute of Machine Design, Faculty of Mechanical Engineering, Cracow University of Technology.

*** Ph.D. Ewa Skrzypczak-Pietraszek, Chair and Department of Pharmaceutical Botany, Jagiellonian University Collegium Medicum.

1. Introduction

Even after a statistical process control (SPC) tuning, an industrial process is affected by instabilities induced by many known and unknown factors. Therefore, the process must be continuously tuned up to produce goods which meet consumer requirements. Many of those factors which control such processes and their proper settings are crucial for the final success. Some factors may be affected by instability or a drift which becomes a source of the whole process instability. A typical SPC reacts if the deviations of important parameters go over the trigger limit, however it is *a posteriori* operation and some scrap is unavoidable. Typically, the process is more sensitive to a few factors while the rest is less important. The selection of these factors is one of the most important phases in SPC [1].

In the 1930s and 1940s, the standard approach to make this selection was to use the Yates's factorial design [2] and to construct the Pareto ranking. In 1948 Placket and Burman proposed a more effective approach [3]: screening designs based on Hadamard matrices. All these approaches have the same requirement: all tests have to be conducted before the analysis may be processed. It means that the costs are constant and the engineering heuristic knowledge is not applied *a priori* to reduce the cost.

In the 1950s and 1960s, the aerospace engineer D. Shainin changed this requirement through his "Red X" approach. Its most spectacular application was related to the reliability assessment of the Lunar Expedition Module (NASA Apollo missions) produced by Grumman where Shainin was responsible for the quality [4].

The ideas which influenced the core concept of the Shainin's approach date back to the results of 19th century Italian sociologist W. Pareto, later in the 1950s enhanced by J. Juran [5]. He created the following statement [6]: "vital few and trivial many". This statement has been mistakenly named Pareto principle, however the particular form has been expressed by Juran. In the 1990s Juran tried to explain this mistake [7], but it was too late. The name "Pareto principle" appeared to be unchangeable.

2. Methods

A clear detection of the most dominant factor is shown in two of Shainin's heuristics phases: the"Component Search" and "Variable Search" developed in 1956 and 1973, respectively. The mathematical structure of both is the same, however in the"Component Search" swapping is applied to physical components, while in the "Variable Search" – to the settings of selected factors.

The analysis starts from the selection of "Green Y", the quantitative variable of interest which should be stabilized. Then two objects are selected, the best product (BoB – Best of Bests) and the worst product (WoW – Worst of Worsts) from a production lot. Next, both objects are twice disassembled and reassembled in the "Component Search" or the process is reset and tuned in the "Variable Search". After each rebuild/resetting, the "Green *Y*" is measured. The aim of this procedure is to determine the noise originated from the disassembly/reassembly process or adjustment devices. At this time, two subsets of three measurements are obtained.

The first analysis starts from two subsets $\mathbf{M}_{\text{BoB}}$ and $\mathbf{M}_{\text{WoW}}$, each containing three measurements. The noise analysis is provided based on median and ranges, as opposed to the classic mean and standard deviations. Shainin argued that such statistics are more robust to instability from outliers. The median and ranges are calculated for BoB:

$$\begin{aligned} m_{\text{BoB}} &= \text{median}\,(\mathbf{M}_{\text{BoB}}) \\ d_{\text{BoB}} &= \max(\mathbf{M}_{\text{BoB}}) - \min(\mathbf{M}_{\text{BoB}}) \end{aligned} \tag{1}$$

and for WoW:

$$\begin{aligned} m_{\text{WoW}} &= \text{median}\,(\mathbf{M}_{\text{WoW}}) \\ d_{\text{WoW}} &= \max(\mathbf{M}_{\text{WoW}}) - \min(\mathbf{M}_{\text{WoW}}) \end{aligned} \tag{2}$$

Next, the difference between the medians and average range are calculated:

$$\begin{aligned} D &= \left| m_{\text{BoB}} - m_{\text{WoW}} \right| \\ d &= \frac{\left| d_{\text{BoB}} - d_{\text{WoW}} \right|}{2} \end{aligned} \tag{3}$$

The median interval D is treated as the measure of a significance difference between BoB and WoW, while the average range d is treated as a measure of noise factors from the assembly process or adjustment devices. The ratio between these two variables i.e. D divided by d is the key value which decides about the further analysis. The critical value of the ratio is set by Shainin at 1.25. This is the first of "magic numbers" placed in this approach. The value was argued as median/range critical level equivalent for typical t Student test for equality of two means.

If the ratio is less than 1.25, it means that the noise from the assembly process/adjustment devices is too loud and it should be reduced first i.e. the assembly process/adjustment devices should be repeatable earlier than the main analysis starts. It should be noted that such a noise reduction may require additional expenses like e.g. repairing of machines in machining industry or significant changes of raw materials. It may be very difficult in e.g. biochemistry and biotechnology processes [8–10], where noise factors origin directly from raw materials and from the natural or semi-natural environment.

If the ratio is greater than 1.25, it means that the noise from the assembly process/adjustment devices is small enough and this noise will not mask the effects from controlled factors. If these conditions are satisfied, then the control lines may be calculated based on values from Eqs. 1–3, first for BoB:

$$\begin{aligned} \text{UCL}_{\text{BoB}} &= m_{\text{BoB}} + 2.776 \cdot \frac{d}{1.81} \\ \text{LCL}_{\text{BoB}} &= m_{\text{BoB}} - 2.776 \cdot \frac{d}{1.81} \end{aligned} \tag{4}$$

and next for WoW:

$$\begin{aligned} \text{UCL}_{\text{WoW}} &= m_{\text{WoW}} + 2.776 \cdot \frac{d}{1.81} \\ \text{LCL}_{\text{WoW}} &= m_{\text{WoW}} - 2.776 \cdot \frac{d}{1.81} \end{aligned} \tag{5}$$

The "magic" values, 2.776 and 1.81, are described by Bhote [11] as taken from *t* Student distribution, however the authors could not find any precise reference to any statistical source.

Subsequently, a specific control card is created based on mentioned control lines and two triplets associated with BoB and WoW. The next points on this card are taken from measurement made at the sequential swapping of components. After each swap, a decision needs to be made about the component/factor status: not-important, important (Pink X), the most important (Red X). The status is read from the mutual position of measurements on the control card (Fig. 1).

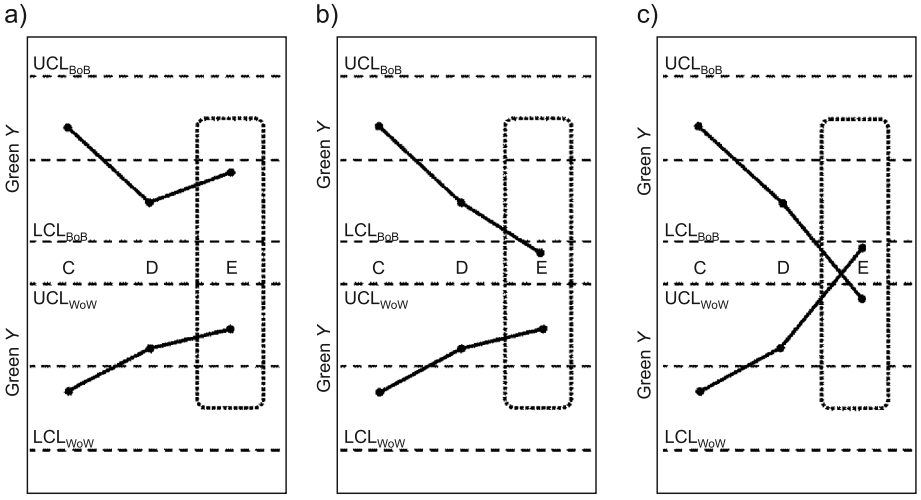

Fig. 1. Possible behavior of the response: a) not-important component/factor, b) important component/factor (Pink X), c) the most important component/factor (Red X)

If both measures are located inside respective control lines (Fig. 1a), it means the swapped component/factor is not important. If at least one measure is located outside its control lines but relative position to the second measure will not be replaced (Fig. 1b), it means the swapped component/factor is important (Pink X), but it does not explain all variability – other important factors are expected. If both measures are located outside their control lines and their relative position is swapped (Fig. 1c), it means the swapped component/factor is the most important (Red X).

The aim of the research was to check when Red X is detected and whether the interaction may mask the existence of Red X.

3. Results

The first check was conducted based on a fixed-effect model with an interaction for two factors *A*, *R* and additive term ε (Eq. 6):

$$\text{Green } Y = \mu + A + R + AR + \varepsilon \tag{6}$$

Factor A represents potential Red X while R describes effects of other components. The additive term ε describes the noise from the disassembly/assembly process and the additive μ describes the mean response. Two test objects, BoB and WoW are modelled at maximum contrasts i.e. at opposite effects:

$$\begin{aligned} \text{Green } Y_{\text{BoB}}(+1,+1) &= \mu + a + r + ar + \varepsilon_{\text{BoB}} \\ \text{Green } Y_{\text{WoW}}(-1,-1) &= \mu + (-a) + (-r) + ar + \varepsilon_{\text{WoW}} \end{aligned} \tag{7}$$

The responses after a swap of A component are described by Eq. 8:

$$\begin{aligned} \text{Green } Y_{\text{BoB}|A}(-1,+1) &= \mu - a + r - ar + \varepsilon_{\text{BoB}} \\ \text{Green } Y_{\text{WoW}|A}(+1,-1) &= \mu + a - r - ar + \varepsilon_{\text{WoW}} \end{aligned} \tag{8}$$

The Red X detection is made when – after a swap of A component – the response of BoB is worse than the response of WoW:

$$\text{Green } Y_{\text{BoB}|A} < \text{Green } Y_{\text{WoW}|A} \tag{9}$$

After substituting respective terms from Eq.8, the condition is transformed into:

$$a > r + \frac{\varepsilon_{\text{BoB}} - \varepsilon_{\text{WoW}}}{2} \tag{10}$$

The form of the expression shows that the interaction effect AR was completely eliminated. It means that the interaction cannot mask Red X detection. If the value of noise realizations are relatively small, the fact of Red X detection means that such factor explains more than 50% of the total variability.

4. Conclusions

The fixed-effect model with linear effects and an interaction was created to describe the process of detection of the most important factor in Shainin's Red X approach. The theoretical analysis reveals that the interaction does not interfere with the detection process, which means that the interaction existence or non-existence is not important for the detection procedure. Additionally, it was concluded that Red X factor explains more than 50% of the total variability if noise factors are relatively small i.e. D/d is far from the limit 1.25.

References

[1] Montgomery D.C., *Introduction to Statistical Quality Control*, John Wiley & Sons, Hoboken, 1997.

[2] Yates F., *Complex experiments*, J. Roy. Statist. Soc., vol. Suppl.2, 1935, 181-247.

[3] Plackett R.L., Burman, J.P., *The design of optimum multifactorial experiments*, Biometrika, vol. 33, 1946, 305-325.

[4] Shainin D., *Reliability: Managing a reliability program*, "Apollo lunar module engine exhaust products", Science, vol. 166, 1969, 733-738.

[5] Juran J.M., *Quality Control Handbook*, McGraw-Hill, New York 1951.
[6] Juran J.M., *Universals in Management Planning and Controlling*, The Management Review, vol. 43 (11), 1954, 748-761.
[7] *The Non-Pareto Principle; Mea Culpa*, [in:] Juran J.M. (Ed.), Juran on Quality by Design, Free Press, New York 1992, 68-71.
[8] Pietraszek J., Skrzypczak-Pietraszek E., *The Optimization of the Technological Process with the Fuzzy Regression*, Terotechnology, vol. 874, 2014, 151-155.
[9] Skrzypczak-Pietraszek E., Pietraszek J., *Seasonal Changes of Flavonoid Content in Melittis melissophyllum L. (Lamiaceae)*, Chemistry & Biodiversity, vol. 11 (4), 2014, 562-570.
[10] Skrzypczak-Pietraszek E., Slota J., Pietraszek J., *The influence of Lphenylalanine, methyl jasmonate and sucrose concentration on the accumulation of phenolic acids in Exacum affine Balf. f. ex Regel shoot culture*, Acta Biochimica Polonica, vol. 61 (1), 2014, 47-53.
[11] Bhote K.R., *World Class Quality: using design of experiment to make it happen*, AMACOM, New York 1991.

TECHNICAL TRANSACTIONS | **CZASOPISMO TECHNICZNE**
MECHANICS | MECHANIKA
4-M/2016

MARIUSZ DOMAGAŁA*

LATTICE-BOLTZMAN METHOD IN CFD MODELLING OF DIRECT ACTING RELIEF VALVE

MODELOWANIE CFD ZAWORU PRZELEWOWEGO BEZPOŚREDNIEGO DZIAŁANIA Z ZASTOSOWANIEM METODY SIATKOWEJ BOLTZMANA (LBM)

Abstract

This paper presents the modelling of a direct acting relief valve with the use of the new approach of CFD techniques which uses the Lattice Boltzman Method (LBM). It allows for eliminating the biggest problem that occurs during the simulation of a valve operation, which is the motion of a working component. During traditional CFD modeling, a deformed mesh has to be used in such a case, which may lead to the occurrence of computational cells with negative volume and, as a consequence, remeshing of fluid domain.

Keywords: LBM, *CFD*, *FSI*, *direct acting relief valve*

Streszczenie

W artykule przedstawiono zastosowanie metody symulacji numerycznych przepływu wykorzystującą metodę siatkową Boltzmana (LBM) w modelowaniu zaworu przelewowego bezpośredniego działania. Umożliwia ona wyeliminowanie największego problemu, jaki występuje podczas symulacji pracy zaworu przelewowego tradycyjnymi metodami CFD, którą jest konieczność wykorzystywania deformującej się siatki modelu dyskretnego.

Słowa kluczowe: LBM, *CFD*, *FSI*, *zawór przelewowy bezpośredniego działania*

DOI: 10.4467/2353737XCT.16.239.5988

* Ph.D. Eng. Mariusz Domagała, Institute of Applied Informatics, Faculty of Mechanical Engineering, Cracow University of Technology.

1. Introduction

Modelling of fluid power components at working conditions is a challenge, even by means of sophisticated simulation tools like computational fluid dynamics (CFD). A direct relief valve, which has a relatively simple structure, may cause a lot of modelling problems. In the simplest case, it consists of a lift component (cone or sphere) and spring whose rate and initial deflection determine the opening pressure and valve characteristic. Despite the significant development of CFD method and its possibilities in fluid-structure interaction (FSI) simulations, which includes mesh deformations, which may lead to the occurrence of distorted cells with negative volume [1, 2]. A solution may be the use of automating remeshing procedure, however, it requires much more computational time and resources. A new approach of FSI named Immersed Solids, which was presented during the modelling of the relief valve in [2], does not use grid deformations. Solid objects occupy the same volume as the fluid domain, which contains this object. However, such an approach does not allow for capturing flow forces accurately enough. Previous research [2] has shown that flow forces that arise on lift components differ from those obtained from the traditional CFD modelling. The flow forces, which appear during a valve operation have essential meaning for the modelling of a relief valve and therefore an efficient way of simulation valves in working conditions is still requested. A new quality in modelling FSI of hydraulic valves may give a new approach of numerical flow simulation based on the Lattice Boltzman Method (LBM).

2. Lattice Boltzman Method approach in fluid flow

The Lattice Boltzman Method (LBM) is a particle-based method, which is an improved modification of Lattice Gas Automata. Recently, LBM becomes more and more popular as an alternative to the conventional FEM or FVM based CFD approaches. A direct connection of LBM with the kinetic theory of gases may be adopted particularly for fluid-structure interaction simulations. LBM uses a spatial discretization method named lattice which consists of discrete points with a discrete set of velocity directions located in the Cartesian

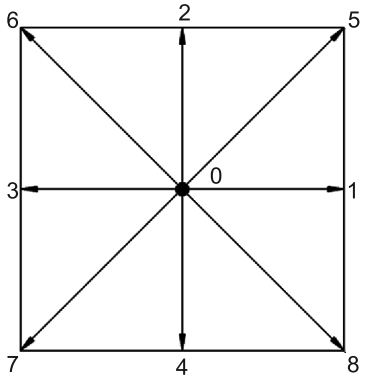

Fig. 1. D2Q9 lattice

space. The set of velocities uses a common terminology which describes the dimension problem and a number of velocity vectors: D_nQ_m, where n stands for dimension, while m for velocity directions. An example of two dimensional lattice is presented in Fig. 1.

There are many approaches of LBM, but all of them have a common feature which is time stepping model based on the propagate-collide scheme. The Boltzman equation for continuum space with discrete velocities can be presented as [3]:

$$\frac{\partial f_i}{\partial t} + \mathbf{e}_i \cdot \Delta f_i = \Omega_i, \quad i = 1, \ldots, b \tag{1}$$

where:

Ω_i – is the collision operator,
$\mathbf{e}_i$ – is a set of discrete velocities,
b – is a number of velocities directions, $b = 4$ for a two dimensional lattice,
f_i – is the probability distribution function.

If we assume $\Omega_i = 0$ the Eq. 1. Is discretized on the lattice in the following way:

$$f_i(\mathbf{r} + \mathbf{e}_i, t + dt) = f_i(\mathbf{r}, t) + \Omega_i(f_1, \ldots, f_b), \quad i = 1, \ldots, b \tag{2}$$

The density and momentum can be derived from the following equations:

$$\rho = \sum_{i=1}^{b} f_i \tag{3}$$

$$\rho \mathbf{v} = \sum_{i=1}^{b} f_i \mathbf{e}_i \tag{4}$$

The collision operator Ω_i is modelled as a relaxation of the probability distribution function towards an equilibrium state. One of the most common approaches uses single relaxation time based on the Bhatnagar-Gross-Krook approximation [3]:

$$\Omega_i = \frac{1}{\tau}(f_i^{eq} - f_i) \tag{5}$$

where:

τ – is relaxation time,
f_i^{eq} – is the local equilibrium function.

The local equilibrium function f_i^{eq} is derived directly from the Maxwell-Boltzman distribution with the same macroscopic variables of the pre-collision state satisfying mass and momentum conservation and can be expressed as follows [3]:

$$f_i^{eq} = \rho w_i \left(1 + \frac{e_{i\alpha} u_\alpha}{c_s^2} + \frac{u_\alpha u_\beta}{2c_s^2} \left(\frac{e_{i\alpha} e_{i\beta}}{c_s^2} - \delta_{\alpha\beta} \right) \right) \tag{6}$$

where:

u – is macroscopic velocity,
δ – is the Kronecker symbol,
w_i – is weighting constant,
α, β – spacial components of vectors appearing in the equation,

3. Object of study

The direct acting relief valve with a cone shape lift element presented schematically on Fig. 2 is the object of the study.

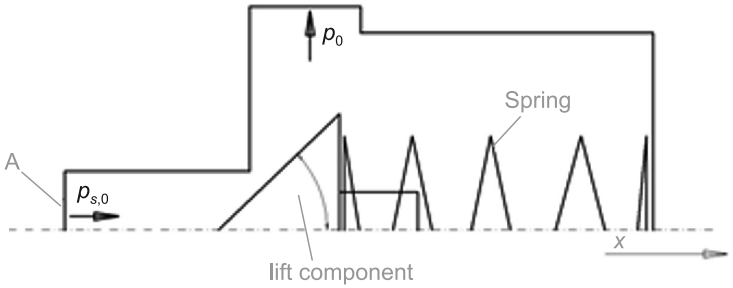

Fig. 2. A scheme of direct acting relief valve

The main aim of the relief valve is to secure the hydraulic system against excessive rise of pressure. When the pressure at the hydraulic line rises (port A) and exceeds the value of valve opening (p_s), the spring yields and the lift element releases working fluid to the tank. The position of lift element depends on forces acting on it, where the flow forces are the most difficult to evaluate. Additionally, due to the lack of damping element, during the operation the lift element may oscillate until the equilibrium state is found.

4. FSI simulation using LBM

The Lattice Boltzman Method is a relatively new approach of flow simulations and is still under development, while traditional CFD approaches using the finite element method (FEM) or the finite volume method (FVM) have existed for decades. One of the commercial LBM applications was implemented in XFlow CFD code. A model of relief valve presented in Fig. 2. was used in XFlow to create a lattice for numerical calculations (Fig. 3.).

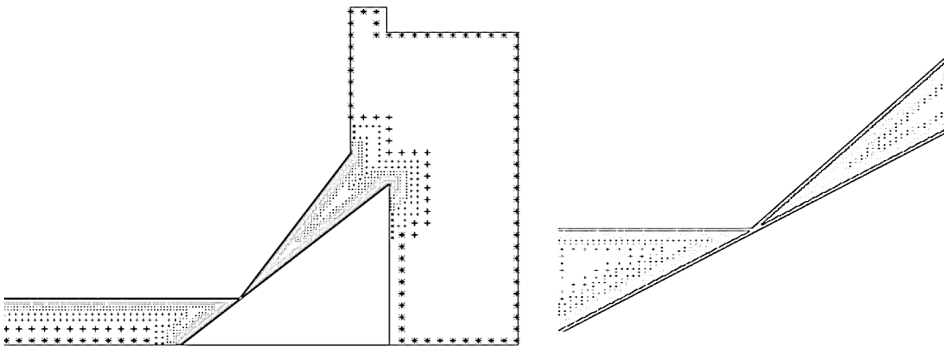

Fig. 3. Lattice for relief valve model

The created lattice is not uniform at the fluid domain, in the area of valve seat and lift element the distance between lattice nodes are much smaller to allow for the described accurate flow at the gap between the lift component and valve seat. The huge advantage of the LBM approach is no necessity of creating a grid, which allows for creating one model for simulation for various flow conditions. Another advantage of LBM is the possibility of rigid body simulation with interaction between valve components (collisions) as well. In the case of the presented relief valve it gives the possibility of simulation condition when the valve is opened and a sudden drop of pressure in the hydraulic line occurs. It leads to a situation when the lift component due to the spring force may hit at the valve seat and then reflect. The results of such conditions were shown in Fig. 4. At initially opened valve (pressure at the hydraulic line $p > p_s$) suddenly pressure drops below the value of opening. The response of the valve is presented in the lower plot in Fig. 4.

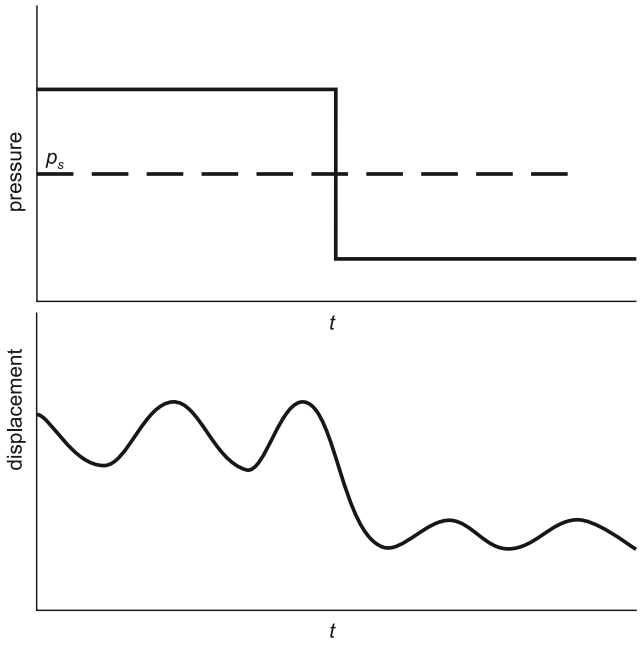

Fig. 4. Pressure in the hydraulic line (upper plot) and the displacement of lift element (lower plot)

The position of the lift element of relief valve was obtained at one model without any modifications and necessity of generating various lattice nodes for different positions of the lift element. The presented results were obtained for 2D model, which does not exactly describe the valve presented in Fig. 2, therefore the results presented in Fig. 4 do not include units. The aim of the conducted simulations was to verify possibilities of the LBM method in a relatively short time in modelling dynamics of the relief valve.

The presented results were obtained for a model which includes interaction between the valve seat and lift element. They were treated as rigid bodies with the ideal elastic model of collision.

5. Conclusions

This paper presents an attempt to use the LBM method for simulation dynamics of a direct acting relief valve. For such purpose, a commercial CFD code named XFlow was used. The created model was used for the investigations of the relief valve during a sudden drop of pressure in the hydraulic line below the value in which the valve is opening. Numerical simulations allowed for obtaining a response of valve components on such conditions, as the displacement of lift element. The application of the LBM method also allowed for simulation valve dynamics, taking into account phenomena like collision between the lift element and valve seat.

LBM seems to be a very promising tool in modelling dynamics of hydraulic valves, which allows for investigating not only flow phenomena during fluid flow but also interaction between valve components. It breaks the limits in simulation of dynamic system during fluid flow and gives much wider possibilities than the traditional approach of CFD tools based on the FEM or FVM. The only disadvantage is that the lattice nodes have to be created in a proper way close to the boundary with complex geometry.

References

[1] Domagała M.J., *Metodyka modelowania zaworów maksymalnych bezpośredniego działania*, Ph.D. thesis, Kraków 2007 [in Polish].

[2] Domagała M., *Modelling of direct acting relief valve using CFD-FSI simulation*, Technical Transactions, vol. 2-M/2015, 43-48.

[3] *XFlow*, Theory guide, Madrid 2016

[4] Perumal D.A., Dass A.K., *A Review on the development of lattice Boltzmann computation of macro fluid flows and heat transfer*, Alexandria Engineering Journal, vol. 54, 2015, 955-971.

[5] Yua D., Meia R., Luob L., Shyy W., *Viscous flow computations with the method of lattice Boltzmann equation*, Progress in Aerospace Sciences, vol. 39, 2003, 329-367.

TECHNICAL TRANSACTIONS | **CZASOPISMO TECHNICZNE**
MECHANICS | MECHANIKA
4-M/2016

RENATA DWORNICKA*, JACEK WESÓŁ**

STUDY OF THE SELECTED CHARACTERISTIC OF ARTIFICIAL PNEUMATIC MUSCLES

BADANIA WYBRANYCH CHARAKTERYSTYK MUSKUŁÓW PNEUMATYCZNYCH

Abstract

McKibben pneumatic artificial muscles (PAMs) allow for a proper representation of static and dynamic movement characteristics of biomechanical systems. These actuators have features similar to physiological muscles such as ability to generate high value of force in short time and elastic and damping properties. McKibben muscles have a nonlinear character – the value of a generated force depends not only on the pressure but also on the stroke. In the presented paper, the authors exemplify basic traits of these actuators and present drawn characteristics of a force to stroke at a constant pressure.

Keywords: McKibben artificial pneumatic muscle, *biomechanical systems*

Streszczenie

Sztuczne muskuły pneumatyczne McKibben umożliwiają dobre odwzorowanie ruchu układów motorycznych istot żywych w układach mechanicznych. Siłowniki te posiadają cechy upodobniające je do mięśni fizjologicznych, m.in. możliwość generowania dużych wartości sił w krótkim czasie oraz korzystne własności sprężyste i tłumiące. Siłowniki te cechują się nieliniowymi charakterystykami pracy, a wartość generowanej przez nie siły zależy nie tylko od ciśnienia, ale również od stopnia ich skrócenia. W prezentowanym artykule przedstawiono budowę oraz podstawowe cechy tych siłowników, a także charakterystyki generowanej siły w funkcji skrócenia mięśnia przy stałym ciśnieniu wyznaczone na skonstruowanym na te potrzeby stanowisku laboratoryjnym.

Słowa kluczowe: sztuczny muskuł pneumatyczny McKibben, *układy biomechaniczne*

DOI: 10.4467/2353737XCT.16.240.5989

* Ph.D. Eng. Renata Dwornicka, Institute of Applied Informatics, Faculty of Mechanical Engineering, Cracow University of Technology.

** M.Sc. Eng. Jacek Wesół, Department of Process Control, Faculty of Mechanical Engineering and Robotics, AGH University of Science and Technology.

1. Introduction

Human muscles have the ability to shorten to about 40–50% of the beginning length. The value of the force created by a muscle ranges between 50–110 N/cm^2. The development of biomedical engineering and rehabilitation disciplines have created the need for artificial muscles. They were applied as driving means of mobile anthropomorphic and humanoid robots as well as a drive for artificial limbs. The pneumatic muscle may be classified as an elastic pneumatic pulling unilateral actuator. The dynamic characteristics allow for a very good mapping of a motion for the motoric system of living beings. It was very well presented for the Mowgli robot [1]. Pneumatic muscles were successfully applied in constructions supporting human motoric moving [2]. For the first time, they allowed for obtaining the metabolic cost of the machine closely to a physiological one. The average energy consumption measured for the suit amounted to about 386.7 W, being almost identical to the result of 381.8 W, measured for the control sample without the suit.

The pneumatic muscle is produced in several types, including McKibben or PLAM. In the recent years, the construction of McKibben muscles was enhanced and commercialized e.g. by FESTO, a company which produces Fluidic Muscles [3]. In the production series of FESTO, there are muscles with the pulling force of 630 N, 1500 N and 6000 N [3], and the frequency of up to 150 Hz [4].

2. The construction and operation of the muscle

A radially deformable tube is the most important element of muscle construction. The tube is made of rubber, latex or silicone and it is disposed in a braid made of non-stretchable fibers. A flexible tube is usually made of latex because of the higher fatigue resistance comparing to silicone [5]. Other materials may also be used, however, this element should be made of elastic materials with low Shore's hardness. Polyester braids are most commonly used as an outer sheath. Metallic braids are also used but the higher mass of a muscle and quicker rubbing of the internal elastic cord is the disadvantage of such a solution. The purpose of the braid is to transform radial deformations into axial deformations. In the McKibben PAMs, the braid structure is helical and crossed. It enables the distribution of forces like in a pantograph (Fig. 1).

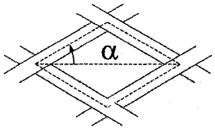

Fig. 1. Structure of a typical braid in McKibben PAM [6]

The capability to activate a large axial force from a relatively small mass and a small cross-section area is a significant advantage of McKibben's PAMs. The peak value of a generated force is almost eight times higher for Fluidic Muscle actuators than for a classic pneumatic actuator with the same cross-section area.

The PAM is activated by compressed air introduced into the muscle's internal space. The pressurized air pushes against the membrane wall and the membrane transmits the generated force to the PAM's braid [7]. This simultaneously results in the swelling and shortening of the PAM. The PAM's shortening and its pulling force are controlled by a pressure value.

The movements performed by PAM, constructed and acting in this way, are smooth and do not show irregularities typical for classic actuators. The design which uses flexible tubes allows for obtaining high elasticity while the contact of the flexible membrane with the braid introduces significant damping properties.

To sum up, the static and dynamic properties of PAM, and especially the ability to generate a large peak force, provide a very good mapping of the biomechanical system work.

3. Operating characteristics of the pneumatic artificial muscle

Fiber braids are arranged diagonally to form a four-bar linkage structure. It allows for converting a radial deformation into the axial one. Although this structure is simple and effective, it introduces some limitations of the actuator. Geometric dependencies make the force generated by the PAM decrease with the increasing of the braid's angle α. Deformations in the radial direction are limited by the geometry of a braid, so the PAM has a relatively small range of shrinkage. The value of the maximum reduction is about 25% of the initial value in the case of McKibben PAMs. The relationship between a generated force and the PAM shrinkage is not linear. It depends on both the degree of the shrinkage as well as the pressure inside the PAM. Typically, the operating characteristics of PAM are defined as a relationship between the force and the percentage shortening at a constant pressure.

This paper describes an investigation of the modified version of McKibben PAMs. These actuators were made as elements of a flexible suit supporting motion motoric (Fig. 2).

Fig. 2. A flexible suit supporting a motion motoric driven by McKibben PAMs

The suit was developed in the AGH University of Science and Technology in the years 2014–2015 [8]. The actuators were completely produced from polymer materials. The flexible membrane was made from a latex tube of 8 mm in diameter and a 2 mm thick wall. The braid was made from a standard polymer braid. The hooks were realized by placing an inactive part of the braid in a latex warp. To increase the flexibility of the actuator, standard metal terminals were replaced by polyethylene ones (one of the terminal was blinded). The connection of the flexible membrane with terminals and the braid was made as pre-stressed ties produced from a nylon-latex composite. It allows for avoiding a quick wipe of the PAM in the place of the polymer-metal contact. The working length of PAM was 33 cm. Muscles were examined on a specially designed test stand (Fig. 3) with one degree of freedom. The stand allows for measuring simultaneously the force, shrinkage and pressure.

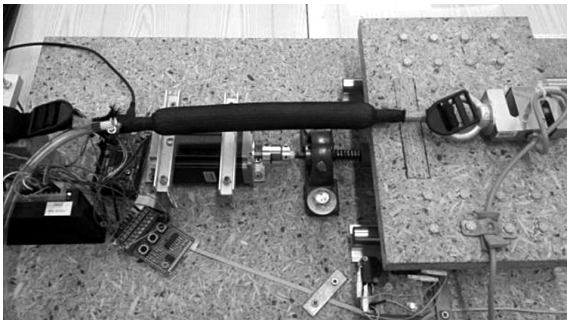

Fig. 3. The test stand for the examination of PAMs

The study was to determine the static characteristics of the actuator. It allows for introducing the relationship between the force and shrinkage into the control model. The control of a force allows subsequently for controlling the torque obtained in the biomechanical system. During the test, the PAM is stretched between the fixed-attachment

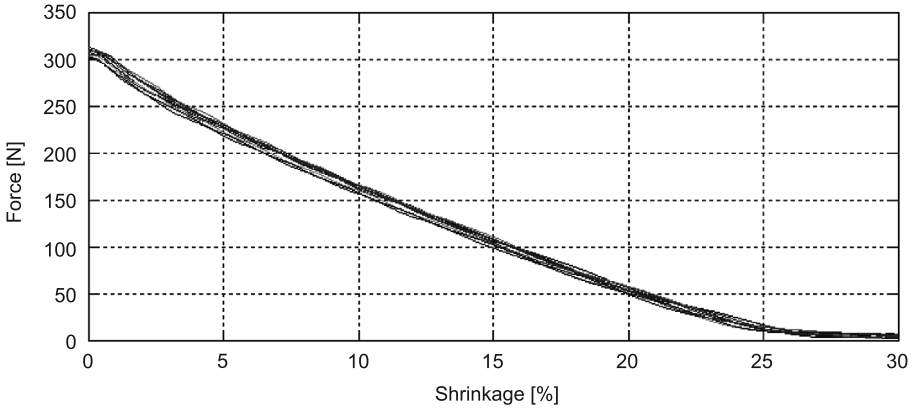

Fig. 4. The relationship between the force and PAM shrinkage obtained for 10 cycles

of the support and the trolley. The trolley is moved by a trapezoidal screw with a stroke of 4 mm while the screw is driven by a stepper motor with a resolution of 400 steps per rotation. The force is measured by a strain gauge with the supply of 10 V. The voltage measurement is made by means of an acquisition card with 16 bit resolution in the range of 0.2 to 0.2 V and a sampling frequency of 100 Hz. The characteristics were achieved by introducing pressure of 4 bar into the PAM and then shortening the PAM's length at a constant speed equal to 10 mm/s.

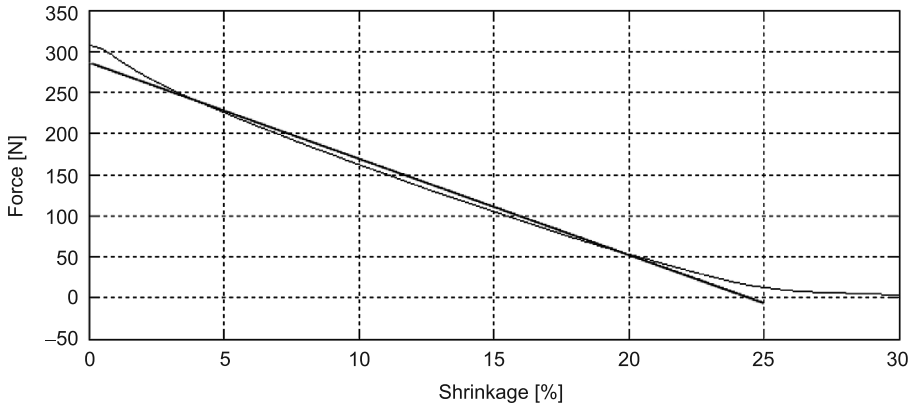

Fig. 5. The linear approximation of the averaged relationship in the range of the shrinkage from 0 to 25% (slope $a = -11.67$, intercept $b = 286.4$)

The obtained characteristics (Fig. 4 and Fig. 5) show a small dispersion. The standard deviation of the shrinkage ranges from 1.34 N to 5.02 N at the assigned value of the force. The average relationship between the force and the shrinkage shows small dynamics of changes in the range of 0–25%. The standard deviation of linear approximation ranges from 1.1 mN up to 11.2 N. The non-linearity is significantly visible in the beginning of the shrinkage range and at 25% of shrinkage, where the plot has a parabolic shape. The modified actuators actively generated a force in the range from 0% up to 26% of shrinkage.

4. Summary

The McKibben artificial pneumatic muscles are an interesting concept of the motion source construction in biomechanical systems. It allows for generating large forces in a short time, which significantly exceeds the capability of conventional actuators. In this paper, the relationships between the force and shrinkage at constant pressure were presented. The obtained characteristics have some non-linearity. The investigation allowed for determining the static characteristics of the actuator. The knowledge of such characteristics makes it possible to introduce a specific relationship between a force and a shrinkage into the control model and – subsequently – to control the force at the variable shrinkage, which derives e.g. from the phase of a movement.

References

[1] Niiyama R., Nagakubo A., Kuniyoshi Y., *Mowgli: A bipedal jumping and landing robot with an artificial musculoskeletal system*, Proc. 2007 IEEE Int. Conf. on Robotics and Automation, IEEE, 2007, 2546-2551.

[2] Wehner M. et al., *A lightweight soft exosuit for gait assistance*, Proc. of IEEE Int. Conf. "Robotics and Automation (ICRA) 2013", 2013, 3362-3369.

[3] *Fluidic Muscle DMSP/MAS*, https://www.festo.com/rep/en_corp/assets/pdf/info_501_en.pdf (date of access 2016-06-20).

[4] *Textile industry: Pneumatic spring for tensioning warp beams in looms*, https://www.festo.com/net/SupportPortal/Files/381403/ Referenzblatt_Wernli_en_V01_M.pdf (date of access 2016-06-20).

[5] Klute G.K., Hannaford B., *Fatigue characteristics of McKibben artificial muscle actuators*, Proc. of IEEE/RSJ International Conference "Intelligent Robots and Systems", 1998, 1776-1781.

[6] Sanchez A., Mahout V., Tondu B., *Nonlinear parametric identification of McKibben artificial pneumatic muscle using flatness property of the system*, Proc. of IEEE International Conference on Control Applications, Triestrem Italy 1–4 September 1998, WA-02, 70-74.

[7] Dindorf R., Łaski P., *Muskuły pneumatyczne. Budowa, parametry, zastosowanie*, Pneumatyka, vol. 2, 2003, 46-48.

[8] Nawrocka A., Bułka J., Folwarczny Ł., Iwaniec M., Izworski A., Mięsikowska M., Moskwa S., Orzechowski T.S., Radziszewski L., Wesół J., Wochlik I., *Wybrane zagadnienia inżynierii biomedycznej*, AGH, Kraków 2014.

TECHNICAL TRANSACTIONS | CZASOPISMO TECHNICZNE
MECHANICS | MECHANIKA
4-M/2016

NORBERT RADEK*, JACEK PIETRASZEK**, AGNIESZKA SZCZOTOK***

PROPERTIES OF ANTI-WEAR ELECTRO-SPARK DEPOSITED COATINGS

WŁAŚCIWOŚCI POWŁOK PRZECIWZUŻYCIOWYCH NANOSZONYCH OBRÓBKĄ ELEKTROISKROWĄ

Abstract

The paper is concerned with the performance properties of electro-spark deposited coatings. The properties were assessed by analyzing the coating microstructure, X-ray diffraction, microgeometry, microhardness, and corrosion tests. The studies were conducted using WC-Co-Al_2O_3 electrodes produced by the sintering of powders. The anti-wear coatings were electro-spark deposited over C45 carbon steel by means of an EIL-8A. These coatings are likely to be applied in sliding friction pairs and as protective coatings.

Keywords: electro-spark deposition, *coating*, *properties*

Streszczenie

W artykule przedstawiono wyniki badań właściwości powłok nanoszonych elektroiskrowo. Ocenę właściwości przeprowadzono na podstawie obserwacji mikrostruktury, analizy składu fazowego oraz pomiarów mikrotwardości, chropowatości i badań korozyjnych. Badania przeprowadzono, wykorzystując elektrody WC-Co-Al_2O_3, które zostały wytworzone przez spiekanie proszków. Przeciwzużyciowe powłoki zostały naniesione elektroiskrowo na próbki ze stali C45 za pomocą urządzenia EIL-8A. Ze względu na swoje właściwości powłoki tego typu mogą być stosowane w ślizgowych węzłach tarcia oraz jako powłoki ochronne.

Słowa kluczowe: obróbka elektroiskrowa, *powłoka*, *właściwości*

DOI: 10.4467/2353737XCT.16.241.5990

* D.Sc. Ph.D. Eng. Norbert Radek, Assoc. Prof., Centre for Laser Technologies of Metals, Faculty of Mechatronics and Machine Design, Kielce University of Technology.

** D.Sc. Ph.D. Eng. Jacek Pietraszek, Assoc. Prof., Institute of Applied Informatics, Faculty of Mechanical Engineering, Cracow University of Technology.

*** Ph.D. Eng. Agnieszka Szczotok, Institute of Materials Science, Faculty of Materials Science and Metallurgy, Silesian University of Technology.

1. Introduction

Electro-spark deposition (ESD) is a cheap high-energy process. Developed in the post--war period, the technology has been frequently modified. Its main advantages are the ability to select precisely the area to be modified, the ability to select the coating thickness, which may range from several to several dozen micrometers, good adhesion of a coating to the substrate, and finally, inexpensive and simple equipment for coating deposition.

The processes of coating formation on metal parts including electro-spark deposition involve mass and energy transport accompanied by chemical, electrochemical and electro-thermal reactions [1, 2]. Today, different electro-spark deposition techniques are used; they are suitable for coating formation and surface microgeometry formation [3, 4].

The EDS process is depicted schematically in Fig. 1.

Coatings produced by electro-spark deposition are applied:

– to protect new elements,
– to recover the properties of worn elements.

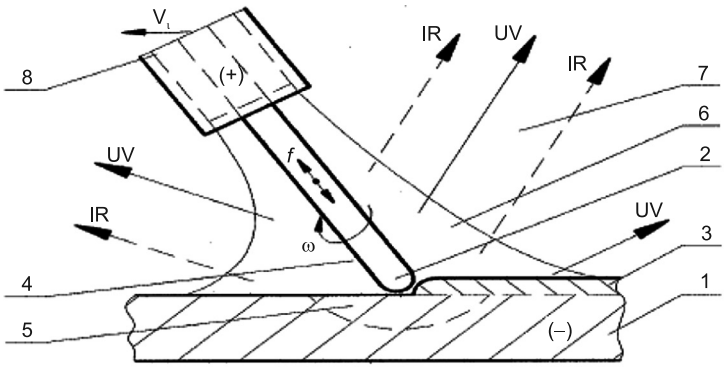

Fig. 1. Scheme of surface layer forming by electro-spark deposition method: 1 – material of base (cathode), 2 – working electrode (anode), 3 – created coating with established operational features, 4 – plasma, 5 – diffusive or reactive-diffusive zone, 6 – nearer surrounding (shielding gas), 7 – further surrounding (air), 8 – electrode holder with channels supplying gas, IR – infrared radiation, UV – ultraviolet radiation [2]

Electro-spark alloying is becoming more and more popular as a surface processing technology. Electro-spark deposited coatings are frequently applied in industry, for example, to produce implants or cutting tool inserts. The coatings are deposited with manually operated equipment or robotized systems.

As electro-spark coatings are reported to be resistant to wear and corrosion, they can be applied, for instance, to:

– ship propeller components,
– casting moulds,
– fuel supply system components,
– exhaust system components.

2. Experimental

Coatings were deposited on the C45 grade plain-carbon steel by the ESD method, using a portable EIL-8A electro-spark deposition facility (TRIZ, Ukraine). Electrodes containing 85% WC, 10% Co and 5% Al_2O_3 were produced using the powder metallurgy hot pressing route [5].

The powders were mixed for 30 minutes in the chaotic motion *Turbula T2C* mixer. The mixture was then poured into rectangular cavities of a graphite mould, each 6 × 40 mm in cross section, and consolidated by passing an electric current through the mould under uniaxial compressive load. A 3 minute hold at 950°C and under a pressure of 40 MPa allowed for obtaining electrodes of porosity $<$ 10% and strength sufficient to maintain integrity when installed in the electrode holder.

The equipment used for electro-spark alloying was an EIL-8A model. Basing on the results of previous research as well as instructions given by the producer, the following parameters were assumed to be optimal for ESA:

– voltage, $U = 230$ V,
– capacitor volume, $C = 150$ μF,
– current intensity, $I = 2.4$ A.

The electro-spark deposition equipment is illustrated in Fig. 2.

Fig. 2. EIL-8A electro-spark deposition – equipment

3. Results and discussion

3.1. Microstructure and X-ray diffraction analysis

A microstructure analysis was conducted for WC-Co-Al_2O_3 coatings, using the Joel JSM-5400 scanning electron microscope.

Fig. 3 illustrates the microstructure of an ESD WC-Co-Al_2O_3 coating. It is clear that the thickness of the obtained layers ranged from 34 to 64 μm, whereas the heat affected zone (HAZ) ranged approximately from 23 to 31 μm into the substrate. Fig. 3 also depicts a clear boundary between the coating and the substrate, pores and microcracks.

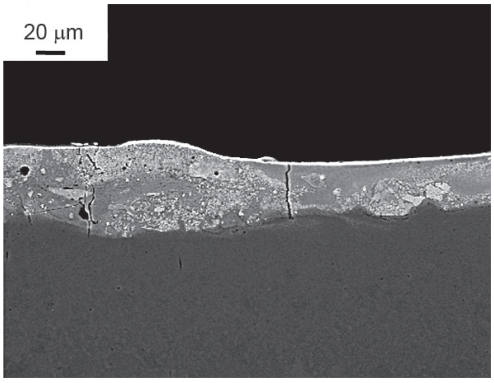

Fig. 3. WC-Co-Al_2O_3 coating microstructure after electro-spark alloying

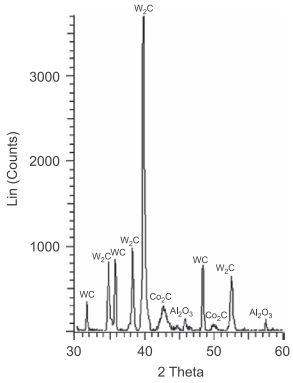

Fig. 4. X-ray diffraction pattern of the WC-Co-Al_2O_3 coating

A Philips PW 1830 X-ray diffractometer with CuKα radiation, operating at 40 kV and 30 mA, was used for identification phase (s). As shown in Fig. 4, the superficial layer of the coating consists of WC and W_2C as well as a small amount of Co_2C and Al_2O_3. W_2C is known to appear as an intermediate during the formation and dissolution of WC. Moreover, it has been found that peaks from the W_2C phase are most intense.

3.2. Microhardness and roughness measurements

The microhardness of the specimens with WC-Co-Al_2O_3 coatings was analyzed applying a load of 0.4 N and using the Vickers method. The indentations were made consecutively in three zones: the coating, the heat affected zone (HAZ) and the base material. The average microhardness of the base material after ESA was 279 HV0.4. The value was the same as the one at the initial state. The average microhardness of the WC-Co-Al_2O_3 coating was 906 HV0.4. Thus, there was a 225 percent increase compared to that of the base material. The microhardness of the heat affected zone after electro-spark alloying was 38 % higher in relation to that of the base material.

The roughness of the WC-Co-Al_2O_3 coatings was quantitatively assessed using the Topo L120 surface profiler.

The roughness was measured in two directions, perpendicular to each other. Then, the average value was calculated: Ra = 6,16 − 7,79 μm.

The steel specimens without coatings (C45) had the roughness from 0.42 to 0.44 μm.

Figure 5 presents an example of the two-dimensional surface microgeometry measurement of the WC-Co-Al_2O_3 coatings.

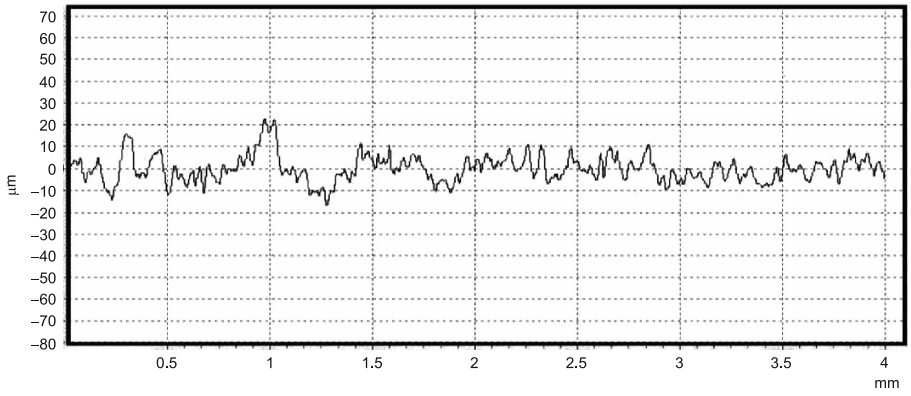

Fig. 5. Surface microgeometry of the WC-Co-Al_2O_3 coating deposited

3.3. Corrosion resistance tests

The corrosion resistance of the WC-Co-Al_2O_3 coatings and the underlying substrate were analyzed by using a computerized system for electrochemical tests, Atlas'99, produced by Atlas-Sollich. The potentiodynamic method was applied, which is reported to be one of the most effective methods of electrochemical testing.

The cathode polarization curve and the anode polarization curve were determined by polarizing the samples with a potential shift rate of 0.2 mV/s in the range of ±200 mV of the corrosive potential, and with 0.4 mV/s in the range of higher potentials. Samples with a marked area of 10 mm in diameter were polarized up to a potential of 800 mV. The polarization curves were drawn for the samples exposed for 24 hours to a 3.5% NaCl solution so that the corrosive potential could be established. The tests were performed at 21±1°C.

The results are summarised in Table 1.

Table 1

Corrosion current densities of the tested materials

Material	Corrosion current density (I_k), μA/cm^2
C45	35.4
WC-Co-Al_2O_3	16.8

The WC-Co-Al_2O_3 coating was reported to have the highest corrosion resistance. The corrosion current density of the coating was 16.8 μA/cm^2, while that of the C45 steel

substrate was 35.4 μA/cm^2. Applying the WC-Co-Al_2O coating improved the sample corrosion resistance by approx 52%. The fusion of the coating and the substrate resulted in a considerable heterogeneity of electrochemical potentials on the coating surface. The microcracks in the surface layer also contributed to the intensification of the corrosion processes.

4. Summary

The following conclusions can be drawn from the analysis and test results:

1. The microstructure analysis revealed that the coating thickness was 34−64 μm, whereas the heat affected zone ranged approximately from 23 to 31 μm. The coatings possessed microcracks and pores.
2. A significant increase in roughness Ra was reported for specimens with WC-Co-Al_2O_3 coatings. Higher roughness, however, is not always considered a disadvantage. Under certain circumstances, valleys in the roughness profile act as lubricant reservoirs, which increases the rate of heat transfer and that of catalysis.
3. The microhardness of the WC-Co-Al_2O_3 coating produced by electro-spark alloying was 906 HV0.4, while that of the base material – C45 steel – was 279 HV0.4.
4. The obtained I_k values indicate over 52% increase in corrosion resistance of the ESD coated sample compared to the uncoated C45 steel substrate.
5. The coating surface is composed of WC and W_2C besides a small amount of Co_2C and Al_2O_3.

References

[1] Galinov I.V., Luban R.B., *Mass transfer trends during electrospark alloying*, Surface & Coatings Technology, 79, 1996, 9-18.

[2] Ozimina D., Scholl H., Styp-Rekowski M., *Formowanie przeciwzużyciowych warstw wierzchnich obróbką elektroiskrową. Wybrane zagadnienia obróbek skoncentrowaną wiązką energii*, rozdział 2, 2003, 104-109.

[3] Radek N., *Determining the operational properties of steel beaters after electrospark deposition*, Eksploatacja i Niezawodność – Maintenance and Reliability, 4, 2009, 1016.

[4] Chang-bin T., Dao-xin L., Zhan W., Yang G., *Electro-spark alloying using graphite electrode on titanium alloy surface for biomedical applications*, Appl. Surf. Sci., 257, 2011, 6364-6371.

[5] Konstanty J., *Powder metallurgy diamond tools*, Elsevier, Oxford 2005.

TECHNICAL TRANSACTIONS | CZASOPISMO TECHNICZNE
MECHANICS | MECHANIKA
4-M/2016

JACEK PIETRASZEK*, ANDRZEJ SOBCZYK**,
EWA SKRZYPCZAK-PIETRASZEK***, MACIEJ KOŁOMYCKI***

THE FUZZY INTERPRETATION OF THE STATISTICAL TEST FOR IRREGULAR DATA

ROZMYTA INTERPRETACJA TESTU STATYSTYCZNEGO DLA NIEREGULARNYCH DANYCH

Abstract

The well-known statistical tests have been developed on the basis of many additional assumptions, among which the normality of a data source distribution is one of the most important. The outcome of a test is a *p*-value which may is interpreted as an estimation of a risk for a false negative decision i.e. it is an answer to the question "how much do I risk if I deny?". This risk estimation is a base for a decision (after comparing with a significance level α): reject or not. This sharp trigger – *p*-level greater than α or not – ignores the fact that a context is rather smooth and evolves from "may be" through "rather not" to "certainly not". An alternative option for such assessments is proposed by a fuzzy statistics, particularly by Buckley's approach. The fuzzy approach introduces a better scale for expressing decision uncertainty. This paper compares three approaches: a classic one based on a normality assumption, Buckley's theoretical one and a bootstrap-based one.

Keywords: statistical test, *normality of distribution*, *fuzzy statistics, bootstrap*

Streszczenie

Powszechnie znane testy statystyczne były opracowane przy wielu dodatkowych założeniach. Jednym z najważniejszych jest normalność rozkładu populacji źródłowej. Wynikiem testu jest wartość *p*, która jest interpretowana jako ocena ryzyka decyzji fałszywie negatywnej, tj. jest to odpowiedź na pytanie „ile ryzykuję jeżeli neguję?". Ta ocena ryzyka jest podstawą do podjęcia decyzji (po porównaniu z krytycznym poziomem istotności α): odrzucić czy nie. Takie ostre przełączenie – wartość *p* większa od α czy też nie – ignoruje fakt, że kontekst jest raczej gładki i ewoluuje od „może tak" przez „raczej nie" do „zdecydowanie nie". Alternatywą dla takich ocen jest statystyka rozmyta, a szczególnie podejście Buckleya. Podejście rozmyte wprowadza lepszą skalę do wyrażenia niepewności decyzji. Niniejszy artykuł porównuje trzy podejścia: klasyczne zakładające normalność, teoretyczne Buckleya i bootstrapowe.

Słowa kluczowe: test statystyczny, *normalność rozkładu*, *statystyka rozmyta*, *bootstrap*

DOI: 10.4467/2353737XCT.16.242.5991

* D.Sc. Ph.D. Eng. Jacek Pietraszek, Assoc. Prof., Institute of Applied Informatics, Faculty of Mechanical Engineering, Cracow University of Technology.
** D.Sc. Ph.D. Eng. Andrzej Sobczyk, Assoc. Prof., Institute of Machine Design, Faculty of Mechanical Engineering, Cracow University of Technology.
*** Ph.D. Ewa Skrzypczak-Pietraszek, Chair and Department of Pharmaceutical Botany, Jagiellonian University Collegium Medicum.
**** M.Sc. Eng. Maciej Kołomycki, Institute of Applied Informatics, Faculty of Mechanical Engineering, Cracow University of Technology.

1. Introduction

The typical statistical approach leads from a certain knowledge about a sample to an uncertain knowledge (more precisely: hypothesis) about a general population from which the sample was taken. The non-parametric test is the first step, the parametric test for the selected and previously not rejected distribution is the second step. Computed estimators define the most probable distribution and its value is the limit to which a long series frequency goes. This definition involves simultaneously Kolmogorov axiom-based probability [1] and von Mises frequency-based probability [2].

As the beginning of a fuzzy approach to statistical problems, statistical hypothesis testing, in particular, the article of Casals and Giles [3] may be recognized. They generalized Neymann-Pearson lemma, where a concept of a fuzzy information system proposed by Tanaka et al. [4] was utilized. It allowed to construct the uniformly most powerful test for point-based hypotheses with the assumed precise significance level. It is characteristic of this approach that a fuzzy event taken from a limited set of fuzzy observations is considered and values of a membership for all considered events must sum to strict 1. In 2004, Buckley [5] proposed and then in 2006 [6] extended a different approach introducing fuzzy conditions, particularly fuzzy significance level. In 2006 Grzegorzewski [7] proposed a general classification of a possible fuzzy generalization for the classic theory of a statistical hypothesis testing, where three main elements constituting a decision system were distinguished. The theory of a statistical hypothesis testing is only the specific element of the system. The three main elements are: data, hypothesis and conditions. Each of these elements may be described precisely or imprecisely. The traditional theory requires the precise description for each of these elements, however all possible combinations are eight.

In the terms of Grzegorzewski's model, the Casals and Giles's proposal may be described as the triplet: fuzzy data, crisp hypothesis and crisp conditions. Buckley's proposal may be treated as: crisp data, crisp hypothesis and fuzzy conditions. To authors' knowledge, other combinations have not been proposed until now (Table 1).

In the further section, the authors evaluate the test for the equal of means and compare the results from classic, Buckley's and bootstrap approaches.

Table 1

Triplets of possible crisp/fuzzy combinations of Grzegorzewski's model

	HYPOTHESIS			
	crisp		fuzzy	
	DATA		**DATA**	
CONDITIONS	crisp	fuzzy	crisp	fuzzy
crisp	classic	Casals & Giles	*not known*	*not known*
fuzzy	Buckley	*not known*	*not known*	*not known*

2. Materials and Methods

2.1. Raw Data

The raw data was taken from the biochemistry investigation [8]. The dataset was divided into two subsets, each of 20 values (Table 2).

Table 2

The raw data

Data source	Values
Series H	4.50; 3.96; 4.11; 5.01; 4.87; 4.31; 3.20; 5.09; 4.61; 4.70 4.49; 3.51; 3.19; 3.29; 2.55; 3.10; 4.11; 3.10; 3.21; 4.67
Series M	4.00; 3.06; 5.90; 4.86; 5.70; 5.21; 3.51; 4.29; 4.61; 5.49 4.30; 4.90; 5.51; 4.39; 4.01; 3.90; 3.70; 2.81; 5.42; 3.50

The data are values of the callus tissue growth factor related to two variants H and M of the special medium modified with various additives. The test of means equality should detect possible differences between effects of these two variants.

2.2. Classic test

The means and the standard deviations for both variants were calculated using classic formulas:

$$\overline{x} = \frac{1}{n}\sum_{i=1}^{n} x_i, \tag{1}$$

$$s^2 = \frac{1}{n-1}\sum_{i=1}^{n} (x_i - \overline{x})^2. \tag{2}$$

The test for the equality of means with an unknown but mutually equal variances was performed with test statistic t calculated from the formula:

$$t = \frac{\overline{x}_M - \overline{x}_H}{\sqrt{\dfrac{(n_H - 1)s_H^2 + (n_M - 1)s_M^2}{n_H + n_M - 2}\left(\dfrac{1}{n_H} + \dfrac{1}{n_M}\right)}}, \tag{3}$$

where distribution of t goes asymptotically to t Student distribution with $(n_{\mathrm{H}} + n_{\mathrm{M}} - 2)$ degree of freedom.

2.3. Buckley's approach

The detailed calculations related to the above-mentioned data were described by Pietraszek and Skrzypczak-Pietraszek [9]. In short, the test statistic has been fuzzified according to formula:

$$\hat{T}[\alpha] = \frac{\Delta \hat{x}[\alpha]}{\sqrt{\frac{\hat{\sigma}_1^2[\lambda]}{n_1} + \frac{\hat{\sigma}_2^2[\lambda]}{n_2}}}, \tag{4}$$

where both variances and the means difference are of specific triangular form. It should be noted that Eq. 4 is specifically designed for unknown means and known variances but unfortunately Buckley did not a present formula for the variant with the unknown variances.

2.4. Bootstrap approach

The bootstrap procedure was conducted according to Shao and Tu [10] instructions. Both of the raw subsets were treated as sources for bootstrap draw, i.e. both subsets were randomly replicated and the test statistic *t* was evaluated from (Eq. 3) and then collected. After 40 000 draws, the collected values were transformed into descriptive statistics and a histogram.

3. Analysis

3.1. Classic approach

The descriptive statistics were evaluated for both subsets (Table 3). The test statistic *t* has the value of 1.789 at 38 degrees of freedom. It led to the *p*-value of 0.082.

Table 3

The descriptive statistics for raw data series

Data source	Mean	Variance	Standard deviation	Sample size
Series H	3.98	0.59	0.77	20
Series M	4.45	0.82	0.90	20

3.2. Buckley's approach

The fuzzified estimators of descriptive statistics were calculated for both the subsets. Next, the fuzzified estimator of the test statistic *t* was calculated according to Eq. 4. The result is presented in Fig. 1. as a triangular-like form of the fuzzy number.

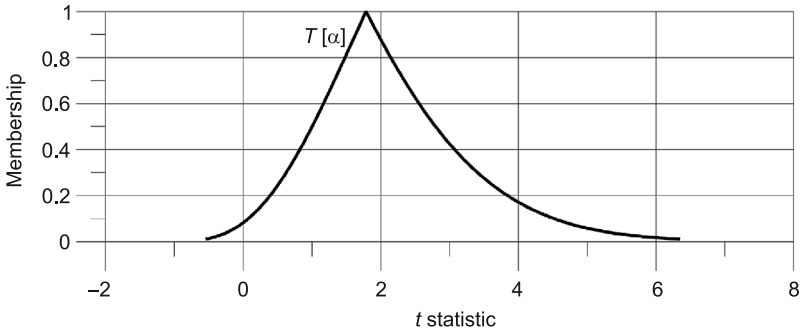

Fig. 1. Fuzzy estimator of test statistic *t* obtained for the fuzzified test of means equality

3.3. Bootstrap approach

The bootstrap approach was made in the following manner: the draws were made from both subsets creating new subsampled bootstrap subsets. Then, the test statistic *t* was evaluated based on descriptive statistics calculated for both subsets. The value of the test statistic was collected and next iteration of the bootstrap process was initiated. After 40 000 iteration, the test statistic *t* collection was processed and its descriptive statistics (Table 4) and the histogram (Fig. 2) were created. The *p*-value evaluated from the bootstrap was 0.067.

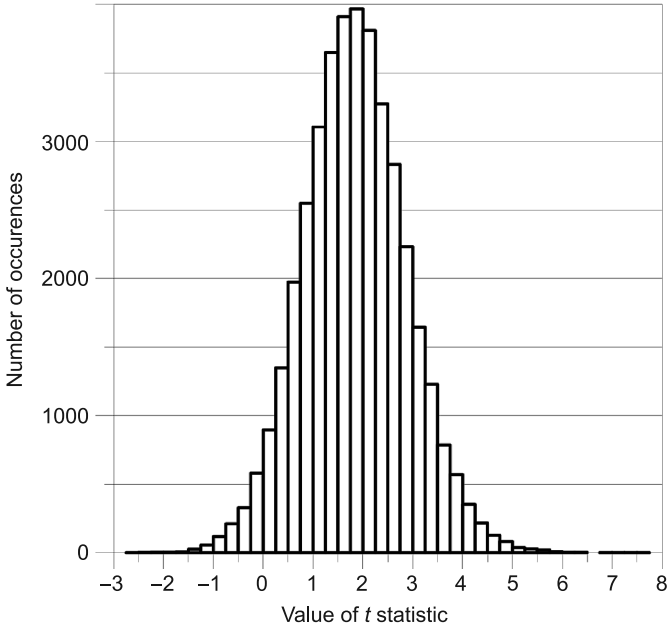

Fig. 2. Distribution of the test statistic *t* obtained from the bootstrap approach

Table 4

The descriptive statistics for the bootstrapped distribution of the test statistic T

Statistic	Value
Minimum	–2.72
Maximum	7.74
Mean	1.85
Median	1.83
Variance	1.06

4. Conclusion

The main characteristics of all approaches are consistent and the decisions which may be made on these results are the same: do not reject equality of the data subset means. On the contrary, the contexts of these approaches are different. The classic one assumes the normality of data and asymptotic equality of the test statistic t with Student distribution. The bootstrap approach is non-parametric and reveals the shape of distribution derived from raw data without additional assumptions. The Buckley's fuzzy approach expresses the subjective opinion about the possibility of such a value for the test statistic t. While the classic and the bootstrap approaches have the same deeper foundations, the Buckley's is far more different because of subjective foundations. The Buckley's approach appears to be useful if the description of data is vague.

References

[1] Kolmogoroff A., *Grundbegriffe der Wahrscheinlichkeitsrechnung*, Springer, Berlin, Heidelberg 1933.

[2] von Mises R., *Mathematical Theory of Probability and Statistics*, Academic Press, New York 1964.

[3] Casals M.R., Gil M.A., Gil P., *On the use of Zadeh's probabilistic definition for testing statistical hypotheses from fuzzy information*, Fuzzy Sets and Systems, vol. 20, 1986, 175-190.

[4] Tanaka H., Okuda T., Asai K., *Fuzzy information and decision in statistical model*, [in:] Gupta M.M., Ragade R.K., Yager R.R. (Ed.), Advances in Fuzzy Sets Theory and Applications, North--Holland 1979, 303-320.

[5] Buckley J.J., *Fuzzy Statistics*, Springer, Heidelberg 2004.

[6] Buckley J.J., *Fuzzy probability and Statistics*, Springer, Heidelberg 2006.

[7] Grzegorzewski P., *Wspomaganie decyzji w warunkach niepewności. Metody statystyczne dla nieprecyzyjnych danych*, EXIT, Warszawa 2006.

[8] Skrzypczak-Pietraszek E., *Polysaccharides in the herb and callus cultures of Melittis melissophyllum L. (Lamiaceae)*, Ph.D. thesis, CM UJ, Kraków 1999.

[9] Pietraszek J., Skrzypczak-Pietraszek E., *A comparison of statistical analysis and fuzzy analysis related to an example of callus tissue growth of Melittis melissophyllum L. with various variants of Murashige and Skoog's medium*, Polish Journal of Environmental Studies, vol. 18 (3B), 2009, 290-293.

[10] Shao J., Tu D., *The Jackknife and Bootstrap*, Springer, New York 1995.

CONTENTS

TREŚĆ

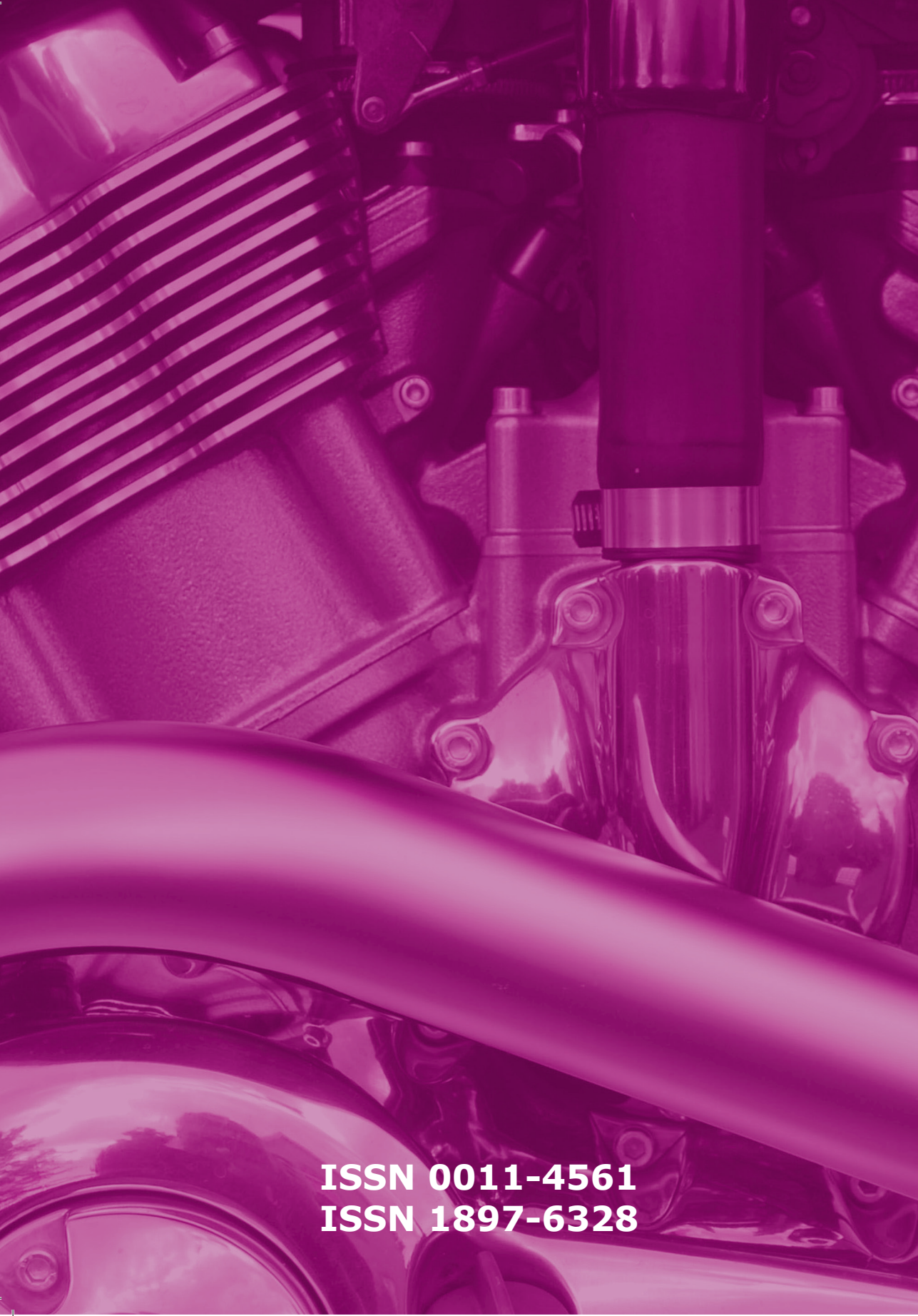

ISSN 0011-4561
ISSN 1897-6328